Synthesis, assembly, and intracellular trafficking of members of the cys-loop and P2X families of ligand-gated ion channels

Kumulative Dissertation
zur Erlangung des Doktorgrades
der Naturwissenschaften

vorgelegt beim Fachbereich
Chemische und Pharmazeutische Wissenschaften
der Johann Wolfgang Goethe-Universität
in Frankfurt am Main

von
Sven Sadtler
aus Bad Homburg

Frankfurt am Main (2005)
(D F 1)

vom Fachbereich Chemische und Pharmazeutische Wissenschaften der
Johann Wolfgang Goethe-Universität als Dissertation angenommen

Dekan:	Prof. Dr. Schwalbe
Gutachter:	Prof. Dr. Lambrecht
	Prof. Dr. Schmalzing
Datum der Disputation:	14.12.2005

Danksagung

Ich danke Prof. Dr. Günter Lambrecht für die Aufnahme in seinen Arbeitskreis, für seine Anregungen sowie für die stetige Diskussionsbereitschaft. Ohne die freundliche und unkomplizierte Übernahme in Seinen Arbeitskreis wäre die Fertigstellung dieser Arbeit an der Johann Wolfgang Goethe-Universität in Frankfurt am Main nicht möglich gewesen.

Für die Aufnahme in seinen Arbeitskreis zu Beginn meiner Doktorarbeit und die freundliche Überlassung des Themas danke ich Prof. Dr. Günther Schmalzing. Ich verdanke Ihm jede erdenkliche fachliche Unterstützung sowie zahlreiche anregende Gespräche. Herrn Prof. Dr. Günther Schmalzing hat mich in jeder Phase der Arbeit sehr sachkundig und richtungweisend begleitete, mich stets ermuntert und viel Geduld gezeigt.

Herzlichen Dank auch allen Mitarbeitern und Mitarbeiterinnen des Arbeitskreises von Herrn Prof. Dr. Günther Schmalzing für das stets gute Arbeitsklima sowie für die große Diskussionsbereitschaft. Ein ganz besonderer Dank möchte ich hierbei an Dr. Cora Büttner richten, die mir in den ersten Wochen mit Ihrer Betreuung stets zur Seite stand und diese Arbeit mit vielen interessanten Ideen und zahlreichen Diskussionen unterstützt hat. Einen ganz besonderen Dank auch an Dr. Bernd-Uwe Failer für viele hilfreiche Anregungen und Diskussionen.

Auch allen anderen Mitarbeitern und Mitarbeiterinnen des Pharmakologischen Instituts für Naturwissenschaftler möchte ich für die gute Zusammenarbeit und das stets gute Arbeitsklima bedanken.

Einen ganz besonderen Dank möchte ich zum Schluss auch an meine Mutter, meine Brüder, meine Freundin und meine Freunde richten. Danke für Eure Unterstützung und Euer Verständnis in den letzten Jahren.

TABLE OF CONTENTS

3. Results

4. Discussion

5. Deutsche Zusammenfassung

TABLE OF FIGURES

1. Introduction

1.1 Basic architecture of the glycine receptor

The anion-conductive inhibitory glycine receptor (GlyR) belongs to the cys-loop superfamily of pentameric ligand-gated ion channels (LGIC), which includes the nicotinic acetylcholine receptors (nAChRs), the γ-aminobutyric acid receptors ($GABA_ARs$ and $GABA_CRs$), and the 5-hydroxytryptamine type 3 receptor ($5HT_3R$). GlyRs mediate fast postsynaptic inhibition in the spinal cord and the brain stem of the mammalian central nervous system. Four genes encoding the ligand-binding GlyR α subunit (α1-α4) and a single gene for the structural β subunit are known in vertebrates (for review, see Kuhse et al., 1995; Harvey & Betz, 2000). These subunits form functional α homo-pentameric or αβ hetero-pentameric chloride channels (Kuhse et al., 1993; Langosch et al., 1988).

The different GlyR subunits share a common modular structure (Fig. 1).

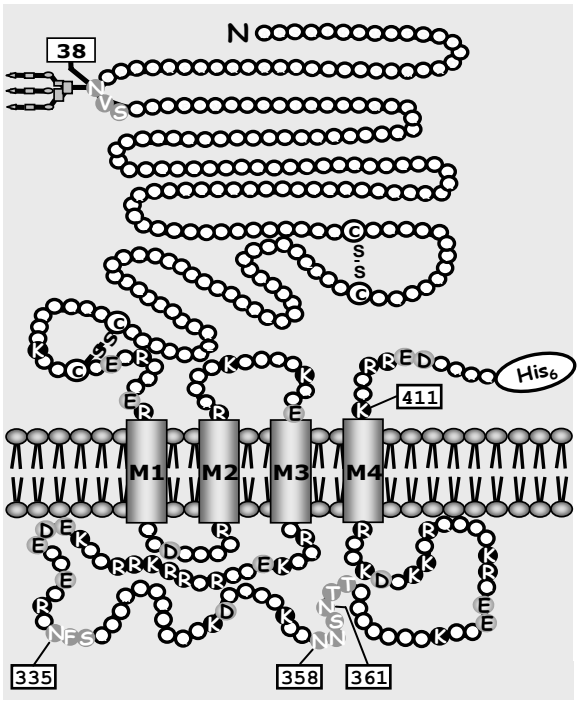

Fig. 1. Sequence and Membrane topology of the GlyR α1 subunit.
The membrane topology and predicted boundaries of the transmembrane segments are based on the original model (Harvey & Betz, 2000). NX(T/S) sequons are indicated with grey symbols combined with white lettering. Notably, only one of the sequons (^{38}NVS) is located on the predicted ectodomain, whereas the three others (^{335}NFS, ^{358}NNS, ^{361}NTT) are located on the cytoplasmic M3-M4 loop. Basic residues (Lys, Arg) are highlighted with filled black symbols and white lettering, whereas acidic residues (Glu, Asp) are highlighted in grey. *His6*, C-terminal hexahistidyl tag.

They consist of a more than 200 amino acids long N-terminal ectodomain, which is followed by four membrane-spanning regions, M1–M4. M1 and M2 as well as M2 and M3 are separated by short hydrophilic loops, whereas a large endodomain of 83 amino acids separates M3 from M4 (designated here as M3-M4 loop). The N-terminal ectodomain comprises not only part of the agonist binding site, but also controls the specificity of subunit oligomerization (Verrall & Hall, 1992). It further includes a 15 amino acids long cysteine loop and a cleavable signal peptide that directs the N-terminus of the polypeptide into the endoplasmic reticulum (ER), where N-glycosylation either at one (α1, α3, α4) or at two consensus sites (α2, β) occurs.

1.2 GlyR topology: The classical model and new determinants

In the classical model of intracellular protein topogenesis the orientation of the signal sequence determines the overall topology of the mature protein by initiating the transport of the following amino acids over the ER membrane (Blobel, 1980; Rapoport et al., 1996). Accordingly, downstream hydrophobic sequences simply serve as alternate stop transfer- and signal anchor sequences, which cause the nascent polypeptide to follow passively the lead of the preceding transmembrane segment and thereby direct the sequential insertion of the membrane domains. In most prokaryotic proteins, the orientation of the signal sequence follows the "inside- or cis-positive rule" (von Heijne & Gavel, 1988), predicting that the transmembrane orientation depends on the charge of the flanking amino acids, and that the more positively charged segment retains on the cytoplasmic (cis) side. Arginines and lysines may interact with the negatively charged head groups of phospholipids (van Klompenburg et al., 1997) and the negative-inside transmembrane potential (Andersson & von Heijne, 1994). Histidines in contrast have almost no effect because of their low average degree of ionization at physiological pH (Andersson et al., 1992). Negatively charged residues seem to affect the topology of prokaryotic proteins only when present in high numbers (Nilsson & von Heijne, 1990).

For eukaryotic proteins, the cis-positive rule does not correlate sufficiently with the orientation of the first transmembrane segment. Here, according to the charge difference hypothesis, also negative charged amino acids have to be taken into account and their number has to be subtracted from the number of positive residues. The segment which carries the more positive net charge will face the cytosol (Hartmann et al., 1989). Besides the charge difference also the hydrophobicity of the signal sequence and its length (Sato et al., 1990; Wahlberg & Spiess, 1997) play important roles for the orientation of the first transmembrane segment. Also glycosylation at sites near the signal sequence has been shown to affect topology (Goder et al., 1999).

Even though a variety of membrane proteins follow the classical insertion model (Wessels & Spiess, 1988; Lipp et al., 1989; Harley & Tipper, 1996; Gafvelin et al., 1997), there is growing evidence that the initial translocation events may not necessarily dictate the topology of the entire mature protein (Wilkinson et al., 1996; Beltzer et al., 1991; Andrews et al., 1992). The correct positioning of the following transmembrane segments in multispanning proteins seems to depend on additional downstream topogenic information (Goder & Spiess, 2001). To address this issue, the GlyR α1 M3-M4 loop was investigated for potential motives that may have an influence on the correct protein topology.

1.3 Distribution and density of LGICs

The efficiency of synaptic transmission depends critically on a dense packing of neurotransmitter receptors in the postsynaptic membrane. Different mechanisms that trigger receptor distribution and density at the plasma membrane have been demonstrated for LGICs. In differentiating muscle fibers, for instance, the postsynaptic density of nAChRs at the developing motor endplate is regulated by gene expression, efficient internalisation and degradation of extrasynaptic receptors, synaptic clustering by rapsyn and slowing down the turnover of synaptically accumulated nAChRs (Colledge & Froehner, 1998; Sanes & Lichtman, 1999). Denervation (Sanes & Lichtman, 1999) or treatment with α-bungarotoxin

(Akaaboune et al., 1999) leads to an increase in nAChR turnover and a postsynaptic loss of nAChRs (Xu & Salpeter, 1999).

In this context, endocytosis is often considered to be a crucial step in the regulation of postsynaptical nAChR density, because receptor degradation only occurs after internalisation and lysosomal targeting (Xu & Salpeter, 1999; Pumplin & Fambrough, 1982). Moreover, different studies revealed that exo- and endocytosis of receptors plays a dynamic role in regulating synaptic efficacy at glutamatergic synapses of the central nervous system (Turrigiano, 2000; Lüscher et al., 2000). In hippocampal neurons high frequency stimulation leads to an increase of AMPA receptors in the dendritic spines during long term potentiation (Shi et al., 1999), whereas the clathrin-mediated receptor internalization might be a crucial step in long term depression in the cerebellum (Wang & Linden, 2000; Man et al., 2000).

Like the nAChRs and glutamatergic receptors, also the inhibitory GlyR is known to undergo efficient endocytosis. Blockade of GlyRs by strychnine in cultured spinal neurons leads to internalization of the receptors into an endosomal compartment (Kirsch & Betz, 1998; Levi et al., 1998). Concomitantly, the blocked GlyRs fail to co-localize with gephyrin, a peripheral membrane protein that anchors GlyRs and $GABA_A$Rs in the postsynaptic membrane (Kneussel & Betz, 2000). Also gephyrin-deficient mice lack $GABA_A$R clusters at synapses and show an increased intracellular $GABA_A$R immunoreactivity (Kneussel et al., 1999a). These results indicate that binding to gephyrin at the postsynaptical membrane may prevent endocytotical internalisation of $GABA_A$Rs and GlyRs.

In summary, a variety of processes, driven either by development or neuronal activity, lead to changes in LGIC density at the postsynaptical membrane by affecting membrane incorporation, surface stability and receptor endocytosis. Especially the mechanisms that trigger internalization have been intensively studied. As only cytosolically exposed portions of a receptor molecule are capable of interacting with cytoskeletal elements, the question arises whether the M3-M4 loop of the GlyR α1 subunit contains information involved in the internalisation and degradation processes. Due to its well analysed molecular structure, subunit assembly and cell surface incorporation the homomeric GlyR is particularly suited for such an analysis.

1.4 Assembly of nicotinic α7 subunits in *Xenopus* oocytes

The most intensively studied member of the cys-loop superfamily of LGICs is the cation-conductive nAChR. Like GlyRs all nAChRs are thought to share a pentameric structure. The best characterized nAChR, situated at neuromuscular junctions, is composed of four homologous gene products with a stoichiometry of $(\alpha 1)_2\beta 1\gamma\delta$ (fetal) or $(\alpha 1_2)\beta 1\varepsilon\delta$ (adult). Eleven additional genes, eight encoding nAChR α subunits (α2–α7, α9, α10) and three encoding β subunits (β2–β4), have been found in the mammalian nervous system. In contrast to α subunits 2-6, which need to heteropolymerize with at least one of the β subunit isoforms to form functional nAChRs (McGehee & Role, 1995; Sargent, P.B., 1993; Le Novere et al., 2002), α7 and α9 subunits homopolymerize to functional ion channels when expressed in *Xenopus* oocytes (Couturier et al., 1990; Anand et al., 1993; Séguela et al., 1993) and certain cells of neuronal origin (Puchacz et al., 1994; Quik et al., 1996; Blumenthal et al., 1997; Cooper & Millar, 1997). Moreover, endogenous α7 homopentamers have been convincingly demonstrated in a PC12 cell line and rat brain (Chen & Patrick, 1997; Drisdel & Green, 2000). In contrast, transient transfection of non-neuronal cell lines with α7 subunit cDNA resulted in little or no production of functional nAChRs, although high levels of α7 mRNA and α7 protein were observed (Cooper & Millar, 1997; Kassner & Berg, 1997). Also certain neuronal cell lines, including those PC12 cells which lack endogenous α7 nAChRs, did not produce functional nAChRs from transfected α7 cDNA (Blumenthal, et al., 1997). Obviously, the assembly, maturation and/or stabilization of functional homo-pentameric nAChRs do critically depend on additional cellular factors which are present only in a subset of cells (Blumenthal et al., 1997; Kassner & Berg 1997; Helekar & Patrick, 1997; Halevi et al., 2002; Helekar et al., 1994). Interestingly, a comparable cell-specific receptor formation is not found with other members of the cys-loop superfamily of LGICs, such as the homooligomeric $5HT_3A$ or GlyR α1 receptors.

To determine the step that requires those additional cellular factors for proper receptor formation, homo-pentameric α7 nAChRs were expressed in *Xenopus* oocytes and analyzed via the blue native PAGE technique. As a control the homooligomeric $5HT_3A$ receptor was used, which exhibits 51% amino acid sequence homology with the nAChR α7 subunit (Ortells & Lunt, 1995).

1.5 Quaternary structure of P2X receptors (LGIC class III)

On the basis of their amino acid sequences and membrane threading patterns, LGICs have been grouped into three major classes (Le Novere & Changeux, 2001; North, R.A., 1996): (i) the nicotinic acetylcholine receptor superfamily discussed above, (ii) the cationic glutamate receptor (iGluR) family including AMPA (α-amino-3-hydroxyl-5-methyl-4-isoxazole propionic acid), NMDA (N-methyl-D-aspartate), and kainate receptors; and (iii) the ATP-gated P2X receptor family. The class I LGIC members consist of a pentameric barrel stave-like array of homologous subunits arranged in a circular order around a central ion channel. Also iGluRs were first thought to share a pentameric architecture. However, both biochemical and electrophysiological data favor the view that iGluRs form tetramers similar to K^+ channels (for references see Dingledine et al., 1999). The architecture of the class III LGICs, the P2X receptors, is still controversially discussed. The seven known P2X isoforms (designated $P2X_1$ to $P2X_7$) form multiple functional homomultimeric and heteromultimeric cation-channels (Brake et al., 1994; Valera et al., 1994; Bo et al., 1995; Chen et al., 1995; Buell et al., 1996; Collo et al., 1996; Surprenant et al., 1996; Soto et al., 1997) and open in response to extracellular ATP released from neuronal and non-neuronal cells (Bodin & Burnstock, 2001). All P2X subunits share a common membrane topology with cytosolic N and C termini, two membrane-spanning hydrophobic domains (M1 and M2), and a large intervening hydrophilic extracellular loop. From kinetic data (Ding & Sachs 2000) and the structural similarity to the inward rectifying K^+ channel, a tetrameric organization was anticipated also for P2X receptors. However, several biochemical and electrophysiological studies have demonstrated that recombinant P2X receptors possess a trimeric architecture (Nicke et al., 1998, 1999, 2003; Stoop et al., 1999; Rettinger et al., 2000).

Against this background, the assembly properties and oligomeric states of slowly desensitizing homomeric P2X receptors were carefully re-evaluated with biochemical methods. The studies focused in particular on $P2X_2$ homomers and $P2X_{1+2}$ heteromers. Because of their known inability to form functional homomeric receptors in *Xenopus* oocytes, $P2X_6$ subunits were also investigated. In addition to blue native PAGE analysis selective cell surface radioiodination followed by chemical cross-linking of plasma membrane-bound P2X receptors was used as a novel and independent approach.

2. Materials and Methods

2.1 cDNA constructs

Site-directed mutagenesis was performed using the QuickChange™ site-directed mutagenesis kit (Stratagene) using the human α1 GlyR subunit cDNA in vector pNKS2# (Gloor et al., 1995) as a template. For protein purification, a His_6 tag was introduced at the 3′ end of the coding region. All constructs were verified by sequencing. Amino acids were numbered according to their position in the mature protein sequence.

2.2 cRNA synthesis

Linearized plasmid DNAs were used for *in vitro* synthesis of cRNAs as described in Schmalzing et al., 1991. cRNA concentrations were determined by optical density readings at 260 nm.

2.3 Oocyte Expression

Defolliculated *Xenopus* oocytes were injected with 50 nl aliquots of capped cRNAs (0.5 µg/µl) and kept at 19°C in sterile frog Ringer's solution (ORi: 90 mM NaCl, 1 mM KCl, 1 mM $CaCl_2$, 1 mM $MgCl_2$, and 10 mM Hepes, pH 7.4) supplemented with 50 mg/litre gentamycin (Schmalzing et al., 1991). One to three days after cRNA injection, glycine responses were measured by two-electrode voltage-clamp recording at a holding potential of -70 mV. Electrophysiological measurements were kindly performed by Dr. Bodo Laube (MPI für Hirnforschung, Frankfurt).

2.4 Metabolic labeling with L-[^{35}S]methionine and cell surface radioiodination with ^{125}I-sulfo-SHPP

cRNA-injected and non-injected control oocytes were metabolically labeled by overnight incubation with L-[^{35}S]methionine (>40 TBq/mmol; Amersham Biosciences) at about 100 MBq/ml (0.1 MBq per oocyte) in frog Ringer's solution at 19°C and chased with 1 mM unlabeled methionine as indicated.

For selective labeling of plasma membrane-bound receptors, the injected oocytes were incubated for 3 days at 19°C. Then the oocytes were washed in oocyte-PBS (30 mM sodium phosphate, 70 mM NaCl, 1 mM $MgCl_2$, 0.1 mM $CaCl_2$) and placed in 0.5 ml polypropylene tubes on ice. Sulfo-SHPP was iodinated at ambient temperature by rapid subsequent addition of sulfo-SHPP (Pierce) in 2 µl of DMSO, 18.5 MBq of carrier-free Na^{125}I (NEN), 10 µl of 5 mg/ml of chloramines T in 0.5 M sodium phosphate buffer pH 7.5, 100 µl of 1 mg/ml of DL-α-hydroxyphenylacetic acid in 0.1 M NaCl, and 10 µl of 12 mg/ml of sodium metabisulfite in 0.05 M sodium phosphate buffer pH 7.5. A 10 µl aliquot of this reaction mix was immediately added per 10–12 oocytes. After 60 min of incubation on ice with occasional gentle mixing, oocytes were rinsed with Ca-free ORi. Where indicated, surface radioiodinated oocytes were first washed in frog Ringer's solution to remove unbound ^{125}I-sulfo-SHPP and then incubated for another 20 h at 19°C.

2.5 Protein Purification

His-tagged α1 GlyR receptors were purified by Ni^{2+}-NTA agarose chromatography. As elution can be achieved by competitive displacement with imidazole, denaturing agents such as SDS can be avoided (Nicke et al., 1998), thus allowing to release natively purified proteins in a non-denatured state. Oocytes were homogenized in detergent buffer (20 µl/oocyte) consisting of 0.1 M sodium phosphate buffer pH 8.0, 1% (w/v) digitonin (Serva, water-soluble), 10 mM iodacetamide to prevent artificial cross-linking of polypeptides by disulfide bonds, and the protease-inhibitors Pefa block-SC (100 µM), Leupeptin (50 µM), antipain (10 µM), and pepstatin (5 µM), all purchased from Biomol. Detergent extracts were cleared by centrifugation (10 min at

10,000 g and 4°C), diluted 5-fold with detergent buffer (same composition as the homogenisation buffer, but without iodacetamide), supplemented with Ni^{2+}-NTA agarose (Qiagen) and imidazole/HCl pH 8.0 (final concentration 10 mM). After 30 min of end-over-end mixing at ambient temperature, beads were washed five times with ice-cold detergent buffer consisting of 0.1 M sodium phosphate buffer pH 8.0, 0.2% (w/v) digitonin (Serva, water-soluble), 1 mM iodacetamide, 25 mM imidazole/HCl pH 8.0, and 100 µM Pefa block-SC. Proteins were released from the Ni^{2+}-NTA agarose beads by two rounds of continuous gentle shaking, each for 10 min at ambient temperature, with non-denaturing elution buffer consisting of 250 mM imidazole/HCl pH 7.6 and 0.5 % (w/v) digitonin (Calbiochem, water-soluble). Eluted proteins were kept at 0°C until analyzed.

2.6 SDS-PAGE and blue native PAGE

For SDS-PAGE (Sodium Dodecyl Sulfate - Polyacrylamide Gel Electrophoresis) or Tricine-SDS-PAGE (Schägger & von Jagow, 1987), proteins were supplemented with the appropriate SDS sample buffer containing 20 mM dithiothreitol, and electrophoresed in parallel with [^{14}C]labeled molecular mass markers (Rainbow; Amersham Biosciences) on linear SDS-polyacrylamide gels. Where indicated, samples were treated prior to SDS-PAGE with either endoglycosidase H (Endo H) or peptide-*N*-glycosidase F (PNGase F; both enzymes were purchased from New England Biolabs) in the presence of 1% (w/v) Nonidet P-40 to counteract SDS inactivation of PNGase F. Blue native PAGE (Schägger et al., 1994; Nicke et al., 1998) was performed immediately after protein purification. Purified proteins were supplemented with blue native sample buffer to final concentrations of 10% (v/v) glycerol, 0.2% (w/v) Serva blue G, and 20 mM sodium 6-amino-*n*-caproate, and applied onto polyacrylamide gradient slab gels. Where indicated, samples were treated prior to blue native PAGE with 8 M urea to induce partial dissociation of receptor complexes into lower order intermediates. Both SDS- and blue native polyacrylamide gels were fixed, dried, and exposed to BioMax MS film (Eastman Kodak Co.) at -80°C. For quantification, the dried gels were exposed to a PhosphorImager screen and scanned using a Storm 820 PhosphorImager (Amersham Biosciences). Individual bands were quantified with the ImageQuant software.

3. Results

3.1 UBIQUITINATION PRECEDES INTERNALIZATION AND PROTEOLYTIC CLEAVAGE OF PLASMA MEMBRANE-BOUND GLYCINE RECEPTORS

Received for publication, March 8, 2001, and in revised form, September 7, 2001
Published in J. Biol. Chem., Nov 2001; 276: 42978 - 42985; 10.1074/jbc.M102121200.

Cora Büttner‡, Sven Sadtler‡, Anne Leyendecker‡, Bodo Laube§, Nathalie Griffon§, Heinrich Betz§, and Günther Schmalzing‡

From the ‡Department of Pharmacology, Biocenter of the Johann Wolfgang Goethe University, Marie Curie Strasse 9, Frankfurt am Main 60439, and the §Department of Neurochemistry, Max Planck Institute for Brain Research, Deutschordenstrasse 46, Frankfurt am Main 60528, Germany

The paper describes that the α1 GlyR is subjected to ubiquitination in *Xenopus laevis* oocytes; the study dealing with the subject of this paper was already in progress when I joined the lab. Early experiments (mainly done by Cora Büttner) showed that (after hetorologous expression in *Xenopus* oocytes and isolation by Ni^{2+}-NTA-agarose chromatography under nondenaturing conditions) α1-His subunits migrated with an apparent mass of 48 kDa on a reducing Tricine-SDS-PAGE gel. Subsequent to a 20h chase interval, additional 35 and 13 kDa proteins, which were not present immediately after the [^{35}S]methionine labeling pulse, were isolated. These data indicated that the α1-His subunit was proteolytically cleaved into two defined fragments of 35 kDa and 13 kDa during the chase period. Additional experiments with the *N*-glycosidases Endo H and PNGase F revealed that the GlyR α1 subunit must have already left the ER and passed beyond the Golgi apparatus before cleavage occurred.

To visualize selectively the plasma membrane-bound α1-His GlyRs, the outer cell surface of oocytes was radioiodinated with ^{125}I-sulfo-SHPP, a membrane-impermeant Bolton-Hunter derivative (Thompson et al., 1987). These experiments revealed that the truncated forms of the α1-His GlyR were exclusively intracellularly located. This data indicated that homopentamers consisting of nicked subunits were either not routed to the cell surface or that cleavage occurred in a compartment distal from the plasma membrane. Unexpectedly, besides the full length 48 kDa subunit two additional bands of 55 and 62 kDa, and occasionally a third band of 69 kDa, were resolved by the Tricine-SDS-PAGE. Like the 48 kDa subunit, these polypeptides were Endo H resistant, but reduced by 3 kDa upon PNGase F treatment, indicating that they all carried a single complex-type *N*-glycan. Blue native PAGE analysis of the surface radioiodinated GlyR combined with Tricine-SDS-PAGE in the second dimension revealed that the 55 and the 62 kDa polypeptides were integral parts of the α1-His pentamer and not co-isolated accessory proteins. These results indicated that the 55 and the 62 kDa bands originate from α1-His subunits, to which one or two molecules of 7 kDa were conjugated *en route* to the plasma membrane or at the plasma membrane itself.[1]

[1] The experiments and results described in this chapter were mainly performed and achieved by Cora Büttner

3.1.1 The α1 GlyR can be isolated from the cell surface through hexahistidyl-tagged ubiquitin

Taking the findings of Cora Büttner into account, my thesis work initially focused on the identification of the molecular nature of the 7 kDa molecules that were conjugated to the GlyR α1-His subunits. The ladder-like pattern of α1-subunit bands differing from each other by ~7 kDa was strongly reminiscent of that of other polypeptides conjugated to one, two, and three molecules of ubiquitin, a protein of 76 amino acids. To examine whether ubiquitin is conjugated to the GlyR and accounts for the additional 55 and the 62 kDa bands at the plasma membrane, antibodies to ubiquitin were used in a first approach. However, no ubiquitin was detectable by Western blot analysis of recombinant GlyRs affinity-purified from *Xenopus* oocytes. Because this result may be due to a low abundance of the GlyR in the purified preparations, human His-ubiquitin was co-expressed together with a non-histidyl-tagged GlyR α1 subunit, to examine whether GlyRs can be isolated through covalently attached His-ubiquitin. As it can be seen from control purifications from [^{35}S]methionine-labeled oocytes (Fig. 2*C*) His-ubiquitin was efficiently expressed in this system. By using the co-expression approach, non-tagged α1 GlyR could be purified through His-tagged ubiquitin from surface-radioiodinated oocytes (Fig. 2*A*). Analysis by Tricine-SDS-PAGE showed the same ladder-like pattern as when the His-tagged α1 GlyR was expressed alone. This experiment revealed that the 55 and 62 kDa polypeptides indeed derive from mono- and di-ubiquitinated forms of the 48 kDa α1 subunit. The fact that a major fraction of the co-purified α1 subunits exists also in the non-ubiquitinated 48 kDa form indicates that not all α1 subunits within the homopentamer are ubiquitinated. Similar results were obtained when commercially available recombinant His-ubiquitin protein was used together with non-tagged GlyR α1 cRNA (Fig. 2*B*).

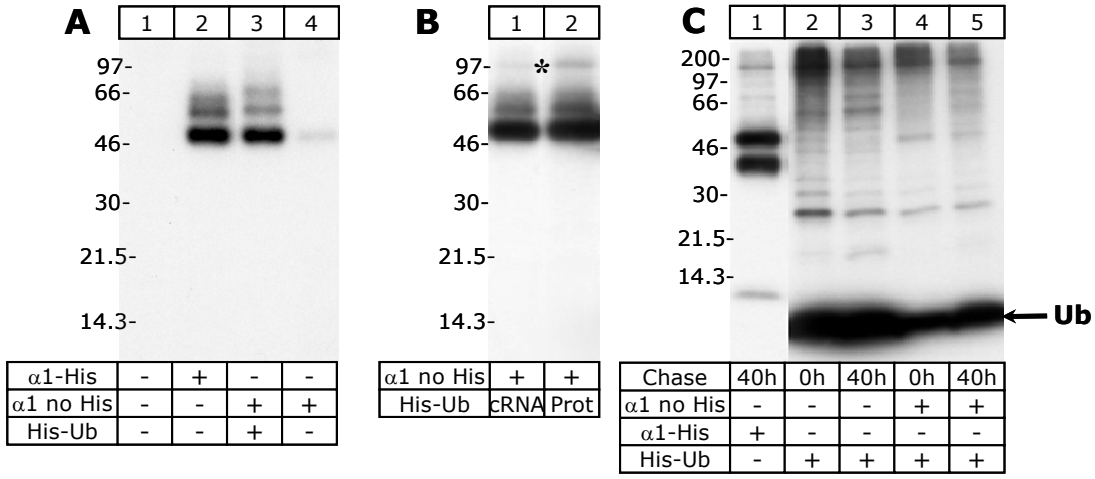

Fig. 2. GlyR α1 is ubiquitinated at the plasma membrane.
Autoradiographies of reducing Tricine-SDS-polyacrylamide gels are shown. *Panels A* and *B*, 3 days after injection of the indicated cRNAs, oocytes were surface labeled for 1 h at 0°C with ^{125}I-sulfo-SHPP. Oocytes were immediately extracted with digitonin, and proteins were purified under non-denaturing conditions by Ni^{2+}-NTA-agarose chromatography. The non-tagged GlyR α1 subunit (*α1 no His*) could be isolated in large amounts in both His-ubiquitinated and nonubiquitinated form upon co-expression of His-ubiquitin (*panels A* and *B*) or co-injection of recombinant His-ubiquitin protein (*His-Ub prot*, *panel B*). * indicates a protein band that was also isolated from non-injected control oocytes in this particular experiment. *Panel C*, proteins were purified by Ni^{2+}-NTA-agarose chromatography from [^{35}S]methionine-labeled oocytes injected with the indicated cRNAs. Note that *lanes 4* and *5* show solely small amounts of non-ubiquitinated GlyR α1 subunit, but no His-ubiquitinated GlyR α1 subunit co-isolated with His-ubiquitin. *Ub*, His-ubiquitin.

Control experiments confirmed that only traces of GlyR protein were purified by the same method when the non-tagged GlyR α1 was expressed without His-ubiquitin. These traces consistently accounted for ≤5% of the GlyR α1 subunit obtained after co-injection of His-ubiquitin.

Notably, the same approach with [^{35}S]methionine-labeled oocytes did not result in a co-isolation of significant amounts of GlyR α1 subunits (Fig. 2*C*). This observation suggests that ubiquitination occurs predominantly or exclusively at the plasma membrane and thus comprises only the fraction of GlyRs that are incorporated into the plasma membrane at the time of the experiment.

3.1.2 The α1-His GlyR is cleaved after internalization

These results strongly indicated that the ladder-like pattern of α1 subunit bands differing from each other by ~7 kDa was due to the conjugation of one, two, and three molecules of ubiquitin. However, it was still unclear at which trafficking step to and from the plasma membrane the α1 GlyR was proteolytically nicked. To address this question, plasma membrane-bound GlyRs of cRNA-injected *Xenopus* oocytes were labeled with ^{125}I-sulfo-SHPP. Subsequently, the oocytes were incubated for a further 20 h either at 19°C or at 0°C to allow for endocytosis or to block endocytosis, respectively. The truncated 35 kDa form and the cleaved 13 kDa fragment could only be isolated from oocytes that were kept for 20 h at 19°C, but not from oocytes that were kept on ice. These results indicate that cleavage does neither take place *en route* to the plasma membrane nor at the plasma membrane itself, but in a later compartment, *i.e.* in the endocytotic pathway.

3.1.3 Arginine substitution of lysine residues between M3 and M4 abolishes ubiquitination of the α1 GlyR in the plasma membrane, but does not block its internalization and lysosomal cleavage[2]

The GlyR α1 subunit harbors ten cytoplasmic lysine residues, which are all located in the large intracellular loop between transmembrane segments M3 and M4 (see Fig. 1). Monoubiquitin attached to lysine residues of endocytic membrane proteins has been demonstrated to be a signal for sorting of cargo into vesicles that bud into the late endosome lumen for delivery into the lysosome (for review see Hicke & Dunn, 2003). To investigate whether the observed ubiquitination of α1 GlyRs in *Xenopus* oocytes is a prerequisite for internalisation and cleavage of the receptor into the 35 and 13 kDa fragments, all ten lysine residues of intracellular loop were replaced by arginines, which cannot be ubiquitinated. After surface radioiodination, the so called GlyR no-K mutant appeared exclusively as a 48 kDa polypeptide on the Tricine-SDS-PAGE gel. In contrast the wild type GlyR α1 subunits migrated in the non-

[2] The following two chapters contain unpublished Data

ubiquitinated 48 kDa form and the 55, 62 and 69 kDa ubiquitinated forms (Fig. 3*A*). The loss of ubiquitination confirms that only the lysine residues of the intracellular loop between M3 and M4 are used to attach ubiquitin to the GlyR α1 subunit.

To examine whether ubquitination deficiency has a direct influence on GlyR α1 cleavage, the injected oocytes were metabolically labeled with [^{35}S]methionine. In contrast to expectations, however, the GlyR α1 no-K mutant and the parent α1-His GlyR were subjected to a similar degree of proteolytic cleavage (Fig. 3*B*). This suggests that abolition of ubiquitination does not impair internalization.

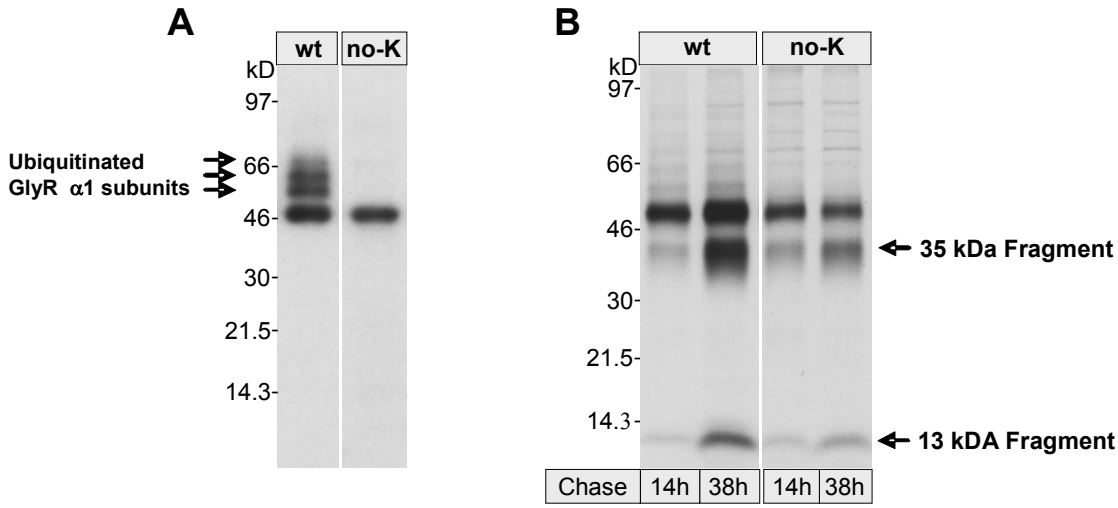

Fig. 3. Loss of ubiquitination does not abolish lysosomal cleavage.
Panel A, Oocytes injected with 25 ng of cRNA for GlyR α1-His (wt) or GlyR α1-His no-K were incubated for 3 days at 19°C and then labeled with membrane-impermeant ^{125}I-sulfo-SHPP. Receptors were purified by Ni^{2+}-NTA chromatography from 1% digitonin extracts of oocytes, and analysed by discontinuous Tricine-SDS-PAGE (13-10-4% acrylamide), followed by autoradiography. The GlyR α1-His no-K mutant does not show any ubiquitinated forms (*lane 2*). *Panel B*, Oocytes injected with 25 ng of cRNA for GlyR α1-His or GlyR α1-His no-K were metabolically labeled with [^{35}S]methionine for 4h at 19°C. Cells were then chased for 14 h or 38 h. Receptors were purified by Ni^{2+}-NTA chromatography from 1% digitonin extracts of oocytes, and analysed by discontinuous Tricine-SDS-PAGE (13-10-4 % acrylamide), followed by autoradiography. Despite the loss of ubiquitination, the GlyR α1-His no-K mutant shows a wild-type like cleavage behavior.

3.1.4 Internalization of GlyR is regulated by at least two signals, ubiquitination and ^{339}Y

Since ubiquitination appeared not to constitute a dominant signal for internalization, the sole tyrosine located on the M3-M4 loop of the GlyR α1 subunit, ^{339}Y, was considered as a residue potentially relevant for endocytosis. Single tyrosines are well known to constitute crucial residues of various endocytosis motives involved in internalization and targeting of membrane proteins to cellular compartments like endosomes and lysosomes. To assess its possible role as an endocytic signal, ^{339}Y was replaced by alanine. But the GlyR Y^{339}A-α1-His mutant was proteolytically cleaved to virtually the same degree into 35 kDa and 13 kDa fragments as the wild type GlyR (Fig. 4*A*). If, however, ^{339}Y was eliminated in addition to all the cytoplasmic ubiquitination sites, the proteolytic cleavage of the corresponding mutant (designated Y^{339}A-α1-His no-K) during a 38 h chase interval was greatly reduced (Fig. 4*B*).

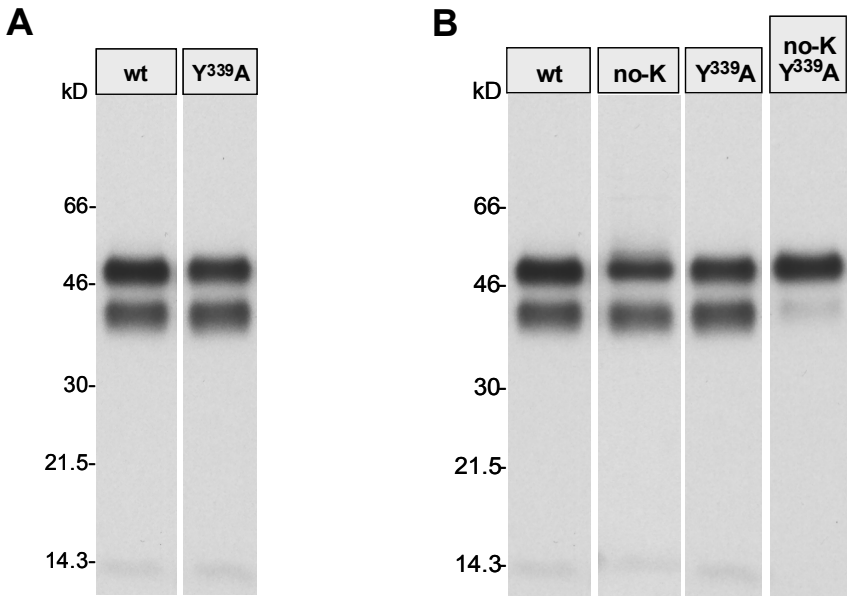

Fig. 4. Replacement of Y^{339} and ubiquitination-sites leads to a reduction of α1-GlyR cleavage
Oocytes injected with 25 ng of cRNA for either GlyR α1-His, GlyR α1-His no-K, Y^{339}A GlyR α1-His or Y^{339}A GlyR α1-His no-K were metabolically labeled with [^{35}S]methionine for 4h at 19°C. Cells were then chased for 38h. Receptors were purified by Ni^{2+}-NTA chromatography from 1% digitonin extracts of oocytes, and analyzed by discontinuous Tricine-SDS-PAGE (13-10-4% acrylamide), followed by autoradiography. *Panel A*, GlyR Y^{339}A-α1-His does not show a modified cleavage behavior (*lane 2*). *Panel B*, Y^{339}A GlyR α1-His no-K is cleaved significantly less than the wild-type or the single mutants (*lane 4*)

The degree of cleavage of the various mutants compared to the wild type α1 GlyR was quantified by PhosphorImager analysis (Fig. 5).

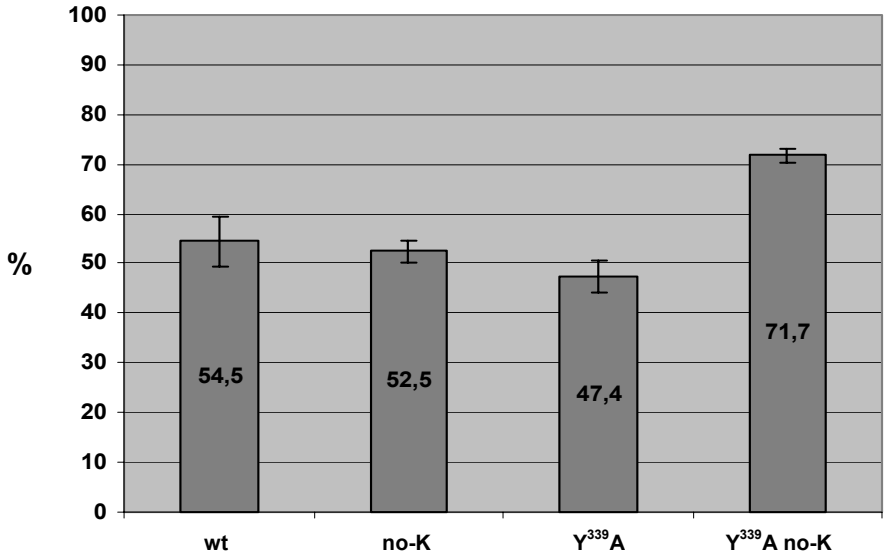

Fig. 5. Percentage of intact wt- and mutant GlyR α1 subunits after a 36h chase internal.
Oocytes injected with 25 ng of cRNA for GlyR α1-His, α1-His no-K, Y^{339}A-α1-His or Y^{339}A-α1-His no-K were metabolically labeled [^{35}S]methionine for 4 h at 19°C and then chased for 38 h. Receptors were purified by Ni^{2+}-NTA chromatography from 1 % digitonin extracts of oocytes, and analyzed by discontinuous Tricine-SDS-PAGE (13-10-4 % acrylamide). The dried gels were subjected to phosphoimage analyses for protein quantification. Error bars represent standard deviations of the means of three independent experiments.

The percentages of the non-cleaved wild type α1-His, the no-K mutant, and the Y^{339}A mutant did not differ significantly from each other. The ubiquitination deficient mutant carrying the additional Y^{339}A mutation, however, was significantly less proteolysed. This may suggest that two endocytosis pathways operate in *Xenopus* oocytes to mediate the internalisation of GlyRs. One pathway may depend on ubiquitin as a signal, whereas the second pathway may involve a tyrosine-based motif. The results can best be reconciled with the view that to two endocytotic pathways can compensate for each other if one of the pathways is blocked.

3.2 A BASIC CLUSTER DETERMINES TOPOLOGY OF THE CYTOPLASMIC M3-M4 LOOP OF THE GLYCINE RECEPTOR α1 SUBUNIT

Received for publication, December 23, 2002, and in revised form, February 21, 2003
Published in J. Biol. Chem., May 2003; 278: 16782 - 16790 ; 10.1074/jbc.M213077200.

Sven Sadtler‡, Bodo Laube§, Alhassan Lasub§, Annette Nicke‡, Heinrich Betz§, and Günther Schmalzing‡

From the ‡Department of Molecular Pharmacology, Medical School of the Technical University of Aachen, Wendlingweg 2, D-52074 Aachen, Germany and §Department of Neurochemistry, Max Planck Institute for Brain Research, Deutschordenstrasse 46, D-60528 Frankfurt am Main, Germany

This paper describes that the correct topology of the GlyR α1 subunit depends critically on six positively charged residues within a basic cluster, RFRRKRR, located in the large cytoplasmic loop a few residues downstream to M3. The role of the basic cluster for the proper transmembrane folding has first been noticed during my work about ubiquitination of α1-GlyRs in *Xenopus laevis*. To examine the role of this cluster in detail, a large number of charge neutralization GlyR α1 mutants were subsequently created and investigated both biochemically and functionally. My contribution to this study involved the generation of most of the charge mutants as well as the entire biochemical examination of these mutants regarding their synthesis, assembly capacity, and post-translational processing in *Xenopus* oocytes.

3.2.1 Alanine substitution of basic residues of the α1-His chain downstream to M3 results in a mixed orientation of the M3-M4 loop

The starting point of this study was the analysis of two charge neutralization GlyR α1 mutants designated $^{316–320}$A-α1-His and $^{316–322,325}$A-α1-His, with either four or seven of the basic residues C terminal to M3 replaced by alanines (see Fig. 7). The two GlyR mutants did not show any differences in the shape of the glycine-induced currents or in the glycine potency compared to the wild-type GlyR α1 when analysed in *Xenopus* oocytes by two-electrode voltage-clamp electrophysiology. However, in three independent experiments, each with five to ten oocytes, the maximal current of the $^{316–320}$A-α1-His receptor was significantly reduced in amplitude, from 4.7 ±1.2 to 2.3 ±0.8 μA compared to the parent α1-His receptor.

Next the synthesis and post-translational processing of the parent α1-His GlyR and the charge neutralization mutants were compared. As in the experiments described above, the wild-type α1-His polypeptide migrated as a single band at 48 kDa when analyzed by reducing Tricine-SDS-PAGE subsequent to isolation by Ni^{2+}-NTA-agarose chromatography from [^{35}S]methionine-labeled *Xenopus* oocytes (Fig. 6*A* and *B*, *lane 1*). Endo H treatment of α1-His subunits that were isolated directly after the [^{35}S]methionine pulse led to a mass shift from 48 kDa to 45 kDa protein core. The difference of 3 kDa corresponds to the mass of a single *N*-glycan removed from ^{38}N of the sole *N*-glycosylation motif ^{38}NVS in the N-terminal extracellular domain (see Fig. 1) (Griffon et al., 1999). In contrast to the parent α1-His polypeptide, the $^{316–320}$A-α1-His and the $^{316–}$

^{322,325}A-α1-His mutants migrated as double bands of apparent masses of 48 and 54 kDa when analyzed under the same conditions (Fig. 6*A*, *lanes 2 & 3*). Endo H or PNGase F treatment of the two mutants (only shown for $^{316–320}$A-α1-His in Fig. 6*B*, *lanes 5 & 6*) resulted in mass shifts from 48 kDa and 54 kDa to the 45 kDa α1-His protein core. These data indicate that the mass difference of 6 kDa between the 48 kDa and the 54 kDa band results from additional (most probably two) N-glycans, each with a single mass of 3 kDa.

Deglycosylation at low Endo H concentrations displayed a ladder-like pattern of four bands (Fig. 6*C*, *lanes 8* and *9*) corresponding to polypeptides from which one, two, and three N-glycans had been cleaved off. The fully deglycosylated 45 kDa polypeptide was prominent at high Endo H concentrations (*lanes 10-12*).

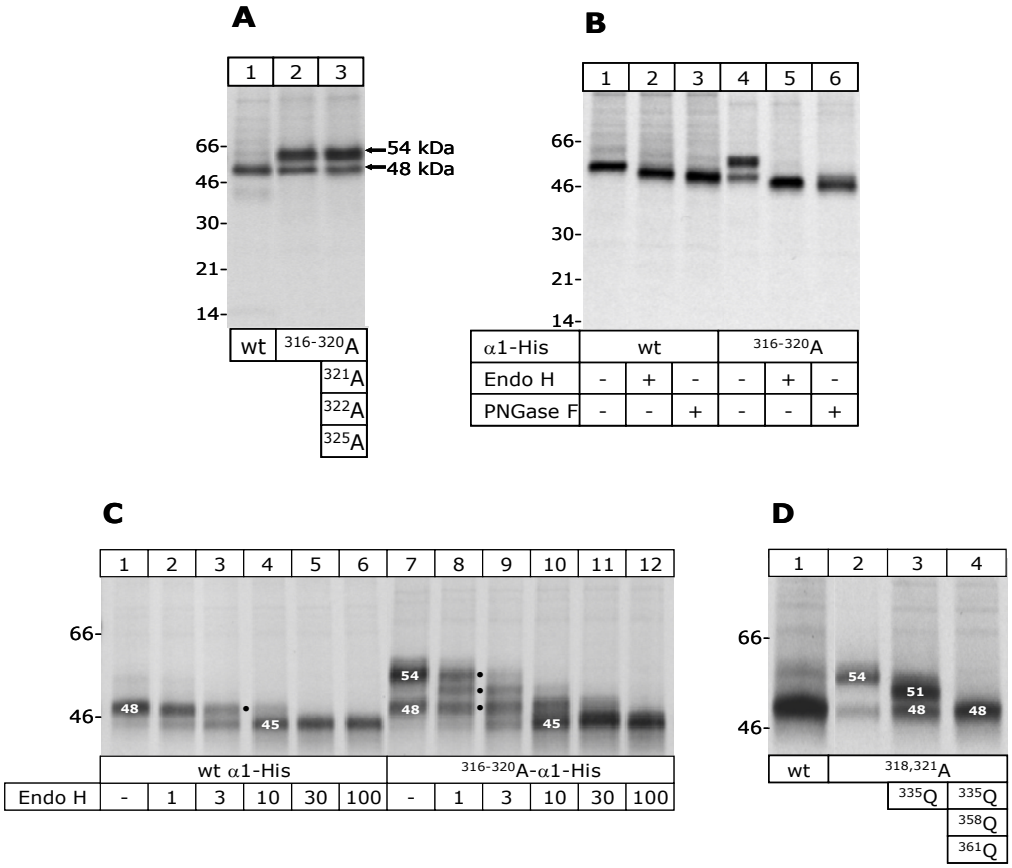

Fig. 6. *N*-Glycan status of GlyR α1-His subunits with neutralized basic charges downstream to M3. Oocytes were injected with indicated cRNAs, labeled overnight with [^{35}S]methionine, and extracted with digitonin. Proteins were natively purified by Ni^{2+}-NTA-agarose chromatography, denatured with Tricine-SDS sample buffer, and resolved by reducing Tricine-SDS-PAGE (4/10/13 % acrylamide). Autoradiographs of the gels are shown. *Panel A*, the wild-type GlyR α1-His subunit migrates as a 48 kDa polypeptide. Neutralization of positively charged amino acids leads to the appearance of an additional 54 kDa polypeptide. *Panel B*, the same samples as in *A* were denatured with reducing Tricine-SDS sample buffer and then incubated for 2 h with Endo H or PNGase F as indicated. The 54 kDa form of the $^{316–320}$A-α1-His mutant was reduced to the 45 kDa protein core by deglycosylation with Endo H or PNGase F. *Panel C*, the indicated polypeptides were incubated with increasing amounts of Endo H (in percent of maximum amount of enzyme used). *Panel D*, elimination of *N*-glycosylation sequons located in the M3-M4 loop results in mass shifts, which corroborate that the misfolded 54 kDa polypeptides carries *N*-glycans at Asn335 and Asn358 (or Asn361).

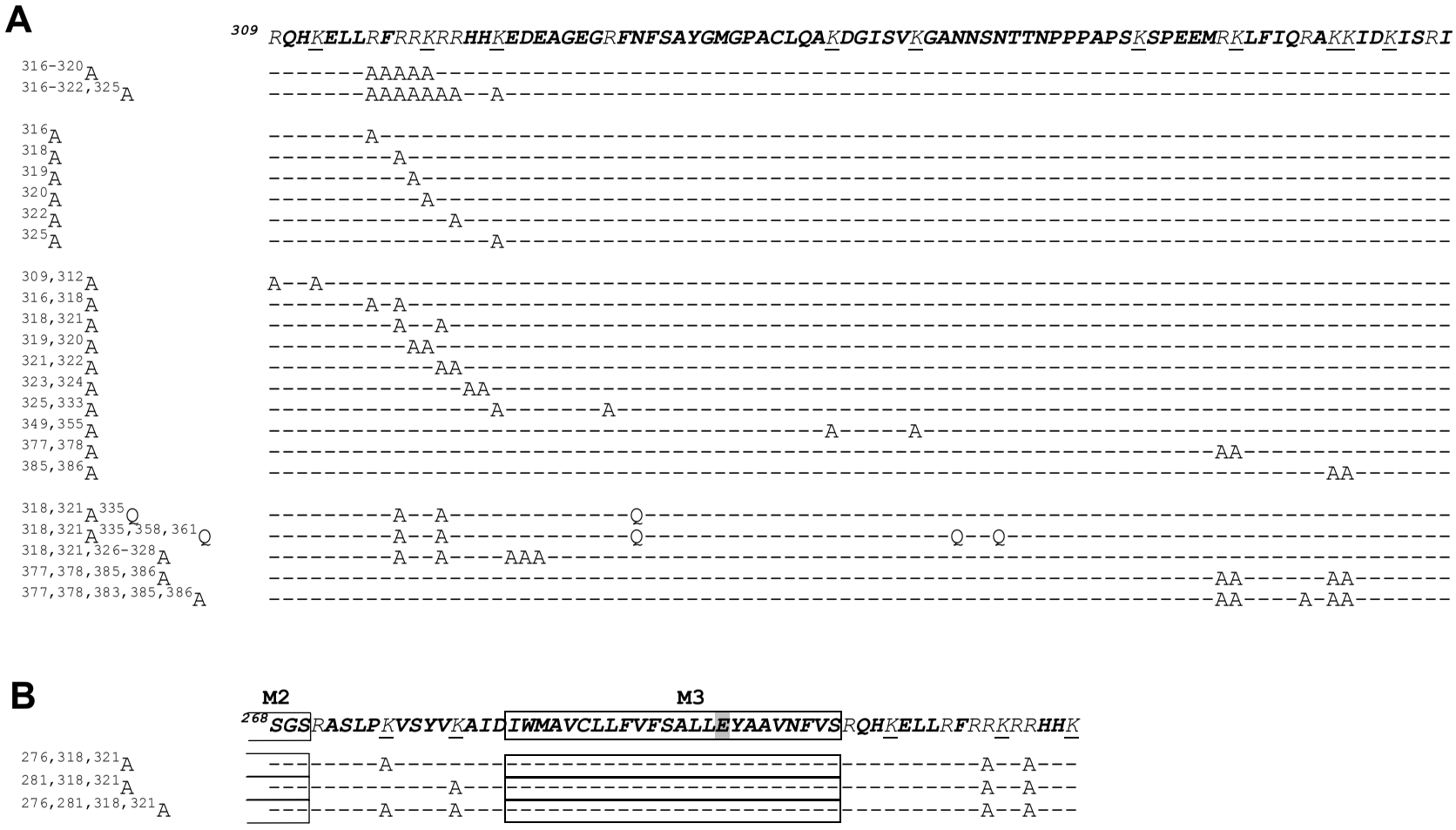

Fig. 7. Sequence of the human GlyR α1 subunit mutants created

Panel A, GlyR α1 subunit constructs carrying mutations solely in the M3-M4 loop. The entire sequence of the M3-M4 loop is shown without the flanking transmembrane segments M3 and M4. Charged residues were replaced by alanine, whereas asparagine was replaced by glutamine. *Panel B*, the amino acid sequence of the hydrophobic stretches thought to represent the transmembrane segments M3 and M4 (boxed) are shown together with the linking sequence (M2-M3 ectodomain) and the N-terminal part of the M3-M4 loop encompassing the cluster of basic residues.

Provided that the GlyR α1 subunit topology shown in Fig. 1 is correct, ^{38}NVS is the only acceptor site for *N*-linked glycosylation. This led to the conclusion that the two additional *N*-glycans must be attached to glycosylation sites that are inaccessible in the mature GlyR α1 polypeptide but, due to a different topology, accessible in the $^{316–320}$A-α1-His mutant. The GlyR α1 subunit harbors a total of four consensus *N*-glycosylation sites, three of which are located on the cytoplasmic M3-M4 loop, ^{335}NFS, ^{358}NNS, and ^{361}NTT (see Fig. 1). These motifs get accessible to the glycosylation apparatus only when the M3-M4 loop translocates into the ER lumen. Indeed, elimination of ^{335}N of the ^{318,321}A-α1-His mutant by replacement with glutamine resulted in a mass shift from 54 kDa to 51 kDa, corresponding to the loss of one N-glycan with a typical mass of 3. kDa (Fig. 6*D*, *lane 3*). When ^{358}N and ^{361}N were simultaneously eliminated in addition to ^{335}N, the 51 kDa band disappeared as well (Fig. 6*D*, *lane 4*) and only the 48 kDa band was detectable. This data indicates that the two additional *N*-glycans of the 54 kDa α1-His mutant polypeptides are located at ^{335}N and ^{358}N (or ^{361}N). The fact that only two of the three possible glycosylation sites of the endoplamatic loop are used might result from a steric hindrance at the two closely neighboring ^{358}NNS / ^{361}NTT glycosylation sequons.

These results imply that the membrane spanning segment M3 fails to integrate properly into the membrane upon neutralization of positive charges of the M3-M4 loop; as a consequence, the M3-M4 loop adopts a luminal orientation.

3.2.2 GlyRs with an aberrant topology of the M3-M4 loop have an impaired assembly capacity and are unable to leave the ER

To investigate the effect of the aberrant topology on the assembly process, several of the GlyR α1 charge neutralization mutants were analysed by blue native PAGE, a method that is well suited for displaying oligomeric states of receptor proteins (Nicke et al., 1998; Griffon et al. 1999). When purified after an overnight chase intervall, all charge neutralization mutants migrated as perfectly assembled homopentamers regardless of how many basic amino acids were neutralized

downstream to M3 (results not shown). If, however, the charge mutants were purified directly after a 4 h [^{35}S]methionine pulse, a propensity of the mutants to aggregate became apparent, as indicated by the appearance of high molecular weight α1-His protein that migrated at a broad range of masses above that of the pentameric receptor (Fig. 8*A*).

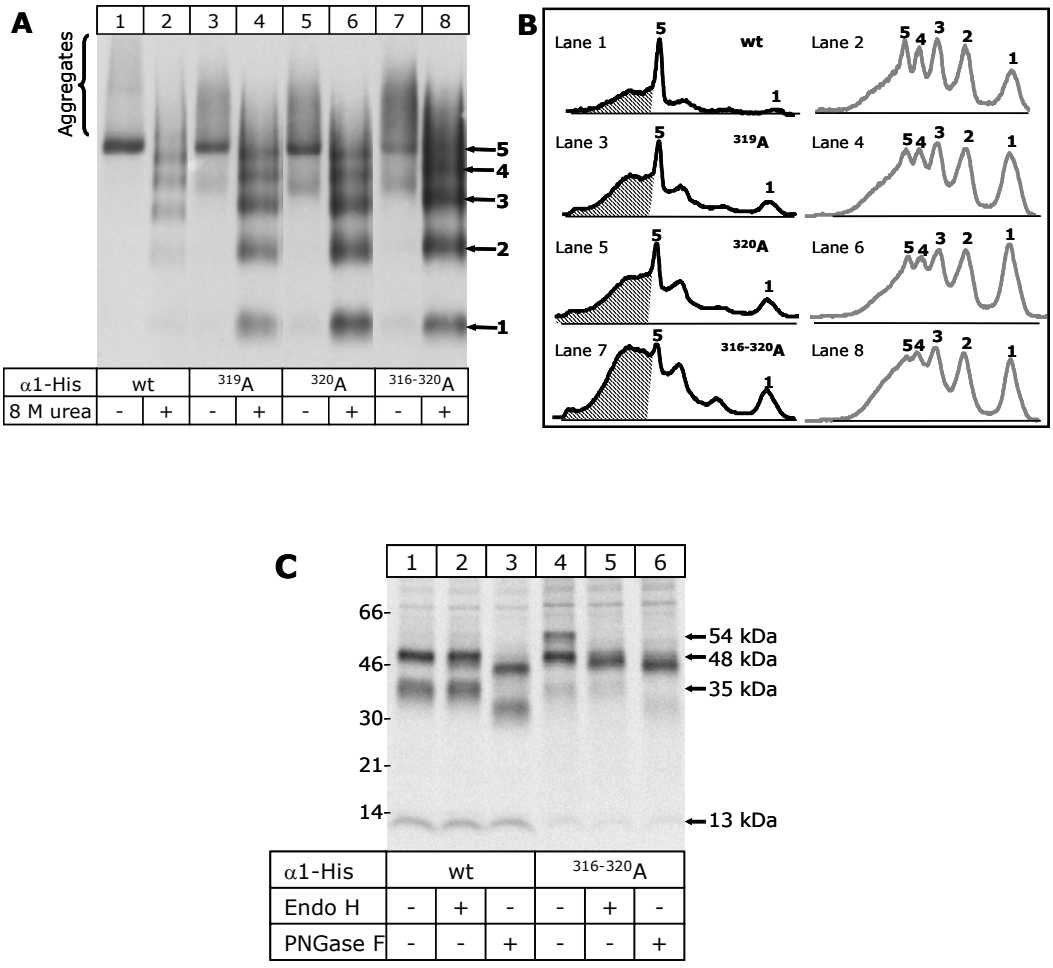

Fig. 8. Assembly and ER exit of GlyR α1-His subunits with neutralized basic charges downstream to M3.

Panel A, α1-His GlyRs natively purified from cRNA-injected oocytes immediately after a 4 h [^{35}S]methionine pulse were resolved by blue native PAGE (4–12 % acrylamide). *Panel B*, quantitative profiles of the protein bands of the *lanes* shown in *A* obtained by PhosphorImager analysis reveal an increased propensity of the α1-His mutants to aggregate (*hatched areas*). *Panel C*, α1-His GlyRs natively purified from cRNA-injected oocytes after a 4 h [^{35}S]methionine pulse and an additional 36 h chase interval were denatured with reducing Tricine-SDS sample buffer and then incubated for 2 h with Endo H or PNGase F as indicated. The monoglycosylated 48 kDa polypeptide was entirely Endo H-resistant, indicating that it had reached the Golgi apparatus. In contrast, the 54 kDa polypeptide persisted in the Endo H-sensitive form, consistent with retention in the ER.

Quantification by PhosphorImager analysis revealed that not only the charge mutants but also the wild-type GlyR α1-His subunits existed partially in an aggregated form shortly after synthesis (Fig. 8*B*). However, the tendency to form aggregates was significantly higher when one charge of the basic cluster downstream of M3 was neutralized ($R^{319}A$, $K^{320}A$; see *lanes 3* and *5*) and increased further upon neutralization of four basic charges ($RFRRK^{316–320}AFAAA$; see *lane 7*). The aggregates of both the wild-type and the mutant GlyR α1 subunits disappeared during a subsequent chase interval (Fig. 8*C, lanes 1 & 4*) and also the hyperglycosylated 54 kDa form decreased relative to the 48 kDa form with increasing chase time (unpublished data). From this we conclude that the high molecular aggregates are predominantly derived from misfolded subunits with a luminally exposed M3-M4 loop and that the hyperglycosylated form of the α1 subunit is subjected to accelerated degradation.

To examine whether α1-His GlyRs with aberrantly folded M3-M4 loop are able to leave the ER, the glycosylation status of the GlyR charge mutants after a 36 h chase interval was investigated (Fig. 8*C*). Many plasma membrane proteins exhibiting *N*-glycans become complex-glycosylated and hence resistant to Endo H during passage of the Golgi apparatus *en route* to the cell surface. As observed in previous experiments, the wild-type GlyR was entirely insensitive to Endo H treatment after a 36 h chase interval (Fig. 8*C*, *lane 2*). In contrast, the hyperglycosylated 54 kDa polypeptide generated from the $^{316–320}$A-α1-His construct was found to be completely in the Endo H sensitive form, indicating that GlyR α1 subunits with aberrantly folded M3-M4 loops are not able to leave the ER (Fig. 8*C*, *lane 5*). This view is supported by a relative decrease in the amounts of the additional 35 and 13 kDa polypeptides, which represent proteolytic cleavage products from endocytotically retrieved GlyRs and hence are indicative of the plasma membrane insertion of the receptor (Büttner et al, 2001). Quantification by PhosphorImager analysis revealed that 57 % of the wild-type α1-His subunit, but only 16 % of the $^{316–320}$A- α1-His mutant, was proteolytically cleaved into the 35 and 13 kDa products.

From these results it can be concluded that GlyRs with an aberrantly folded M3-M4 loop are not exported to the cell surface.

3.2.3. Neutralization of a single basic residue downstream to M3 is sufficient to disturb topology of the M3-M4 loop

To determine how many basic residues can be removed without disturbing membrane topology, GlyR α1 mutants with only one or two alanine substitutions in the ^{316}RFRRKRRHHK motif were generated (see. Fig. 7). Surprisingly, already the exchange of one single basic amino acid was sufficient to create a mixed topology, revealed by the appearance of the hyperglycosylated 54 kDa polypeptide (Fig. 9*A*). As observed before also a minor portion of the wild type GlyR migrated in the misfolded form (Fig. 9*A*, *lane 1*). Quantification by PhosphorImager analysis revealed that 5–10% wild-type α1 subunits possessed a luminally oriented M3-M4 loop shortly after synthesis.

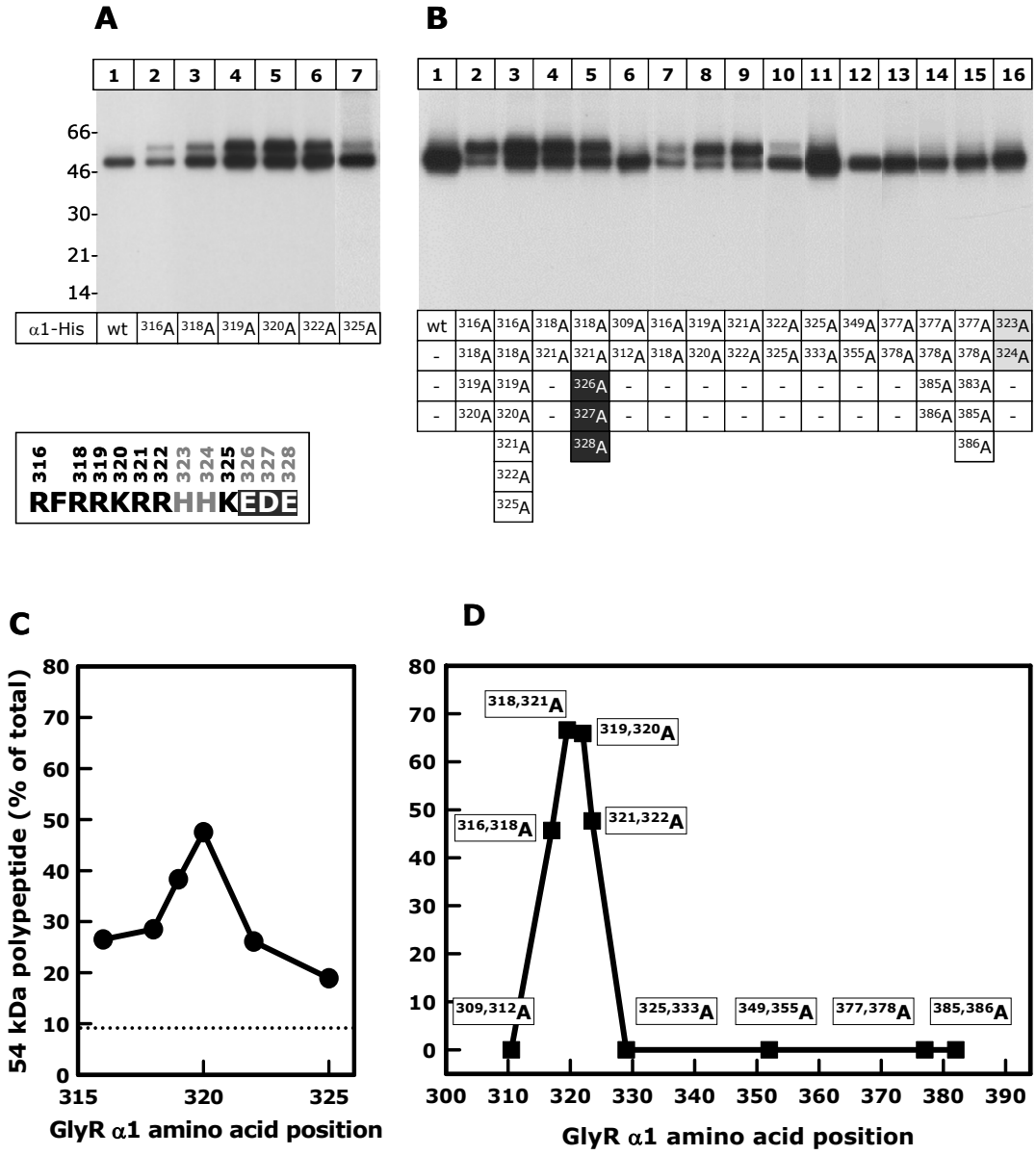

Fig. 9. Positional effects of charged residues on M3-M4 loop topology of the GlyR α1 subunit revealed by alanine scanning mutagenesis.
cRNA injected oocytes were incubated with [^{35}S]methionine for 4 h (*Panel A*) or 14 h (*Panel B*) prior to extraction with digitonin. Proteins were resolved by reducing Tricine-SDS-PAGE. Autoradiographs of the gels are shown. *Panel C* and *D*, protein bands shown in *Panel A* or *B* were quantified by PhosphorImager analysis to determine the fraction of misfolded 54kDa polypeptide of single mutants (*C*) and double mutants (*D*) as a function of the position of the neutralized basic residues. For the double mutants, the arithmetic mean of the amino acid position of the two mutations is plotted. The *dotted line* indicates the relative level of misfolded 54 kDa wild-type α1 subunit in these experiments.

3.2.4. Positional effect of basic residues on M3-M4 loop topology

To investigate a positional effect of the single charge neutralisation of the M3-M4 loop, the relative amounts of 48 kDa and 54 kDa peptides in Fig 9*A* were quantified by PhosphorImager analysis. As it can be seen from Fig. 9*C* the largest effect was found when K^{320} was substituted by alanine, which is located at a distance of ~12 residues from the end of the M3 domain (see Fig. 1). 48 % of the total mutant receptor subunits migrated in the aberrantly folded 54 kDa form directly after a 4 h [^{35}S]methionine pulse. To examine the effect of charge neutralization over the entire M3-M4 loop, a set of double mutants was generated in which two consecutive positively charged amino acids were systematically replaced by alanine (see Fig. 7). The highest relative amounts of aberrantly folded polypeptides were observed when either R^{318} and R^{321} or R^{319} and K^{320} were neutralized by alanine substitution (Fig. 9*D*), indicating that positive charges in the centre of the basic cluster are of particular importance for the topology of the M3-M4 loop. Neutralisation of more than two basic residues in this cluster as in the $^{316–322,325}$A-α1-His mutant did not further increase the relative amounts of the 54 kDa polypeptide (Fig. 9*B*, *lane 3*). Neutralization of basic residues close to M3 (Fig. 9*B*, *lane 6*) or in the C-terminal half of the M3-M4 loop (*lanes 11–14*) showed little or no effect. Even when a total of five basic amino acids in the C-terminal half of the M3-M4 loop was replaced by alanines (*lane 15*) no 54 kDa polypeptide could be observed.

To further investigate whether the net charge in this particular region is responsible for the correct topology of the M3-M4 loop, three negative charges, EDE, immediately downstream of the basic cluster at positions 326–328 were neutralized in the ^{318,321}A-α1-His mutant. As it can be seen from Fig. 9*B*, *lane 5*, this mutant, $^{318,321,326–328}$A-α1-His, still showed a mixed topology. Quantification revealed a relative decrease of the misfolded 54 kDa polypeptide from 60 % (parent ^{318,321}A-α1-His mutant) to 48% ($^{318,321,326–328}$A-α1-His mutant), indicating that increasing the net charge difference (positive charges minus negative charges) can only partially compensate for neutralization of residues within the basic cluster.

3.2.5 Neutralization of basic charges in the M2-M3 ectodomain rescues GlyR α1 mutant topology

Former studies (Gafvelin & Von Heijne, 1994) revealed that the presence of several positive charges on both sides of a transmembrane domain can prevent its correct membrane insertion. To examine whether these findings apply to the charge mutants used in this study two basic amino acids in the short hydrophilic loop connecting M2 and M3, K^{276} and K^{281}, were neutralized by alanine substitution in the ^{318,321}A-α1-His mutant (see Fig. 1 & 7). As it can be seen from Fig. 10*A* (*lanes 3 & 4)* and Fig. 10*B* neutralisation of one of these lysines in the charge mutant ^{318,321}A-α1-His resulted in clearly decreasing amounts of the 54 kDa peptide. Simultaneous neutralisation of both lysines almost fully abolished the fraction of newly synthesized ^{318,321}A-α1-His with luminal M3-M4 loop orientation. This data suggests that the basic cytoplasmic cluster C-terminal to M3 is required to counteract the three basic charges in the M2-M3 ectodomain, which otherwise impede a correct membrane insertion of M3.

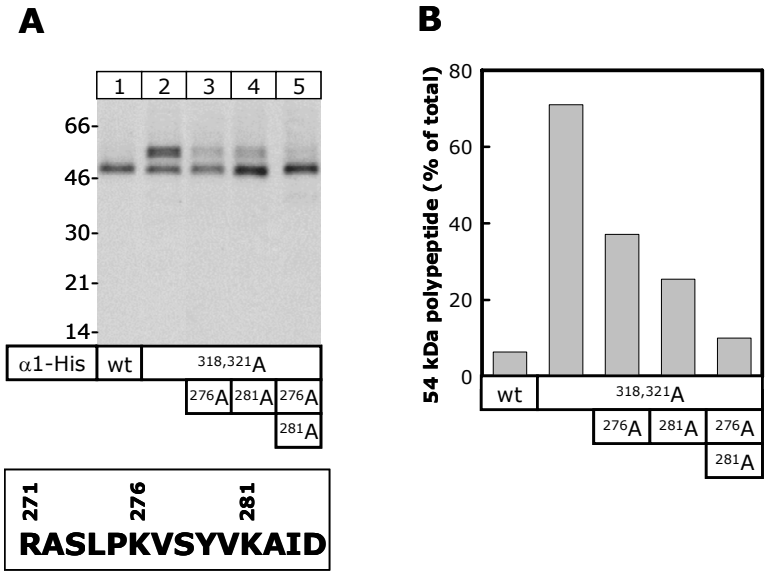

Fig. 10. Effect of simultaneous neutralization of positive charges of the M2-M3 ectodomain and the basic cluster on the disposition of the M3-M4 loop.
Panel A, cRNA-injected oocytes were pulse-labeled with [^{35}S]methionine for 4 h. Proteins were purified from digitonin extracts of these cells and resolved by reducing Tricine-SDS-PAGE. *Panel B*, the relative amount of the misfolded 54 kDa polypeptide in *A* was quantified by PhosphorImager analysis.

3.3 ASSEMBLY OF NICOTINIC α7 SUBUNITS IN *XENOPUS* OOCYTES IS PARTIALLY BLOCKED AT THE TETRAMER LEVEL

Received 5 June 2004; revised 11 August 2004; accepted 12 August 2004
Published in FEBS Letters - 24 September 2004 (Vol. 575, Issue 1, Pages 52-58)

Annette Nicke[1, 2], Heike Thurau[1], Sven Sadtler, Jürgen Rettinger[3] and Günther Schmalzing

Department of Molecular Pharmacology, Medical School of the Technical University of Aachen, Wendlingweg 2, D-52074, Aachen, German.

[1] These authors contributed equally to this work.
[2] Present address: Max Planck Institute for Brain Research, Deutschordenstrasse 46, D-60528 Frankfurt am Main, Germany.
[3] Present address: Max Planck Institute of Biophysics, Marie-Curie-Strasse 13-15, D-60439 Frankfurt am Main, Germany.

The paper describes that *Xenopus* oocytes have a limited capacity to guide the assembly of nicotinic α7 subunits. My contribution to this study was the blue native PAGE analysis of metabolically labeled α7 and $5HT_3A$ receptors as well as the examination of the glycosylation state of metabolically labeled α7 subunits.

3.3.1 Unlike $5HT_3A$ subunits, α7 subunits assemble inefficiently to homopentamers in *Xenopus* oocytes

Subsequent to isolation under non-denaturing conditions from *Xenopus* oocytes $5HT_3A$-His subunits migrated predominantly as homopentamers on the blue native PAGE gels (Fig. 11*A*, *lane 4*). Quantification by PhosphorImager analysis confirmed that $5HT_3A$-His subunits were largely incorporated in the homopentameric complex (Fig. 11*B*, *lane 4*). Treatment with 8 M urea or 0.1 % SDS to weaken non-covalent subunit interactions generated a ladder of five bands, corresponding to one, two, three, four and five copies of the $5HT_3A$-His subunit (Fig. 11*A*, *lanes 5 and 6*). These data are consistent with former studies, all indicating that the $5HT_3A$ receptor has a pentameric structure (Boess et al., 1995; Green et al., 1995). The additional protein band in the non-dissociated sample can be assigned to a minor fraction of homotrimers (Fig. 11*B*, *lane 4*). The absence of significant amounts of intermediate assembly states indicates that the $5HT_3A$Rs attained a pentameric state during or shortly after synthesis while still in the ER.

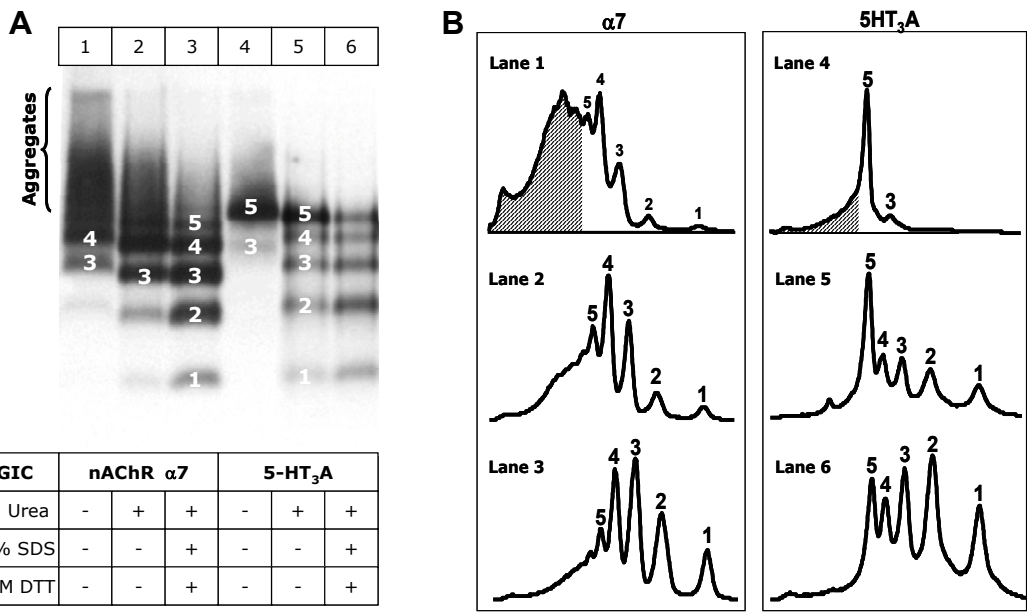

LGIC	nAChR α7			5-HT$_3$A		
8 M Urea	-	+	+	-	+	+
0.1% SDS	-	-	+	-	-	+
0.1 M DTT	-	-	+	-	-	+

Fig. 11. Assembly state of homomeric nAChR α7-His and 5HT3A-His shortly after their synthesis. *Panel A*, Xenopus oocytes were injected with cRNAs for His-tagged a subunits and non-tagged accessory subunits as indicated. After [^{35}S]methionine labeling, LGICs were natively purified from digitonin extracts of these cells. LGICs were immediately resolved by blue native PAGE either without further treatment or after a 1 h incubation at 37°C in the presence of 8 M urea, 0.1 M DTT or 0.1 % SDS as indicated. *Panel B,* quantitative profile of the radioactivity incorporated in the various homooligomers was established by PhosphorImager analysis of individual lanes of the blue native PAGE gel shown in *A*. The origin of the abscissa corresponds to the top of the blue native PAGE gel. Numbers indicate the oligomeric state of the corresponding protein bands. Hatched areas indicate aggregated protein. Lane numbers are the same as in *A*. Experiments were repeated ≥ 3 times with virtually identical results.

In contrast, the recombinant α7-His protein existed in several oligomeric states and also in an aggregated form as indicated by the high molecular mass proteins that migrated at a broad range of masses above that of the pentameric receptor (Fig. 11*A, lane 1*). Treatment either with 8 M urea alone or with 8 M urea, 0,1 % SDS and DTT induced partial dissociation of receptor complexes into lower order intermediates (Fig. 11*A, lanes 2 & 3*).

By comparison with the pattern of bands produced by dissociating treatment of the α7-His protein the discrete protein bands in *lane 1* could be assigned to homotrimers and homotetramers of the α7-His subunit. Quantification by PhosphorImager analysis revealed the presence of monomers, dimers, and pentamers besides the dominant homotetramer (Fig. 11*B*, *lane 1*). However, the quantitative profile clearly shows that the bulk part of α7-His subunits was contained in high

molecular aggregates larger than the homopentamer. These aggregates did not disappear during a subsequent 36 h chase interval (results not shown).

Virtually the same results were obtained when digitonin extracts of LGIC-expressing oocytes were subjected to sucrose density centrifugation, a method more commonly used in this respect. The similar results obtained by either method also demonstrate that blue native PAGE represents a convenient alternative for sucrose density centrifugation.

3.3.2 Solely complex-glycosylated α7 pentamers arrive at the cell surface

Further experiments mainly performed by Anette Nicke showed that the plasma membrane contained exclusively homopentameric α7 nAChRs, albeit in comparably low amounts. No α7-His tetramers or lower order complexes were observed to exist at the cell surface. Deglycosylation experiments revealed that the plasma membrane-bound α7 subunits were entirely Endo H resistant, indicating that all plasma membrane bound α7-His subunits become complex-glycosylated during passage of the Golgi apparatus *en route* to the cell surface. The fraction of complex-glycosylated α7 subunits relative to the total amount of α7 subunits synthesized appears to be very slow as only Endo H-sensitive α7 subunits could be detected when the total cellular pool of α7 subunits was analyed. Selective visualization of plasma membrane bound α7 subunits was required to detect their Endo H resistance.

3.4 TRIMERIC ARCHITECTURE OF HOMOMERIC $P2X_2$ AND HETEROMERIC $P2X_{1+2}$ RECEPTORE SUBTYPES

Received 6 April 2004; revised 25 June 2004; accepted 27 June 2004. Edited by D. Rees. Available online 28 July 2004. Published in J. Mol. Biol. (2004) 342, 333-343

Armaz Aschrafi[1], Sven Sadtler, Cristina Niculescu, Jürgen Rettinger[2] and Günther Schmalzing

Department of Molecular Pharmacology, Medical School of the Technical University of Aachen, Wendlingweg 2, D-52074, Aachen, German.

[1] *Present address:* *Department of Neurobiology, The Scripps Research Institute, 10550 North Torrey Pines Road, La Jolla, CA 92037, USA;*

[2] *Present address:* *Max Planck Institute of Biophysics, Marie-Curie-Strasse 13-15, D-60439 Frankfurt am Main, Germany.*

When I worked about the ubiquitination and membrane tethering of GlyRs, several studies on the quaternary structure of P2X receptors (LGIC class III) were in progress in the lab. All biochemical and electrophysiological data from these studies favoured the view that recombinant P2X receptors possess a trimeric architecture (Nicke et al., 1998, 1999, 2003; Rettinger et al., 2000). However, not all scientist were convinced of a trimeric structure. The present paper represents an extension of previous studies by including several additional homomeric and heteromeric P2X receptors in the analysis. My contribution to this study was the biochemical analysis of the human $P2X_2$ and $P2X_6$ subtypes.

3.4.1 Intracellular rat and human $P2X_2$ subunits exhibit distinct assembly states

Armaz Aschrafi, the main author of the paper showed that subsequent to isolation under non-denaturing conditions from *Xenopus* oocytes the His-$rP2X_2$ protein migrated on blue native PAGE predominantly in an aggregated form. The only discrete protein band detectable could be assigned to homotrimers of the His-$rP2X_2$ subunit. Higher order assembly states could also be detected with recombinant $rP2X_1$, $rP2X_3$, $rP2X_4$ and $rP2X_5$ receptors, but trimers represented the predominant assembly state of these P2X subtypes, indicating that the formation of large amounts of undefined aggregates was unique to $rP2X_2$ subunits. Deglycosylation experiments with Endo H and PNGase F revealed that ~70 % of metabolically labeled $rP2X_2$ subunits acquired Endo H resistance during an extended chase interval. Accordingly, the high amounts of $rP2X_2$ aggregates could not be assigned to ER retention.

Because of the exceptional assembly-behaviour of the $rP2X_2$ protein, its human orthologue was investigated in the same manner. In contrast to $rP2X_2$ subunits, $hP2X_2$ subunits migrated under virtually identical conditions in a single defined assembly state, which could be clearly assigned to a trimer.

3.4.2 $rP2X_2$ receptors exist as individual homotrimers and clusters of homotrimers at the plasma membrane

To visualize selectively the plasma membrane-bound $rP2X_2$ receptors, the outer cell surface of oocytes was radioiodinated with ^{125}I-sulfo-SHPP. In contrast to the His-$rP2X_1$ receptor that migrated in a single defined assembly state, the His-$rP2X_2$ receptor existed at the cell surface in several defined oligomers. These oligomers migrated in a ladder-like pattern of three or four bands, each spaced by the mass of a His-$rP2X_2$ trimer. Accordingly, hexameric and nonameric states can be assigned to the higher mass oligomers. Thus, $rP2X_2$ receptors appear as homotrimers or multimers of homotrimers at the plasma membrane, whereas their intracellular assembly state remained undefined by blue native PAGE.

To determine the quaternary structure of the $rP2X_2$ receptor at the cell surface of intact *Xenopus* oocytes by a second, independent approach, plasma membrane-bound receptors were chemical cross-linked prior to purification. The autoradiogram of the reducing SDS-PAGE gel displayed the formation of an increasing amount of adducts in expense of the monomer at different stages of the cross-linking reaction. Three different bands with molecular weight ~65, ~130, and ~190 kDa could be distinguished corresponding in mass to the $rP2X_2$ monomer, dimer and trimer. Since no bands larger than the 190 kDa band could be detected, these findings add further strong support to the view that functional $rP2X_2$ receptors are organized as homotrimers.

3.4.3 Polymerization of $rP2X_2$ and $rP2X_1$ subunits generates $rP2X_{1+2}$ heterotrimers

Since $P2X_2$ subunits have not only been shown to build stable homotrimers, but also to heteropolymerize with $P2X_1$ (Brown et al., 2002) and $P2X_3$ subunits (Lewis et al., 1995; Chen et al., 1995), the question arose whether a trimeric architecture can also be assigned to heteromultimeric P2X receptors. Therefore, oocytes co-expressing the hexahistidyltagged $rP2X_1$ subunit with the non-tagged $rP2X_2$ subunit were surface

radioiodinated with [^{125}I]sulfo-SHPP. The receptors isolated from oocytes co-expressing rP2X$_2$ and His-rP2X$_1$ subunits migrated on blue native PAGE gels in between that of homotrimeric His-rP2X$_1$ receptors and homotrimeric His-rP2X$_2$ receptors, consistent with the formation of heterotrimeric rP2X$_{1+2}$ receptors. Interestingly, no homomeric His-rP2X$_1$ receptors could be isolated from those oocytes which were co-expressing rP2X$_2$ and His-rP2X$_1$ subunits, indicating that heteromer formation represents the favored assembly pathway. Reanalysis of the rP2X$_{1+2}$ receptor intermediate in the second dimension by SDS-PAGE corroborated this view by resolving two bands of ~57 kDa and ~62 kDa as expected for His-rP2X$_1$ and rP2X$_2$ monomers, respectively. These results clearly indicate that rP2X$_{1+2}$ have a trimeric architecture. Also, the results of cross-linking experiments were fully consistent with the view that rP2X$_{1+2}$ receptors are organized as trimers.

3.4.4 hP2X$_6$ subunits form tetramers and aggregates that are not exported to the plasma membrane of *Xenopus* oocytes

P2X$_6$ subunits represent the sole P2X subtype that is unable to form functional homomeric receptors in *Xenopus* oocytes (North, R.A., 2002; Collo et al., 1996). However, co-expression with P2X$_4$ subunits results in the generation of heteromeric, functional ATP receptors (Le et al., 1998). Subsequent to isolation under non-denaturing conditions from *Xenopus* oocytes the His-hP2X$_6$ protein migrated on the blue native PAGE gel in a single distinct assembly state as well as in an aggregated form as indicated by the high molecular mass proteins (Fig. 12*A*, *lane 3*). Treatment with 8 M urea (*lane 4*) induced partial dissociation of receptor complexes into lower order intermediates, each spaced by the mass of an hP2X$_6$ monomer. By comparison with the pattern of bands produced by dissociating treatment of the His-hP2X$_6$ protein the discrete protein band in Fig. 12*A*, *lane 3* could be assigned to homotetramer of the His-hP2X$_6$ subunit. The coanalyzed rP2X$_3$ receptor and the α1 GlyR migrated as trimers (*lanes 1 & 2*) and pentamers (*lanes 5 & 6*), respectively. Deglycosylation experiments revealed that the metabolically lebeled hP2X$_6$ subunit was completely Endo H-sensitive after an extended chase interval (Fig. 12*B*).

Attempts to visualize selectively plasma membrane-bound homomeric $hP2X_6$ receptors failed, although other homomeric P2X receptors that were expressed in parallel showed high surface expression levels (results not shown). Together, these findings indicate that the tetrameric $hP2X_6$ complex is recognized and retained in the ER by the quality control machinery as an incorrectly assembled protein. Tetramers and aggregates were also observed for the rat orthologue, $rP2X_6$ (results not shown).

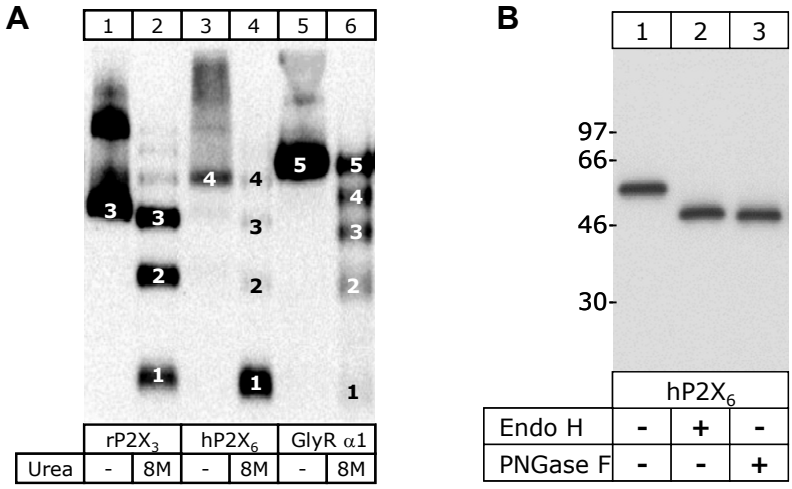

Fig. 12. $hP2X_6$ subunits form aggregates and homotetramers in Xenopus oocytes.
Panel A, metabolically labelled GlyR α1 subunits and $rP2X_3$ subunits, both known to form functional homomeric receptors, migrated as pentamers and trimers, respectively, on the blue native PAGE gel. In contrast, $hP2X_6$ subunits known for their inability to form a functional homomeric receptor in *Xenopus* oocytes, migrated as tetramers and aggregate. *Panel B*, N-glycan content of $hP2X_6$ subunits. The same samples as in *A* were deglycosylated as indicated and resolved by SDS-PAGE. The observed shift, from 56 to 48 kDa (49 kDa calculated protein core), is consistent with the presence of three N-glycans, suggesting that all three consensus sites (^{155}NGT, ^{185}NFT, ^{200}NFS) were used. No complex-glycosylated bands were observed.

4. Discussion

4.1 Ubiquitination of the α1 GlyR: A targeting signal for internalization and lysosomal degradation?

The results presented here strongly indicate that ubiquitination of the recombinant human α1 GlyR at the plasma membrane of *Xenopus* oocytes is involved in receptor internalisation and degradation. Ubiquitination of the human α1 GlyR has been demonstrated by radio-iodination of plasma membrane-bound α1 GlyRs, whose subunits differed in molecular weight by additional 7, 14 or 21 kDa, corresponding to the molecular weights of one, two and three conjugated ubiquitin molecules, respectively, and by co-isolation of the non-tagged human α1 GlyR through hexahistidyl-tagged ubiquitin. Ubiquitin conjugated GlyRs where prominent at the plasma membrane, but could be hardly detected in total cell homogenates, indicating that ubiquitination takes place exclusively at the plasma membrane and not during intracellular routing of the receptor.

After ubiqitination at the plasma membrane the receptor was internalized and proteolytically cleaved into an *N*-terminal 35 kDa and C-terminal 13 kDa fragment. Since α1 GlyR homopentamers could be isolated from cell homogenates even after cleavage, nicking does not cause a dissociation of the α1 subunits (Büttner et al., 2001). This observation is consistent with former studies showing that the critical determinants of assembly are located on the extracellular N-terminal domain of the α1 subunit (Kuhse et al., 1993). A similar importance of extracellular domains for receptor assembly has been demonstrated for $GABA_A$Rs and $GABA_C$Rs (Hackam et al., 1997) as well as for the muscle nAChR (Verrall & Hall, 1992). Moreover, when proteolytically nicked by papain, the nAChR neither shows a tendency to disassemble nor a loss of function. Even extensive proteolysis had no dramatic effect on sedimentation characteristics, toxin binding, the doughnut-like appearance in transmission electron microscopy, or cation channel function (Lindstrom et al., 1980; Huganir & Racker, 1980). By analogy, the nicked α1 GlyR might still function as glycine-gated Cl^--channel, but apparently it is not localized in the plasma membrane.

Altogether, the results presented here place the human α1 GlyR into a class of mammalian membrane proteins, that are ubiquitinated at the cell surface, internalized and routed to lysosomal or lysosomal-like vacuolar degradation (Bonifacino & Weissman, 1998).

On one hand these observations agree with former findings showing hat ubiquitination at the plasma membrane constitutes a general internalisation signal, thus regulating the amount of receptor proteins at the cell surface (Hicke, 1999; Bonifacino & Weissman, 1998). On the other hand, ubiquitination is well known to regulate the degradation of short lived cytosolic proteins by the 26S proteasome (Hershko & Ciechanover, 1998). In addition, ubiquitination followed by proteasomal destruction provides for degradation of many luminal and transmembrane ER proteins that, when abnormally folded or incompletely assembled, are translocated back into the cytosol (Bonifacino & Weissman, 1998). By analogy the results presented here could be interpreted as a cellular reaction to downregulate high amounts of α1 GlyR caused by overexpression. However, several results argue against this view. First, after heterologous expression in *Xenopus* oocytes α1 subunits assembled properly and with high efficiency into functional α1 GlyR homopentamers, as revealed by blue native PAGE and two-electrode voltage clamp. In addition, α1 GlyR homopentamers were translocated efficiently to the Golgi apparatus, as judged from the rapid and complete acquisition of complex-type carbohydrates. Second, compared to abnormally folded or incompletely assembled proteins, which have in general very short half-lifes of less than 1 h, the homo-pentameric α1 GlyR is metabolically stable and shows a half-life in the range of days. Third, the ubiquitinated α1 subunits are contained within the assembled homopentameric α1 GlyR and carry complex-type carbohydrate chains indicative of a localization in the Golgi or later compartments. Moreover, ubiquitination of the α1 subunits seems to be topologically restricted to the plasma membrane, as revealed by surface-labeling experiments. Finally, the proteasome system, which is involved in the degradation of many short lived cytosolic proteins, does not play a role in the degradation process observed here as the proteasome inhibitor lactacystin did not inhibit α1-His cleavage. In contrast, cleavage appears to be mediated by lysosomal serine proteases as phenylmethylsulfonyl fluoride blocked processing almost as efficiently as did NH_4Cl.

The suggestion that ubiquitination of GlyRs serves as a signal for internalisation agrees well with the finding that ubiquitinated GlyR carried only one to three ubiquitin molecules per α1 subunit. While modification by a single ubiquitin molecule or by multiple single ubiquitins on multiple distinct lysine residues is not sufficient to serve as a proteasomal targeting signal (recognition by the proteasome requires branched multiubiquitin chains containing at least four copies of ubiquitin; Thrower et al, 2000), monoubiquitination has been shown to be sufficient for internalisation of the yeast maltose transporter (Lucero et al., 2000) and Ste2p, a yeast G-protein-coupled receptor (Terrell et al., 1998). Monoubiquitin has also been shown to promote endocytosis of an alpha-factor receptor-ubiquitin chimeric protein in the absence of any other internalization signals (Shih et al., 2000). Moreover, cell-surface receptor tyrosine kinases (RTKs) are monoubiquitinated at multiple sites following ligand stimulation (Haglund et al., 2003; Mosesson et al., 2003). Since termination of RTK signaling occurs via endocytosis and lysosomal degradation, (Dikic & Giordano, 2003) monoubiquitination may act as internalization signal, routing the receptor to the lysosome for degradation.

Therefore, it can be assumed that multiple lysine residues within the large cytoplasmic loop of the α1 subunit (Fig. 1) are monoubiquitinated rather than that a single lysine residue carries a branched multiubiquitin chain and that the ubiquitination reactions identified here serve exclusively in labeling GlyRs for removal from the plasma membrane.

4.2 Potential roles of receptor ubiquitination in synaptic development and remodelling

Ubiquitination of the GlyR and related LGICs may play a role in the regulation of receptor abundance at developing and adult synapses by initiating endocytosis and lysosomal degradation. At the developing muscle, extrasynaptic nAChRs in the non-innervated sarcolemmal membrane have been shown to be rapidly internalized, whereas synaptic nAChRs become metabolically stable upon further development of

the neuromuscular junction (Sanes & Lichtman, 1999). In contrast, during withdrawal of nerve terminals from the motor endplate, the postsynaptic membrane is depleted of nAChRs before there is any obvious loss of membrane in the overlying motor nerve ending (Balice-Gordon & Lichtman, 1993). An early loss of postsynaptic nAChRs can also be observed during synapse elimination in reinnervated adult muscles (Rich & Lichtman, 1989). Notably, an identical distribution of ubiquitin and nAChRs in postsynaptic membranes of neuromuscular junctions has been demonstrated (Serdaroglu et al., 1992) as well as a rise in cytosolic ubiquitin in a comparable early stage of response to axonal injury (De Stefano et al., 1998). Altogether, these findings support the view that ubiquitination constitutes an important labeling reaction for enhanced receptor internalization and/or degradation.

It is tempting to assume that ubiquitination plays a role in activity-dependent regulation of synaptical LGICs. A decrease in AMPA receptor abundance at synaptic sites by synaptic activity has been shown to accompany long term depression in the cerebellum (Wang & Linden, 2000; Matsuda et al., 2000) and in hippocampal neurons (Man et al., 2000). Recent studies revealed that AMPA receptors (GLR-1) of C. elegans are ubiquitinated at synapses. When ubiquitination of GLR-1 was experimentally decreased, the amount of GLR-1 at synapses increased and the locomotion behaviour was altered in a manner that is consistent with increased synaptic strength. Overexpression of ubiquitin led to a decrease of GLR-1 at synapses as well as to a decrease in density of GLR-1-containing synapses (Burbea et al., 2002). By analogy, ubiquitination may play a similar role at glycinergic synapses. Ubiquitin conjugation to homopentameric GlyRs expressed in Xenopus oocytes has been presented here. Embryonic GlyRs that were electrically blocked by the selective antagonist strychnine have been shown to be routed rapidly to an endosomal compartment by a yet unidentified pathway, consistent with an inactivity-dependent internalisation (Kirsch & Betz, 1998).

Ubiquitination may also be involved in the receptor isoform switches during development, e.g. the postnatal replacement of the embryonic γ-subunit by the adult ε-subunit in the nAChR of neuromuscular junctions. Comparable isoform switches occur also with glutamate, $GABA_A$, and glycine receptors in the developing central nervous system (for references, see Missias et al., 1997).

A possible consequence of ubiquitin additions to LGIC subunits may be the disruption of protein-protein interactions at the synapse, e.g. the interaction between LGICs with their anchoring proteins. The reduction of synaptic AMPA receptor numbers seen upon induction of long term depression in cerebellar neurons is thought to involve release from the postsynaptic anchoring protein GRIP and subsequent clathrin-dependent endocytosis (Matsuda et al., 2000; Xia et al., 2000). Also GlyRs bind with their β-subunit to a receptor-anchoring protein named gephyrin. This interaction is thought to be crucial for a stable, postsynaptic localization of the receptor (Kneussel & Betz, 2000; Kneussel et al., 1999b; Kirsch et al., 1996). Recruitment of an E3 ligase[3] to one or several α1-subunits within an $\alpha 1_3\beta_2$ heteropentameric GlyR (Langosch et al., 1988) may sterically affect GlyR-gephyrin interactions and even result in ubiquitination of one or several of the 13 lysine residues within the large cytoplasmic loop of a neighbouring β-subunit. Conceivably, such modification might interfere with GlyR anchoring to postsynaptic gephyrin and thus facilitate receptor internalization by endocytosis. Conversely, immobilization of plasma membrane-bound heteromeric GlyRs on a preassembled gephyrin scaffold (Kneussel & Betz, 2000; Sola et al., 2001) could protect receptors against ubiquitination and thus stabilize the postsynaptic receptor pool at the synapse (Changeux & Danchin, 1976). Similar interactions may also occur with $GABA_A$Rs which are also anchored by gephyrin at postsynaptic sites. In cultured hippocampal neurons from gephyrin-deficient mice synaptic $GABA_A$R clusters were absent and intracellular immunoreactivities of $GABA_A$R subunits were found to be strikingly increased compared with wild-type cells (Kneussel et al., 1999a).

In conclusion, all presently available data can be reconciled with the view that ubiquitination of plasma membrane LGICs constitutes an important signal in targeting receptors to intracellular compartments for proteolytic degradation. One may speculate that receptor-protein interactions regulate receptor turnover by affecting ubiquitination reactions directly at the synapse. Such an idea is supported by the observation that multiple membrane proteins of unknown identity are conjugated with ubiquitin in brain synaptic membranes and postsynaptic densities, indicating that ubiquitination of membrane proteins is a widespread phenomenon in the mammalian brain (Chapman et al., 1994).

[3] E3 ligases transfer ubiquitin to the target protein and are the last group of enzymes in a row of three, that are involved in the ubiquitination process

4.3 Ubiquitination and ^{339}Y are involved in the internalization of the α1 GlyR

Ubiquitination of the α1 GlyR at the plasma membrane was no longer detectable when the ten lysine residues of the cytoplasmic loop between transmembrane segments M3 and M4 were replaced by arginines. Despite this proteolytic cleavage continued to take place at the same extent as with the wild type α1 GlyR, suggesting that removal of GlyRs from the plasma membrane and routing to lysosomes for degradation were not dependent on ubiquitination. Also replacing a tyrosine in position 339, which was speculated to be part of an additional endocytosis motif, did not lead to a significant reduction of cleavage of the GlyR α1 subunits. However, a mutant lacking both, ubiquitination sites and ^{339}Y, was significantly less processed. These results may suggest that the GlyR α1 subunit harbors at least two endocytosis motifs, which may act independently to regulate the density of α1 GlyR. Apparently, each of the two signals may be capable of compensating entirely the loss of the other. Such redundant regulation systems are often found at critical points of metabolic pathways and may serve to prevent a fast collapse of cell function in case of a single metabolic disturbance.

4.4 Functional importance of the basic cluster for correct GlyR subunit topogenesis

According to the classic model of membrane integration of polytopic proteins, the hydrophobic M3 region of the α1 GlyR subunit should follow the lead of the preceding transmembrane segment, M2. Because M2 has an N_{cyt}-C_{exo} orientation, M3 should adopt passively the opposite N_{exo}-C_{cyt} orientation, thus acting as a stop-transfer sequence that halts further translocation of the polypeptide chain across the membrane. In contrast, the data presented here clearly demonstrates that the correct orientation of M3 critically depends on the presence of a cluster of basic amino acids, ^{316}RXRRKRR, directly downstream of the M3 transmembrane segment. Between 30 and 80 % of newly synthesizes α1 GlyR subunits M3 failed to integrate into the membrane when at least one basic residue of this cluster was substituted by

a neutral amino acid, indicating that this basic cluster directly downstream to M3 plays a crucial role in proper membrane integration of α1 GlyR subunits. A similar role of positively charged residues in halting translocation of a hydrophobic segment has been described previously (Kuroiwa et al., 1991).

In general, there is growing evidence for polytopic proteins that topologic information is not restricted to the most N-terminal transmembrane domain but spread over the entire polypeptide chain (Goder & Spiess, 2001). One of the determinants is apparently the transmembrane distribution of positive charges, which prevents not only the translocation of N- and C-terminal segments (Zhang et al. 1995), but also of connecting loops of polytopic membrane proteins. (Sato & Mueckler, 1999) demonstrated that positive charges, present at equivalent positions within two different cytoplasmic loops of the glucose transporter Glut1 form critical anchoring points. In addition, internal loops of polytopic membrane proteins have on average a higher content of positively charged residues as compared with external ones (Gafvelin et al., 1997).

Nevertheless, the high percentage of α1 GlyR subunits that failed to integrate properly into the membrane after neutralization of only a single positive residue within the basic cluster was still unexpected, because seven positively charged residues are still left within the 15 residues flanking the C-terminal end of the hydrophobic M3 region. With respect to the charge difference rule this means a surplus of 6 positively charged residues C-terminal and of 2 positively charged residues N-terminal of M3, resulting in a net charge difference Δ(C-N) of +4 for the single charge neutralization mutants. This should be more than sufficient to dictate a N_{exo}-C_{cyt} orientation of a signal anchor sequence. However, despite this excess of positive charges only a minor fraction of the M3 segment adopted the correct N_{exo}-C_{cyt} orientation and most of the M3-M4 loops were translocated incorrectly. In addition, the α1 GlyR subunit harbors a total of 20 positively charged amino acids but only 9 negatively charged residues over the entire M3-M4 loop. With respect to the positive inside rule the excess of 11 positive charges should clearly induce the correct N_{exo}-C_{cyt} orientation of M3.

Taken together neither the charge difference rule nor the positive inside rule are consistent to a biased topology of the apolar M3 domain subsequent to neutralization of one or several positively charged residue. This suggests that the M3 segment by itself is unable to reliably halt translocation.

4.5 Positive charges on the short M2-M3 ectodomain seem to impair the stop-transfer function of the apolar M3 segment

Hydropathy analysis of the M3 domain by the Kyte-Doolittle algorithm with a window of five amino acids provided no indication for an impaired membrane integration. The observation that a proper integration of the M3 domain can be restored in the charge mutants when positive charges on the short M2-M3 loop are neutralized led to the conclusion that these positive charges N-terminal to M3 impose a problem for a proper membrane integration of M3. The three positive charged amino acids of the short M2-M3 loop may impose constraints to the M3 segment to adopt an N_{cyt}-C_{exo} orientation, which is obviously incompatible with the N_{cyt}-C_{exo} orientation of the preceding M2 domain. Therefore, the M3 domain may remain in an unstable state until the cluster of basic residues downstream M3 serves as a stop transfer sequence and constrains M3 into the correct N_{exo}-C_{cyt} orientation. The extreme sensitivity of the M3 transmembrane orientation to neutralization of single basic residues within the ^{316}RXRRKRR sequence suggests that the particular high density of positive charges is essential for keeping the M3-M4 loop on the cis-side of the membrane. After the correct N_{exo}-C_{cyt} insertion additional interactions with the lipid bilayer or integral proteins may stabilize the adopted topology.

Interestingly, positive charges appear to be more easily translocated through the ER than through bacterial membranes, most likely because of the absence of a membrane potential in the ER (Gafvelin et al., 1997). The results presented here imply that basic clusters play an important role in these translocation processes. This view is supported by the finding that basic charged motifs in cytoplasmic loops occur more frequently near cytoplasmic membrane surface than expected from computer-based predictions of the Arg/Lys frequency (Juretic et al., 2002). It is likely that topogenic basic clusters act through electrostatic interactions with negative charges of lipids or proteins (or both). Anionic phospholipids have been shown to interact electrostatically with lysine and arginine residues of membrane proteins in prokaryotes, thus stabilizing protein topology (van Klompenburg et al., 1997; Gallusser & Kuhn, 1990; Bogdanov et al., 2002). A potential role for phospholipids in conformational stabilization of GlyR subunits is also supported by early findings, showing that successful solubilization of the GlyR but not of the nicotinic acetylcholine receptor critically depends on the presence of exogenous

phospholipids (Pfeiffer & Betz 1981). Whether the topogenic basic cluster identified here contributes to phospholipid stabilization of GlyR structure by ensuring its proper topology remains to be determined.

4.6 Incomplete assembly of α7 subunits in *Xenopus* oocytes

Although many non-neuron-derived cells fail to express functional nAChRs at the cell surface when transiently transfected with α7 subunits, *Xenopus* oocytes were always considered as an established exception of this rule. Accordingly, oocytes served frequently in the analysis of electrophysiological and pharmacological properties of the homomeric α7 nAChR. In contrast, the data presented here clearly demonstrates that only a minor fraction of intracellular α7 subunits assemble properly to homopentamers in *Xenopus* oocytes. Blue native PAGE analysis and deglycosylation experiments with Endo H and PNGase F revealed that a large portion of α7 subunits exists as homotetramers and aggregates which remain trapped in the ER in the high-mannose form. Only a limited fraction of the totally synthesized α7 subunits polymerizes properly to homopentamers and acquires complex-type carbohydrates in the Golgi apparatus *en route* to the plasma membrane. Incomplete homopolymerization in *Xenopus* oocytes is neither found with homooligomeric $5HT_3A$ subunits (presented here) nor GlyRα1 subunits (Griffon et al., 1999; Büttner et al., 2001; Sadtler et al., 2003). Since the small amount of $5HT_3A$ homotrimers that was observable directly after the [^{35}S]methionine pulse disappeared completely during a subsequent chase period (data not shown), a trimeric architecture can be considered as transient assembly state of homopentameric $5HT_3ARs$. In contrast, the relative amounts of α7 tetramers and aggregates persisted during the chase interval, suggesting that a significant percentage of the α7 subunits was permanently misfolded and misassembled.

4.7 *N*-Glycan status of α7 nAChRs in Xenopus oocytes

Deglycosylation experiments with Endo H and PNGase F revealed that the small fraction of homopentameric α7 nAChRs that reached the cell surface harbors exclusively Endo H resistant, complex-type carbohydrates. This result was unexpected, since previous studies always showed α7 subunits to carry solely high-mannose type carbohydrates, irrespective of whether they were isolated from native tissue, i.e., brain, or from host cells such as *Xenopus* oocytes or COS cells (Chen et al., 1998). Most likely, the detection of complex-type carbohydrates requires the selective visualization of the plasma membrane-bound α7 nAChR by surface radioiodination. Since complex-glycosylated α7 subunits at the cell surface constitute only a minor fraction of the total α7 subunit pool, it may be impossible to detect this fraction in lysates of metabolically labeled oocytes. Hence, it is likely that small amounts of complex-glycosylated α7 subunits remained undetected in previous studies, in which the plasma membrane-bound nAChRs were not selectively labeled.

4.8 Incompletely assembled α7 nAChRs are retained by the quality control system in *Xenopus* oocytes

The mechanisms that account for the low abundance of functional homopentameric α7 nAChRs at the cell surface of transiently transfected cells are cell type specific. While tsA201 cells of a human kidney epithelial cell line route α7 subunits properly, but in a non-functional form to the cell surface (Rakhilin et al., 1999), COS cells produce properly folded and assembled α7 nAChRs, which remain located in an intracellular pool because they lack trafficking motifs needed for distribution to the plasma membrane (Dineley & Patrick, 2000). The data presented here suggests that large parts of newly synthesized α7 subunits do not assemble properly in *Xenopus* oocytes and are retained in the ER by the ER quality control system (Hurtley & Helenius 1989). A similar mechanism appears to be responsible for the low surface expression of functional α7 nAChRs in HEK293 and fibroblast QT6 cells.

Like *Xenopus* oocytes, these cells produce the α7 protein, but largely fail to assemble it properly (Kassner & Berg, 1997). The need for structural subunits such as homologous subunits, splice variants or folding isomers as well as the absence of specific helper proteins could explain the limited capacity of α7 subunits to polymerize. One such helper protein, RIC-3, has recently been identified to be involved in functional maturation of nAChRs in Caenorhabditis elegans (Halevi et al., 2002).

In summary, the data presented here show that *Xenopus* oocytes efficiently synthesize nicotinic α7 subunits, but do not have the capacity to guide the polymerization of α7 subunits with the same efficiency as other LGIC subunits. Thus, the limited number of functional α7 nAChRs observed at the cell surface can be assigned to inefficient pentameric assembly rather than on inefficient routing of fully assembled α7 receptors. Efficient α7 nAChR formation in *Xenopus* oocytes apparently needs co-assembly with other nAChR subunit isoforms such as β2 (Khiroug et al., 2002) and β3 subunits (Jones et al., 1999) or support from cell type-specific chaperones that guide the assembly process.

4.9 Tetrameric *versus* trimeric organization of P2X Receptors

Although evidence for a trimeric assembly of P2X receptors is accumulating, the architecture of this LGIC class is still under debate. (Kim et al., 1997) demonstrated that refolding of the bacterially expressed extracellular domain of the $P2X_2$ subunit results in the formation of stable tetramers. However, an important cave to these experiments is that multimerization of full length $P2X_2$ subunits is determined by the second transmembrane domain, and not by the extracellular loop (Torres et al., 1999). Further support to the tetramer hypothesis was lent by kinetic data. The inactivation rate of the $P2X_2$ receptor in excised patches has been shown to increase with a Hill coefficient of 4, suggesting that the functional channel has at least four Ca^{2+} binding sites (North, R.A., 2002). However, as mentioned by the author, these data can also be reconciled with other stoichiometries if multiple Ca^{2+} binding sites are present per subunit.

In contrast, the results presented here clearly argue against a tetrameric organization and support the trimer hypothesis. All P2X subtypes that form functional homomeric receptors in *Xenopus* oocytes showed a trimeric aritechture when isolated and analysed under non-denaturating conditions. Tetrameric assemblies were only observed upon expression of $P2X_6$ subunits, which are known for their incapability to form as functional homomeric receptors in *Xenopus* oocytes (North, R.A., 2002). Their complete absence at the cell surface and their sensitivity to Endo H indicates that both $P2X_6$ aggregates and tetramers are recognized and permanently retained by the ER quality control system as incorrectly assembled proteins. This lends indirect support to the view that tetramers are not a functional oligomeric state of P2X receptors. In addition to the results presented here all other functional studies reported so far are in essence consistent with a trimeric channel. Experiments conducted before P2X receptors were cloned suggested that ATP-gated ion channels must bind ATP to each of three identical, non-interacting binding sites to open the channel. (Bean, B.P., 1992). Later single channel studies with recombinant $rP2X_2$ receptors supported this view by determining a Hill coefficient of 2.3 for the opening probability in response to ATP (Ding & Sachs 1999). Also when low agonist concentrations were used to minimize the contribution of cooperative interactions of subunits, initial slopes of 2.5 and 2.7 were derived for homooligomeric $rP2X_2$ and $rP2X_3$ receptors, consistent with three identical, independent binding sites (Jiang et al., 2003). Although these results cannot exclude the existence of more than three ATP binding sites, the data fit best with a model in which the channel proceeds through three ATP binding steps before opening.

Also experiments with concatenated P2X subunit cDNAs argue for a trimeric subunit organisation. Contiguous copies of the $rP2X_2$ subunit carrying a functional reporter mutation could not be inhibited by a cysteine-reactive compound if the reporter mutation was introduced into the fourth copy, indicating that not four but maximally three subunits actively participate in channel formation (Stoop et al., 1999).

In a more biochemically oriented study with concatamers of up to six $rP2X_1$ subunits in series, significant problems were encountered in the interpretation of the electrophysiological data arising from the production of minute levels of lower order by-products such as monomers and dimers (Nicke et al., 2003). These by-products combined to functional multimers equal in mass to the homotrimeric $rP2X_1$ receptor assembled from $rP2X_1$ monomers. Because multimers consisting of more than three

$rP2X_1$ monomers were not observed to appear in the plasma membrane, these results provide additional support for a trimeric architecture of $rP2X_1$ receptors.

The assessment of the oligomeric organization of $rP2X_2$ receptors was unexpectedly complicated by an undefined intracellular assembly state that was not observed with any other P2X receptor. Since blue native PAGE analyses of radio-iodinated oocytes and cross-linking experiments revealed that all plasma membrane-bound $rP2X_2$ receptors exist in a defined assembly state of homotrimers or multiples thereof, it is likely that the amorphous mass observed with metabolically labelled oocytes consists predominantly of those multiples of $rP2X_2$-homotrimers. This view is supported by the finding that a large majority of $rP2X_2$ subunits were insensitive to Endo H, indicating that they were not retained in the ER by the quality control system. Interestingly, $hP2X_2$ subunits do not show a similar amorphous migration on blue native PAGE gels, but migrate in their intracellular form solely as homotrimers. As sequence variability between human and rat $P2X_2$ subunits is almost confined to the C-terminal cytoplasmic domain, this observation points to a role of the long C-terminal tail for the unusual migration of $rP2X_2$ receptors.

Similar (heteromeric) P2X subunits also formed trimers, as shown for co-expressed $P2X_1$ and $P2X_2$ subunits, which assembled efficiently to a $P2X_{1+2}$ receptor that was exported to the plasma membrane. It has recently been suggested that a trimeric $P2X_{2+3}$ receptor would have the composition $P2X_2(P2X_3)_2$ (Jiang et al., 2003). For the heterotrimeric $P2X_{1+2}$ receptor, SDS-PAGE gels indicate that significantly more radioactivity corresponds to the co-isolated non-tagged $P2X_2$ subunits than to His-$P2X_1$ subunits. Assuming that both subunits become labelled by [^{125}I]sulfo-SHPP with similar efficiency, this observation favours the view that the trimeric $P2X_{1+2}$ receptor incorporates one $P2X_1$ subunit and two $P2X_2$ subunits. Surprisingly, the assembly of $P2X_1$ and $P2X_2$ subunits to heteromeric $P2X_{1+2}$ receptors seems to be favoured over an assembly of $P2X_1$ subunits to a homomeric $P2X_1$ receptor. Since $P2X_1$ and $P2X_2$ subunits co-exist in a variety of tissues (Brown et al., 2002) the efficient formation of heteromeric $P2X_{1+2}$ receptors raises the intriguing possibility that ATP-gated currents attributed to homotrimeric $P2X_1$ receptors may at least in some native tissues be mediated by $P2X_{1+2}$ heterotrimers.

4.10 Higher order interactions of plasma membrane-bound homotrimeric $rP2X_2$ receptors: a possible structural basis of coupled gating

The existence as multiples of homotrimers at the plasma membrane was unique to the $rP2X_2$ receptor in the experiments presented here. In previous studies a propensity to form hexamers has been demonstrated for $rP2X_1$ and $rP2X_3$ subunits if n-octylglucoside was used instead of digitonin as detergent for receptor solubilization (Nicke et al., 1998). Accordingly, the clusters of homotrimeric $rP2X_2$ receptors may be considered to form as artefacts similar to the $rP2X_1$ hexamers produced by n-octylglucoside in our previous study. An intriguing alternative possibility, however, comes from a kinetic study showing that multiple $rP2X_2$ receptors in a patch do not open and close independent of each other as expected for individual receptors, but are functionally coupled and partially synchronized (Ding & Sachs, 2002). Cooperative effects resulting from homomeric channel interactions have been demonstrated for a variety of ion channels including nAChRs (Keleshian et al., 2000; Schindler et al., 1984), K^+ channels (Tytgat & Hess, 1992), and Ca^{2+} release channels on the sarcoplasmic reticulum membrane (Marx et al., 2001). Thus, the physical association between $rP2X_2$ homotrimers observed here could well represent the structural basis for the coupled gating behavior, leading to a synchronized opening of neighboring $rP2X_2$ receptors.

5. Deutsche Zusammenfassung

5.1 Der Internalisierung und Proteolyse des GlyRs geht eine Ubiquitinierung an der Zelloberfläche voraus[4]

Der inhibitorische Glycin-Rezeptor (GlyR) gehört zur Superfamilie der pentameren Ligand-gesteuerten Ionenkanäle (LGIC), zu der auch der nikotinische Acetylcholin-Rezeptor (nAChR), die γ-Aminobuttersäure-Rezeptoren ($GABA_AR$ und $GABA_CR$) und der 5-Hydroxytryptamin-Rezeptor-Typ-3 ($5HT_3R$) gerechnet werden. Als postsynaptischer Chloridkanal vermittelt der GlyR in Säugetieren die schnelle Reizweiterleitung an inhibitorischen Synapsen des Zentralnervensystems und des Rückenmarks. In Vertebraten konnten vier verschiedene α-Untereinheiten (α1-α4), die an der Ligandbindung beteiligt sind und eine strukturgebende β-Untereinheit identifiziert werden, die sowohl zu αβ-Heteropentameren als auch zu funktionellen α-Homopentameren assemblieren. Die vier verschiedenen α-Untereinheiten und die ß-Untereinheit haben einen ähnlichen strukturellen Aufbau (vgl. Fig. 1).

Der 200 Aminosäuren zählende N-Terminus umfasst ein Signalpeptid, das die wachsende Peptidkette in das Endoplasmatische Retikulum dirigiert, sowie eine 15 Aminosäuren große Cysteinschleife. Im Endoplasmatischen Retikulum findet bei α1-, α3- und α4-Untereinheiten eine N-Glykosylierung an einem, im Falle der α2- und β-Untereinheit an zwei Glykosylierungsmotiven statt. An den N-Terminus schließen sich vier Transmembrandomänen, M1 bis M4 an. Während M1 und M2 sowie M2 und M3 durch eine lediglich kurze hydrophile Sequenz getrennt sind, befindet sich zwischen M3 und M4 eine ca. 83 Aminosäuren zählende, große cytoplasmatische Domäne, die Gegenstand eines Großteils meiner Untersuchungen war und die im Folgenden als „M3-M4-Schleife“ bezeichnet wird.

Die postsynaptische Dichte Liganden-gesteuerter Ionenkanäle hat einen entscheidenden Einfluss auf die Effizienz der synaptischen Reizweiterleitung. Für nAChRs beispielsweise konnten multiple Mechanismen aufgezeigt werden, die die

[4]Büttner, C., **Sadtler, S**., Leyendecker, A., Laube, B., Griffon, N., Betz, H., Schmalzing, G. (2001) Ubiquitination precedes internalization and proteolytic cleavage of plasma membrane-bound glycine receptors. J Biol Chem. **276**, 42978-42985.

synaptische Verteilung und Dichte der Rezeptoren in der Plasmamembran steuern. Vor diesem Hintergrund wurden die Internalisierung- und Degradations-mechanismen homopentamerer α1-GlyRs näher untersucht.

Die Ergebnisse dieser Studie sowie weiterführende, bisher unveröffentlichter Experimente zeigen, dass die α1-Untereinheit des GlyRs in ihrer cytoplasmatischen Schleife zwischen M3 und M4 (mindestens) zwei verschiedene Internalisierungs- und/oder Degradationsmotive besitzt. Hierbei handelt es sich um zehn Lysinreste, die als Konjugationspunkte für (vermutlich) einzelne Ubiquitinmoleküle dienen, sowie ein als Teil eines Internalisierungsmotives fungierendes Tyrosin in Position 339. Beide Motive sind imstande, den Verlust des jeweils anderen vollständig zu kompensieren. Nach der Ubiquitinierung des GlyRs an der Plasmamembran erfolgt dessen Internalisierung in endosomale Kompartimente und von dort eine Weiter-leitung in die Lysosomen, in denen α1-Untereinheiten in zwei Fragmente von 35 und 13 kDa gespalten werden. Das Proteasom-System scheint an dieser Spaltung nicht beteiligt zu sein. Nachdem inzwischen auch für den AMPA-Rezeptor eine für dessen Internalisierung kritische Ubiquitinierung an Synapsen gezeigt werden konnte (Burbea et al., 2002), könnte Ubiquitinierung einen generellen Internalisierungs-mechanismus für Ligand-gesteuerte Ionenkanäle darstellen.

5.2 Ein basisches Aminosäure-Cluster bestimmt die Topologie der cytoplasmatischen M3-M4-Schleife des α1-GlyRs[5]

Nach dem klassischen Modell der Topogenese von Membranproteinen wird die Gesamt-Topologie eines Proteins von der Orientierung der Signalsequenz bestimmt, die die Einschleusung der Polypeptidkette über die ER-Membran initiiert. Die weiter C-terminal gelegenen hydrophoben Domänen dienen ausschließlich als Stop-Transfer und Ankersequenzen, welche die wachsende Polypeptidkette dazu veranlassen, passiv dem vorangehenden Transmembransegment zu folgen, so dass auf diese Weise die typische Zick-Zack-Faltung polytoper Membraneproteine entsteht.

[5]**Sadtler, S.**, Laube, B., Lashub, A., Nicke, A., Betz, H., Schmalzing G. (2003) A basic cluster determines topology of the cytoplasmic M3-M4 loop of the glycine receptor α1 subunit. J Biol Chem. **278**, 16782-16790.

Obwohl die Topologie vieler Proteine dem klassischen Modell folgt, gibt es zunehmend Hinweise, dass die korrekte Topologie von die Membran mehrfach durchspannenden Proteinen nicht allein von der Orientierung der ersten Transmembrandomäne, sondern auch von verschiedenen, weiter C-terminal gelegenen topogenen Informationen abhängt.

Die hier beschriebene Studie belegt, daß eine Ansammlung sechs basischer Aminosäuren, RFRRKRR, unmittelbar C-terminal der dritten Transmembrandomäne gelegen, entscheidenden Einfluss auf die Topologie der GlyR-α1-Untereinheit hat. Der Austausch einer oder mehrerer basischer Aminosäuren dieses *Clusters* gegen ungeladene Aminosäuren, nicht aber der Austausch anderer basischer Aminosäuren der M3-M4-Schleife, führte zu einer anormalen Faltung der M3-M4-Schleife in das ER-Lumen. Um zu untersuchen, ob die Netto-Ladung für die falsche Ausrichtung der dritten Transmembrandomäne verantwortlich war, wurden in einer Mutante mit zwei neutralisierten basischen Aminosäuren drei dem basischen *Cluster* benachbart gelegene, negativ geladene Aminosäuren durch Alanine ersetzt. Auch wenn ein leichter Rückgang der Menge an inkorrekt gefalteten α1-Untereinheiten beobachtet werden konnte, lagen immer noch knapp 50% des Proteins mit einer ins ER-Lumen gerichteten M3-M4-Schleife vor. Die Falschfaltung konnte jedoch verhindert werden, wenn neben in einer Mutante mit zwei neutralisierten basischen Aminosäuren gleichzeitig zwei der drei basischen Aminosäuren der zwischen M2 und M3 liegenden Ectodomäne neutralisiert wurden.

Diese Ergebnisse zeigen, dass das basische *Cluster* C-terminal von M3 ein kritisches topogenes Motiv für die GlyR-α1-Untereinheit darstellt. Die inkorrekte Faltung der cytoplasmatischen M3-M4-Schleife bei den erstellten α1-Mutanten lässt sich nicht durch das klassische Topogenese-Modell erklären. Nach der „*positiv-inside*“ Regel wäre bei Substitution einer der basischen Aminosäuren des *Clusters* immer noch ein deutlicher Überschuss von vier positiven Aminosäuren auf der C-terminalen Seite von M3 zu verbuchen. Die erhebliche Ladungsdifferenz sollte somit für die korrekte N_{exo}-C_{cyt}-Orientierung von M3 ausreichen. Vermutlich stellt das basische *Cluster* ein für die korrekte Topogenese notwendiges Gegenstück zu den zwei positiv-geladenen Aminosäuren N-terminal von M3 dar, welche ansonsten eine zuverlässige Inkorporation von M3 in die Membran verhindern würden.

5.3 Der Assemblierungsvorgang der nikotinischen α7 Untereinheit in *Xenopus*-Oozyten ist auf der Tetramer-Ebene partiell blockiert[6]

Eines der am intensivsten studierten Mitglieder der *Cys-loop*-Superfamilie Ligand-gesteuerter Ionenkanäle ist der Kationen-selektive nAChR. Wie GlyRs weisen nAChRs eine pentamere Struktur auf. Der am besten charakterisierte nAChR befindet sich an der neuromuskulären Endplatte, setzt sich aus vier homologen Genprodukten zusammen und besitzt die Stöchiometrie $(\alpha 1)_2\beta 1\gamma\delta$ (fetal) bzw. $(\alpha 1_2)\beta 1\varepsilon\delta$ (erwachsen). Insgesamt sind bei Säugern neun Gene, die α-Untereinheiten kodieren (α1-α7, α9 und α10) und vier Gene, die β-Untereinheiten kodieren (β1-β4) bekannt.

Obwohl die meisten nicht-neuronalen Zelllinien Schwierigkeiten haben, α7-Untereinheiten nach einer transienten Transfektion zu funktionellen homopentameren nAChRs zu assemblieren, galten *Xenopus*-Oozyten als etablierte Ausnahme. Verschiedene Veröffentlichungen beschreiben, dass *Xenopus*-Oozyten nach einer Expression von α7- und α9-Untereinheiten funktionelle homopentamere Rezeptoren ausbilden. Die Ergebnisse der hier vorgestellten Studie zeigen jedoch, dass nur ein geringer Teil der in *Xenopus*-Oozyten exprimierten α7-Untereinheiten zu funktionellen homopentameren Rezeptoren assembliert. Der weitaus größte Teil an α7-Untereinheiten assembliert unvollständig zu Tetrameren oder bildet hochmolekulare Aggregate, die nicht imstande sind, das ER zu verlassen. Vermutlich ist die limitierte Assemblierungskapazität in *Xenopus*-Oozyten auf das Fehlen von spezifischen Helferproteinen oder aber auf die Unfähigkeit, strukturell notwendige Faltungsisomere zu bilden, zurückzuführen. Die Ergebnisse von Deglykosylierungs-Experimenten lassen zudem auf eine Zurückhaltung unvollständig assemblierter α7-Untereinheiten im ER durch das ER-Qualitätskontrollsystem schließen. Da eine große Zahl der unvollständig assemblierten α7-Untereinheiten in Form von Tetrameren vorlag, scheint vor allem der Einbau einer fünften α7-Untereinheit zum entstehenden Rezeptorkomplex in Oozyten ein Problem darzustellen.

---

[6]Nicke, A., Thurau, H., **Sadtler, S.**, Rettinger, J., Schmalzing, G. (2004) Assembly of nicotinic α7 subunits in *Xenopus* oocytes is partially blocked at the tetramer level. FEBS Lett. 2004 Sep 24;575(1-3):52-8.

5.4 Homomere $P2X_2$- und heteromere $P2X_{1+2}$-Rezeptoren weisen eine trimere Architektur auf[7]

Auf der Basis ihrer Aminosäuresequenz und Faltung durch die Plasmamembran werden LGICs in drei große Gruppen eingeteilt: Die zuvor beschriebene nAChR-Superfamilie (Klasse I), die Kationen-selektive Glutamatrezeptor-Familie, zu der AMPA-, NMDA- und Kainatrezeptoren gerechnet werden (Klasse II) und die Familie ATP-gesteuerter P2X-Rezeptoren (Klasse III). Während die Architektur der Klasse I und II LGICs aufgeklärt zu sein scheint, wurde die der Klasse III LGICs zu Beginn meiner Dissertation noch kontrovers diskutiert. Obwohl oberflächliche Ähnlichkeiten mit K^+-Kanälen eher für eine tetramere Organisation von P2X-Rezeptoren sprachen, belegten biochemischen Ergebnisse der eignen Arbeitsgruppe eindeutig eine trimere Architektur für homomere $P2X_1$- und $P2X_3$-Rezeptoren.

Vor diesem Hintergrund wurde das Assemblierungsverhalten verschiedener P2X-Rezeptoren sorgfältig mit verschiedenen biochemischen Methoden re-evaluiert. Im Fokus der Untersuchungen standen der homomere $P2X_2$- sowie der heteromere $P2X_{1+2}$-Rezeptor. Auch das Assemblierungsverhalten von $P2X_6$-Untereinheiten, die bekanntermaßen nicht im Stande sind, in *Xenopus*-Oozyten funktionelle Rezeptoren zu bilden, wurde untersucht. Alle in der hier vorgestellten Studie gewonnenen Ergebnisse untermauern die Vorstellung, dass P2X-Rezeptoren an der Zelloberfläche aus drei nicht-kovalent gebundenen Untereinheiten bestehen. Sowohl für die schnell desensibilisierenden $rP2X_1$- und $rP2X_3$-Rezeptoren, als auch für die langsam desensibilisierenden $rP2X_2$-, $rP2X_4$- und $rP2X_5$-Rezeptoren wurden trimere Assemblierungszustände an der Zelloberfläche beobachtet.

Ein außergewöhnliches Assemblierungsverhalten konnte bei metabolischer Markierung für $rP2X_2$-Untereinheiten beobachtet werden. Im Gegensatz zu allen anderen untersuchten P2X-Rezeptoren lagen diese intrazellulär nur zu einem geringen Prozentsatz als Trimere vor. Der weitaus größte Teil assemblierte zu hochmolekulare Aggregaten. Deglykosylierungsexperimente zeigten jedoch, dass die Bildung dieser hochmolekularen Aggregate nicht an eine Zurückhaltung im ER gekoppelt war. Ca. 70% der metabolisch markierten $rP2X_2$-Untereinheiten hatten nach einem verlängerten Chase-Intervall das ER verlassen. Interessanterweise zeigte

[7]Aschrafi, A., **Sadtler, S.**, Niculescu, C., Rettinger, J., Schmalzing, G. (2004) Trimeric Architecture of Homomeric $P2X_2$ and Heteromeric $P2X_{1+2}$ Receptor Subtypes. J Mol Biol. 2004 Sep 3;342(1):333-43.

das humane Ortholog kein solches Verhalten. Unter identischen Versuchsbedingungen konnten beim $hP2X_2$-Rezeptor ausschließlich perfekt assemblierte Homotrimere beobachtet werden. Da der $rP2X_2$-Rezeptor an der Plasmamembran ausschließlich als Homotrimer vorlag, bleibt als einzige Erklärung, dass $rP2X_2$-Rezeptoren auch im ER Homotrimere sind, diese Struktur jedoch aufgrund zusätzlicher (unbekannter) Protein-Protein-Interaktionen bei der blauen nativen PAGE-Analyse maskiert ist.

$hP2X_6$-Untereinheiten wurden intrazellulär, erwartungsgemäß jedoch nicht an der Zelloberfläche nachgewiesen. Im blauen nativen PAGE-Gel wanderten sie in Form von hochmolekularen Aggregaten sowie als Tetramere. Deglykosylierungsexperimente zeigten, dass die isolierten $hP2X_6$-Untereinheiten selbst nach einem verlängerten Chase-Intervall vollständig Endo H sensibel waren. Diese Ergebnisse sprechen dafür, dass tetramere $P2X_6$-Komplexe und $P2X_6$-Aggregate vom ER-Qualitätskontrollsystem als inkorrekt assemblierte Protein erkannt und im ER zurückgehalten werden.

References

Akaaboune, M., Culican, S.M., Turney, G., Lichtman, J.W. (1999).
Rapid and reversible effects of activity on acetylcholine receptor density at the neuromuscular junction in vivo.
Science **286**, 503-507.

Anand, R., Peng, X., Lindstrom, J. (1993).
Homomeric and native α7 acetylcholine receptors exhibit remarkably similar but non-identical pharmacological properties, suggesting that the native receptor is a heteromeric protein complex.
FEBS Lett. **327**, 241-246.

Andersson, H., Bakker, E., von Heijne, G. (1992).
Different positively charged amino acids have similar effects on the topology of a polytopic transmembrane protein in *Escherichia coli*.
J. Biol. Chem. **267**, 1491-1495.

Andersson, H., von Heijne, G. (1994).
Membrane protein topology: effects of $\Delta\mu H^+$ on the translocation of charged residues explain the 'positive inside' rule.
EMBO J. **13**, 2267-2272.

Andrews, D.W., Young, J.C., Mirels, L.F., Czarnota, G.J. (1992).
The role of the N region in signal sequence and signal-anchor function.
J. Biol. Chem. **267**, 7761-7769.

Balice-Gordon, R.J., Lichtman, J.W. (1993).
In vivo observations of pre- and postsynaptic changes during the transition from multiple to single innervation at developing neuromuscular junctions.
J. Neurosci. **13**, 834-855.

Bean, B.P. (1992).
Pharmacology and electrophysiology of ATP-activated ion channels.
Trends Pharmacol. Sci. **13**, 87-90.

Beltzer, J.P., Fiedler, K., Fuhrer, C., Geffen, I., Handschin, C., Wessels, H.P., Spiess, M. (1991).
Charged residues are major determinants of the transmembrane orientation of a signal-anchor sequence.
J. Biol. Chem. **266**, 973-978.

Blobel, G. (1980).
Intracellular protein topogenesis.
Proc. Natl. Acad. Sci. U S A. **77**, 1496-1500.

Blumenthal, E.M., Conroy, W.G., Romano, S.J., Kassner, P.D., Berg, D.K. (1997).
Detection of functional nicotinic receptors blocked by α-bungarotoxin on PC12 cells and dependence of their expression on post-translational events.
J. Neurosci. **17**, 6094-6104.

Bo, X., Zhang, Y., Nassar, M., Burnstock, G., Schoepfer, R. (1995).
A P2X purinoceptor cDNA conferring a novel pharmacological profile.
FEBS Lett. **375**, 129-133.

Bodin, P., Burnstock, G. (2001).
Purinergic signalling: ATP release.
Neurochem. Res. **26**, 959-969.

Boess, F.G., Beroukhim, R., Martin, I.L. (1995).
Ultrastructure of the 5-hydroxytryptamine3 receptor.
J. Neurochem. **64**, 1401-1405.

Bogdanov, M., Heacock, P.N., Dowhan, W. (2002).
A polytopic membrane protein displays a reversible topology dependent on membrane lipid composition.
EMBO J. **21**, 2107-2116.

Bonifacino, J.S., Weissman, A.M. (1998).
Ubiquitin and the control of protein fate in the secretory and endocytic pathways.
Annu. Rev. Cell Dev. Biol. **14**, 19-57.

Brake, A.J., Wagenbach, M.J., Julius, D. (1994).
New structural motif for ligand-gated ion channels defined by an ionotropic ATP receptor.
Nature **371**, 519-523.

Brown, S.G., Townsend-Nicholson, A., Jacobson, K.A., Burnstock, G., King, B.F. (2002).
Heteromultimeric P2X(1/2) receptors show a novel sensitivity to extracellular pH.
J. Pharmacol. Exp. Ther. **300**, 673-680.

Buell, G., Lewis, C., Collo, G., North, R.A., Surprenant, A. (1996).
An antagonist-insensitive P2X receptor expressed in epithelia and brain.
EMBO J. **15**, 55-62.

Burbea, M., Dreier, L., Dittman, J.S., Grünwald, M.E., Kaplan, J.M. (2002).
Ubiquitin and AP180 regulate the abundance of GLR-1 glutamate receptors at postsynaptic elements in *C. elegans*.
Neuron **35**, 107-120.

Büttner, C., Sadtler, S., Leyendecker, A., Laube, B., Griffon, N., Betz, H., Schmalzing, G. (2001).
Ubiquitination precedes internalization and proteolytic cleavage of plasma membrane-bound glycine receptors.
J. Biol. Chem. **276**, 42978-42985.

Changeux, J.P., Danchin, A. (1976).
Selective stabilisation of developing synapses as a mechanism for the specification of neuronal networks.
Nature **264**, 705-712.

Chapman, A.P., Smith, S.J., Rider, C.C., Beesley, P.W. (1994).
Multiple ubiquitin conjugates are present in rat brain synaptic membranes and postsynaptic densities.
Neurosci. Lett. **168**, 238-342.

Chen, C.C., Akopian, A.N., Sivilotti, L., Colquhoun, D., Burnstock, G., Wood, J.N. (1995).
A P2X purinoceptor expressed by a subset of sensory neurons.
Nature **377**, 428-431.

Chen, D., Dang, H., Patrick, J.W. (1998).
Contributions of N-linked glycosylation to the expression of a functional α7-nicotinic receptor in Xenopus oocytes.
J. Neurochem. **70**, 349-357.

Chen, D., Patrick, J.W. (1997).
The α-bungarotoxin-binding nicotinic acetylcholine receptor from rat brain contains only the α7 subunit.
J. Biol. Chem. **272**, 24024-24029.

Colledge, M., Froehner, S.C. (1998).
Signals mediating ion channel clustering at the neuromuscular junction.
Curr. Opin. Neurobiol. **8**, 357-363.

Collo, G., North, R.A., Kawashima, E., Merlo-Pich, E., Neidhart, S., Surprenant, A., Buell, G. (1996).
Cloning of $P2X_5$ and $P2X_6$ receptors and the distribution and properties of an extended family of ATP-gated ion channels.
J. Neurosci. **16**, 2495-2507.

Cooper, S.T., Millar, N.S. (1997).
Host cell-specific folding and assembly of the neuronal nicotinic acetylcholine receptor α7 subunit.
J. Neurochem. **68**, 2140-2151.

Couturier, S., Bertrand, D., Matter, J.M., Hernandez, M.C., Bertrand, S., Millar, N., Valera, S., Barkas, T., Ballivet, M. (1990).
A neuronal nicotinic acetylcholine receptor subunit (α7) is developmentally regulated and forms a homo-oligomeric channel blocked by α-BTX.
Neuron **5**, 847-856.

De Stefano, M.E., Squitti, R., Toschi, G. (1998).
The rise in cytoplasmic ubiquitin levels is an early step in the response of parasympathetic ganglionic neurons to axonal injury followed by regeneration.
J. Neuropathol. Exp. Neurol. **57**, 1000-1012.

Dikic, I., Giordano, S. (2003).
Negative receptor signalling.
Curr. Opin. Cell Biol. **15**, 128-135.

Dineley, K.T., Patrick, J.W. (2000).
Amino acid determinants of α7 nicotinic acetylcholine receptor surface expression.
J. Biol. Chem. **275**, 13974-13985.

Ding, S., Sachs, F. (2000).
Inactivation of P2X2 purinoceptors by divalent cations.
J. Physiol. **522**, 199-214.

Ding, S., Sachs, F. (1999).
Single channel properties of $P2X_2$ purinoceptors.
J. Gen. Physiol. **113**, 695-720.

Ding, S., Sachs, F. (2002).
Evidence for non-independent gating of $P2X_2$ receptors expressed in Xenopus oocytes.
BMC Neurosci. **3**, 17.

Dingledine, R., Borges, K., Bowie, D., Traynelis, S.F. (1999).
The glutamate receptor ion channels.
Pharmacol. Rev. **51**, 7-61.

Drisdel, R.C., Green, W.N. (2000).
Neuronal α-bungarotoxin receptors are α7 subunit homomers.
J. Neurosci. **20**, 133-139.

Gafvelin, G., Sakaguchi, M., Andersson, H., von Heijne, G. (1997).
Topological rules for membrane protein assembly in eukaryotic cells.
J. Biol. Chem. 272, 6119-6127.

Gafvelin, G., von Heijne, G. (1994).
Topological "frustration" in multispanning E. coli inner membrane proteins.
Cell **77**, 401-412.

Gallusser, A., Kuhn, A. (1990).
Initial steps in protein membrane insertion. Bacteriophage M13 procoat protein binds to the membrane surface by electrostatic interaction.
EMBO J. **9**, 2723-2729.

Gloor, S., Pongs, O., Schmalzing G. (1995).
A vector for the synthesis of cRNAs encoding Myc epitope-tagged proteins in Xenopus laevis oocytes.
Gene **160**, 213-217.

Goder, V., Bieri, C., Spiess, M. (1999).
Glycosylation can influence topogenesis of membrane proteins and reveals dynamic reorientation of nascent polypeptides within the translocon.
J. Cell Biol. **147**, 257-266.

Goder, V., Spiess, M. (2001).
Topogenesis of membrane proteins: determinants and dynamics.
FEBS Lett. **504**, 87-93.

Green, T., Stauffer, K.A., Lummis, S.C. (1995).
Expression of recombinant homo-oligomeric 5-hydroxytryptamine3 receptors provides new insights into their maturation and structure.
J. Biol. Chem. **270**, 6056-6061.

Griffon, N., Büttner, C., Nicke, A., Kuhse, J., Schmalzing, G., Betz, H. (1999).
Molecular determinants of glycine receptor subunit assembly.
EMBO J. **18**, 4711-4721.

Hackam, A.S., Wang, T.L,, Guggino, W.B., Cutting, G.R. (1997).
A 100 amino acid region in the GABA rho 1 subunit confers robust homo-oligomeric expression.
Neuroreport **8**, 1425-1430.

Haglund, K., Sigismund, S., Polo, S., Szymkiewicz, I., Di Fiore, P.P., Dikic I. (2003).
Multiple monoubiquitination of RTKs is sufficient for their endocytosis and degradation.
Nat. Cell Biol. **5**, 461-466.

Halevi, S., McKay, J., Palfreyman, M., Yassin, L., Eshel, M., Jorgensen, E., Treinin, M. (2002).
The C. elegans ric-3 gene is required for maturation of nicotinic acetylcholine receptors.
EMBO J. **21**, 1012-1020.

Harley, C.A., Tipper, D.J. (1996).
The role of charged residues in determining transmembrane protein insertion orientation in yeast.
J. Biol. Chem. **271**, 24625-24633.

Hartmann, E., Rapoport, T.A., Lodish, H.F. (1989).
Predicting the orientation of eukaryotic membrane-spanning proteins.
Proc. Natl. Acad. Sci. U S A. **86**, 5786-5790.

Harvey, R.J., Betz, H. (2000).
Structure, diversity, pharmacology, and pathology of glycine receptor chloride channels.
Handbook of Experimental Pharmacology **147**, 479-497.

Helekar, S.A., Char, D., Neff, S., Patrick, J. (1994).
Prolyl isomerase requirement for the expression of functional homo-oligomeric ligand-gated ion channels.
Neuron **12**, 179-189.

Helekar, S.A., Patrick, J. (1997).
Peptidyl prolyl cis-trans isomerase activity of cyclophilin A in functional homo-oligomeric receptor expression.
Proc. Natl. Acad. Sci. U S A. **94**, 5432-5437.

Hershko, A., Ciechanover, A. (1998).
The ubiquitin system.
Annu. Rev. Biochem. **67**, 425-479.

Hicke, L., Dunn, R. (1999).
Regulation of membrane protein transport by ubiquitin and ubiquitin-binding proteins.
Annu. Rev. Cell Dev. Biol. **19**, 141-172.

Hicke, L. (1999).
Gettin' down with ubiquitin: turning off cell-surface receptors, transporters and channels.
Trends Cell Biol. **9** 107-112.

Huganir, R.L., Racker, E. (1980).
Endogenous and exogenous proteolysis of the acetylcholine receptor from *Torpedo californica*.
J. Supramol. Struct. **14**, 13-19.

Hurtley, S.M., Helenius, A. (1989).
Protein oligomerization in the endoplasmic reticulum.
Annu. Rev. Cell. Biol. **5**, 277-307.

Jiang, L.H., Kim, M., Spelta, V., Bo, X., Surprenant, A., North, R.A. (2003).
Subunit arrangement in P2X receptors.
J. Neurosci. **23**, 8903-8910.

Jones, S., Sudweeks, S., Yakel, J.L. (1999).
Nicotinic receptors in the brain: correlating physiology with function.
Trends Neurosci. **22**, 555-561.

Juretic, D., Zoranic, L., Zucic, D. (2002).
Basic charge clusters and predictions of membrane protein topology.
J. Chem. Inf. Comput. Sci. **42**, 620-632.

Kassner, P.D., Berg, D.K. (1997).
Differences in the fate of neuronal acetylcholine receptor protein expressed in neurons and stably transfected cells.
J. Neurobiol. **33**, 968-982.

Keleshian, A.M., Edeson, R.O., Liu, G.J., Madsen, B.W. (2000).
Evidence for cooperativity between nicotinic acetylcholine receptors in patch clamp records.
Biophys. J. **78**, 1-12.

Khiroug, S.S., Harkness, P.C., Lamb, P.W., Sudweeks, S.N., Khiroug, L., Millar, N.S., Yakel, J.L. (2002).
Rat nicotinic ACh receptor α7 and ß2 subunits co-assemble to form functional heteromeric nicotinic receptor channels.
J. Physiol. **540**, 425-434.

Kim, M., Yoo, O.J., Choe, S. (1997).
Molecular assembly of the extracellular domain of $P2X_2$, an ATP-gated ion channel.
Biochem. Biophys. Res. Commun. **240**, 618-622.

Kirsch, J., Betz, H. (1998).
Glycine-receptor activation is required for receptor clustering in spinal neurons.
Nature **392**, 717-720.

Kirsch, J., Meyer, G., Betz, H. (1996).
Synaptic Targeting of Ionotropic Neurotransmitter Receptors
Mol. Cell. Neurosci. **8**, 93-98.

Kneussel, M., Betz, H. (2000).
Clustering of inhibitory neurotransmitter receptors at developing postsynaptic sites: the membrane activation model.
Trends Neurosci. **23**, 429-435.

Kneussel, M., Brandstätter, J.H., Laube, B., Stahl, S., Müller, U., Betz, H. (1999a)
Loss of postsynaptic GABA(A) receptor clustering in gephyrin-deficient mice.
J. Neurosci. **19**, 9289-9297.

Kneussel, M., Hermann, A., Kirsch, J., Betz, H. (1999b)
Hydrophobic interactions mediate binding of the glycine receptor ß-subunit to gephyrin.
J. Neurochem. **72**, 1323-1326.

Kuhse, J., Betz, H., Kirsch, J. (1995).
The inhibitory glycine receptor: architecture, synaptic localization and molecular pathology of a postsynaptic ion-channel complex.
Curr. Opin. Neurobiol. **5**, 318-323.

Kuhse, J., Laube, B., Magalei, D., Betz, H. (1993).
Assembly of the inhibitory glycine receptor: identification of amino acid sequence motifs governing subunit stoichiometry.
Neuron **11**, 1049-1056.

Kuroiwa, T., Sakaguchi, M., Mihara, K., Omura, T. (1991).
Systematic analysis of stop-transfer sequence for microsomal membrane.
J. Biol. Chem. **266**, 9251-9255.

Langosch, D., Thomas, L., Betz, H. (1988).
Conserved quaternary structure of ligand-gated ion channels: the postsynaptic glycine receptor is a pentamer.
Proc. Natl. Acad. Sci. U S A. **85**, 7394-7398.

Le Novere, N., Changeux, J.P. (2001).
LGICdb: the ligand-gated ion channel database.
Nucleic Acids Res. **29**, 294-295.

Le Novere, N., Corringer, P.J., Changeux, J.P. (2002).
The diversity of subunit composition in nAChRs: evolutionary origins, physiologic and pharmacologic consequences.
J. Neurobiol. **53**, 447-456.

Le, K.T., Babinski, K., Seguela, P. (1998).
Central $P2X_4$ and $P2X_6$ channel subunits coassemble into a novel heteromeric ATP receptor.
J. Neurosci. **18**, 7152-7159.

Levi, S., Vannier, C., Triller, A. (1998).
Strychnine-sensitive stabilization of postsynaptic glycine receptor clusters.
J. Cell Sci. **111**, 335-345.

Lewis, C., Neidhart, S., Holy, C., North, R.A., Buell, G., Surprenant, A. (1995).
Coexpression of $P2X_2$ and $P2X_3$ receptor subunits can account for ATP-gated currents in sensory neurons.
Nature **377**, 432-435.

Lindstrom, J., Gullick, W., Conti-Tronconi, B., Ellisman, M. (1980).
Proteolytic nicking of the acetylcholine receptor.
Biochemistry. **19**, 4791-4795.

Lipp, J., Flint, N., Haeuptle, MT., Dobberstein, B. (1989).
Structural requirements for membrane assembly of proteins spanning the membrane several times.
J. Cell. Biol. **109**, 2013-2022.

Lucero, P., Penalver, E., Vela, L., Lagunas, R. (2000).
Monoubiquitination is sufficient to signal internalization of the maltose transporter in *Saccharomyces cerevisiae*.
J. Bacteriol. **182**, 241-243.

Lüscher, C., Nicoll, R.A., Malenka, R.C., Muller, D. (2000).
Synaptic plasticity and dynamic modulation of the postsynaptic membrane.
Nat. Neurosci. **3**, 545-550.

Man, H.Y., Lin, J.W., Ju, W.H., Ahmadian, G., Liu, L., Becker, L.E., Sheng, M., Wang, Y.T. (2000).
Regulation of AMPA receptor-mediated synaptic transmission by clathrin-dependent receptor internalization.
Neuron **25**, 649-662. Erratum in: Neuron (2001), 29, 307.

Marx, S.O., Gaburjakova, J., Gaburjakova, M., Henrikson, C., Ondrias, K., Marks, A.R. (2001).
Coupled gating between cardiac calcium release channels (ryanodine receptors).
Circ. Res. **88**, 1151-1158.

Matsuda, S., Launey, T., Mikawa, S., Hirai, H. (2000).
Disruption of AMPA receptor GluR2 clusters following long-term depression induction in cerebellar Purkinje neurons.
EMBO J. **19**, 2765-2774. Erratum in: EMBO J. (2003), 22, 174.

McGehee, D.S., Role, L.W. (1995).
Physiological diversity of nicotinic acetylcholine receptors expressed by vertebrate neurons.
Annu. Rev. Physiol. **57**, 521-546.

Missias, A.C., Mudd, J., Cunningham, J.M., Steinbach, J.H., Merlie, J.P., Sanes, J.R. (1997).
Deficient development and maintenance of postsynaptic specializations in mutant mice lacking an 'adult' acetylcholine receptor subunit.
Development **124**, 5075-5086.

Mosesson, Y., Shtiegman, K., Katz, M., Zwang, Y., Vereb, G., Szollosi, J., Yarden, Y. (2003).
Endocytosis of receptor tyrosine kinases is driven by monoubiquitylation, not polyubiquitylation.
J. Biol. Chem. **278**, 21323-21326.

Nicke, A., Bäumert, H.G., Rettinger, J., Eichele, A., Lambrecht, G., Mutschler, E., Schmalzing, G. (1998).
$P2X_1$ and $P2X_3$ receptors form stable trimers: a novel structural motif of ligand-gated ion channels.
EMBO J. **17**, 3016-3028.

Nicke, A., Rettinger, J., Büttner, C., Eichele, A., Lambrecht, G., Schmalzing, G. (1999).
Evolving view of quaternary structures of ligand-gated ion channels.
Prog. Brain Res. **120**, 61-80.

Nicke, A., Rettinger, J., Schmalzing, G. (2003).
Monomeric and dimeric byproducts are the principal functional elements of higher order $P2X_1$ concatamers.
Mol. Pharmacol. **63**, 243-252.

Nilsson, I., von Heijne, G. (1990).
Fine-tuning the topology of a polytopic membrane protein: role of positively and negatively charged amino acids.
Cell **62**, 1135-1141.

North, R.A. (2002).
P2X receptors: a third major class of ligand-gated ion channels.
Ciba Found. Symp. **198**, 91-109

North, R.A. (2002).
Molecular physiology of P2X receptors.
Physiol. Rev. **82**, 1013-1067.

Ortells, M.O., Lunt, G.G. (1995).
Evolutionary history of the ligand-gated ion-channel superfamily of receptors.
Trends Neurosci. **18**, 121-127.

Pfeiffer, F., Betz, H. (1981).
Solubilization of the glycine receptor from rat spinal cord.
Brain Res. **226**, 273-279.

Puchacz, E., Buisson, B., Bertrand, D., Lukas, R.J. (1994).
Functional expression of nicotinic acetylcholine receptors containing rat α7 subunits in human SH-SY5Y neuroblastoma cells.
FEBS Lett. **354**, 155-159.

Pumplin, D.W., Fambrough, D.M. (1982).
Turnover of acetylcholine receptors in skeletal muscle.
Annu. Rev. Physiol. **44**, 319-335.

Quik, M., Choremis, J., Komourian, J., Lukas, R.J., Puchacz, E. (1996).
Similarity between rat brain nicotinic α-bungarotoxin receptors and stably expressed α-bungarotoxin binding sites.
J. Neurochem. **67**, 145-154.

Rakhilin, S., Drisdel, R.C., Sagher, D., McGehee, D.S., Vallejo, Y.,
Green, W.N. (1999).
α-bungarotoxin receptors contain α7 subunits in two different disulfide-bonded conformations.
J. Cell. Biol. **146**, 203-218.

Rapoport, TA., Jungnickel, B., Kutay, U. (1996).
Protein transport across the eukaryotic endoplasmic reticulum and bacterial inner membranes.
Annu. Rev. Biochem. **65**, 271-303.

Rettinger, J., Aschrafi, A., Schmalzing, G. (2000).
Roles of individual N-glycans for ATP potency and expression of the rat $P2X_1$ receptor.
J. Biol. Chem. **275**, 33542-33547.

Rich, M.M., Lichtman, J.W. (1989).
In vivo visualization of pre- and postsynaptic changes during synapse elimination in reinnervated mouse muscle.
J. Neurosci. **9**, 1781-1805.

Sadtler, S., Laube, B., Lashub, A., Nicke, A., Betz, H., Schmalzing G. (2003).
A basic cluster determines topology of the cytoplasmic M3-M4 loop of the glycine receptor α1 subunit.
J. Biol. Chem. **278**, 16782-16790.

Sanes, J.R., Lichtman, J.W. (1999).
Development of the vertebrate neuromuscular junction.
Annu. Rev. Neurosci. **22**, 389-442.

Sargent, P.B. (1993).
The diversity of neuronal nicotinic acetylcholine receptors.
Annu. Rev. Neurosci. **16**, 403-443.

Sato, M., Mueckler, M. (1999).
A conserved amino acid motif (R-X-G-R-R) in the Glut1 glucose transporter is an important determinant of membrane topology.
J. Biol. Chem. **274**, 24721-24725.

Sato, T., Sakaguchi, M., Mihara, K., Omura, T. (1990).
The amino-terminal structures that determine topological orientation of cytochrome P-450 in microsomal membrane.
EMBO J. **9**, 2391-2397.

Schägger, H., Cramer, W.A., von Jagow, G. (1994).
Analysis of molecular masses and oligomeric states of protein complexes by blue native electrophoresis and isolation of membrane protein complexes by two-dimensional native electrophoresis.
Anal. Biochem. **217**, 220-230.

Schägger, H., von Jagow, G. (1987).
Tricine-sodium dodecyl sulfate-polyacrylamide gel electrophoresis for the separation of proteins in the range from 1 to 100 kDa.
Anal. Biochem. **166**, 368-379.

Schindler, H., Spillecke, F., Neumann, E. (1984).
Different channel properties of *Torpedo* acetylcholine receptor monomers and dimers reconstituted in planar membranes.
Proc. Natl. Acad. Sci. U S A. **81**, 6222-6226.

Schmalzing, G., Gloor, S., Omay, H., Kroner, S., Appelhans, H.,
Schwarz, W. (1991).
Up-regulation of sodium pump activity in *Xenopus laevis* oocytes by expression of heterologous ß1 subunits of the sodium pump.
Biochem. J. **279**, 329-336.

Séguela, P., Wadiche, J., Dineley-Miller, K., Dani, J.A., Patrick, J.W. (1993).
Molecular cloning, functional properties, and distribution of rat brain α7: a nicotinic cation channel highly permeable to calcium.
J. Neurosci. **13**, 596-604.

Serdaroglu, P., Askanas, V., Engel, W.K. (1992).
Immunocytochemical localization of ubiquitin at human neuromuscular junctions.
Neuropathol. Appl. Neurobiol. **18**, 232-236.

Shi, S.H., Hayashi, Y., Petralia, R.S., Zaman, S.H., Wenthold, R.J., Svoboda, K., Malinow, R. (1999).
Rapid spine delivery and redistribution of AMPA receptors after synaptic NMDA receptor activation.
Science **284**, 1811-1816.

Shih, S.C., Sloper-Mould, K.E., Hicke, L. (2000).
Monoubiquitin carries a novel internalization signal that is appended to activated receptors.
EMBO J. **19**, 187-198.

Sola, M., Kneussel, M., Heck, I.S., Betz, H., Weissenhorn, W. (2001).
X-ray crystal structure of the trimeric N-terminal domain of gephyrin.
J. Biol. Chem. **276**, 25294-25301.

Soto, F., Garcia-Guzman, M., Stuhmer, W. (1997).
Cloned ligand-gated channels activated by extracellular ATP (P2X receptors).
J. Membr. Biol. **160**, 91-100.

Stoop, R., Thomas, S., Rassendren, F., Kawashima, E., Buell, G., Surprenant, A., North, R.A. (1999).
Contribution of individual subunits to the multimeric $P2X_2$ receptor: estimates based on methanethiosulfonate block at T336C.
Mol. Pharmacol. **56**, 973-981.

Surprenant, A., Rassendren, F., Kawashima, E., North, R.A., Buell, G. (1996).
The cytolytic P2Z receptor for extracellular ATP identified as a P2X receptor ($P2X_7$).
Science **272**, 735-738.

Terrell, J., Shih, S., Dunn, R., Hicke, L. (1998).
A function for monoubiquitination in the internalization of a G protein-coupled receptor.
Mol. Cell **1**, 193-202.

Thompson, J.A., Lau, A.L., Cunningham, D.D. (1987).
Selective radiolabeling of cell surface proteins to a high specific activity.
Biochemistry **26**, 743-750.

Thrower, J.S., Hoffman, L., Rechsteiner, M., Pickart, C.M. (2000).
Recognition of the polyubiquitin proteolytic signal.
EMBO J. **19**, 94-102.

Torres, G.E., Egan, T.M., Voigt M,M. (1999).
Identification of a domain involved in ATP-gated ionotropic receptor subunit assembly.
J. Biol. Chem. **274**, 22359-22365.

Turrigiano, G.G. (2000).
AMPA receptors unbound: membrane cycling and synaptic plasticity.
Neuron **26**, 5-8.

Tytgat, J., Hess, P. (1992).
Evidence for cooperative interactions in potassium channel gating.
Nature **359**, 420-423.

Valera, S., Hussy, N., Evans, R.J., Adami, N., North, R.A., Surprenant, A., Buell, G. (1994).
A new class of ligand-gated ion channel defined by P2x receptor for extracellular ATP.
Nature **371**, 516-519.

van Klompenburg, W., Nilsson, I., von Heijne, G., de Kruijff, B. (1997).
Anionic phospholipids are determinants of membrane protein topology.
EMBO J. **16**, 4261-4266.

Verrall, S., Hall, Z.W. (1992).
The N-terminal domains of acetylcholine receptor subunits contain recognition signals for the initial steps of receptor assembly.
Cell **68**, 23-31.

von Heijne, G., Gavel, Y. (1988).
Topogenic signals in integral membrane proteins.
Eur. J. Biochem. **174**, 671-678.

Wahlberg, JM., Spiess, M. (1997).
Multiple determinants direct the orientation of signal-anchor proteins: the topogenic role of the hydrophobic signal domain.
J. Cell. Biol. **137**, 555-562.

Wang, Y.T., Linden, D.J. (2000).
Expression of cerebellar long-term depression requires postsynaptic clathrin-mediated endocytosis.
Neuron **25**, 635-647.

Wessels, HP., Spiess, M. (1988).
Insertion of a multispanning membrane protein occurs sequentially and requires only one signal sequence.
Cell **55**, 61-70.

Wilkinson, BM., Critchley, AJ., Stirling, CJ. (1996).
Determination of the transmembrane topology of yeast Sec61p, an essential component of the endoplasmic reticulum translocation complex.
J. Biol. Chem. **271**, 25590-25597.

Xia, J., Chung, H.J., Wihler, C., Huganir, R.L., Linden, D.J. (2000).
Cerebellar long-term depression requires PKC-regulated interactions between GluR2/3 and PDZ domain-containing proteins.
Neuron **28**, 499-510.

Xu, R., Salpeter, M.M. (1999).
Rate constants of acetylcholine receptor internalization and degradation in mouse muscles.
J. Cell. Physiol. **181**, 107-112.

Zhang, J.T., Lee, C.H., Duthie, M., Ling, V. (1995).
Topological determinants of internal transmembrane segments in P-glycoprotein sequences.
J. Biol. Chem. **270**, 1742-1746.

TABLE OF ATTACHMENTS

THE JOURNAL OF BIOLOGICAL CHEMISTRY
Vol. 276, No. 46, Issue of November 16, pp. 42978–42985, 2001
Printed in U.S.A.

Ubiquitination Precedes Internalization and Proteolytic Cleavage of Plasma Membrane-bound Glycine Receptors*

Received for publication, March 8, 2001, and in revised form, September 7, 2001
Published, JBC Papers in Press, September 17, 2001, DOI 10.1074/jbc.M102121200

Cora Büttner‡, Sven Sadtler‡, Anne Leyendecker‡, Bodo Laube§, Nathalie Griffon§¶, Heinrich Betz§, and Günther Schmalzing‡‖

From the ‡Department of Pharmacology, Biocenter of the Johann Wolfgang Goethe University, Marie Curie Strasse 9, Frankfurt am Main 60439, and the §Department of Neurochemistry, Max Planck Institute for Brain Research, Deutschordenstrasse 46, Frankfurt am Main 60528, Germany

The inhibitory glycine receptor (GlyR) in developing spinal neurones is internalized efficiently upon antagonist inhibition. Here we used surface labeling combined with affinity purification to show that homopentameric α1 GlyRs generated in *Xenopus* oocytes are proteolytically nicked into fragments of 35 and 13 kDa upon prolonged incubation. Nicked GlyRs do not exist at the cell surface, indicating that proteolysis occurs exclusively in the endocytotic pathway. Consistent with this interpretation, elevation of the lysosomal pH, but not the proteasome inhibitor lactacystin, prevents GlyR cleavage. Prior to internalization, α1 GlyRs are conjugated extensively with ubiquitin in the plasma membrane. Our results are consistent with ubiquitination regulating the endocytosis and subsequent proteolysis of GlyRs residing in the plasma membrane. Ubiquitin-conjugating enzymes thus may have a crucial role in synaptic plasticity by determining postsynaptic receptor numbers.

The efficiency of synaptic transmission depends critically on a dense packing of neurotransmitter receptors in the postsynaptic membrane. At fast synapses, ligand-gated ion channels (LGICs)[1] mediate the postsynaptic response. Different lines of evidence indicate that the distribution and density of LGICs in the plasma membrane are regulated tightly. In differentiating muscle fibers, the formation of a densely packed postsynaptic matrix of nicotinic acetylcholine receptors (nAChRs) at the developing motor endplate requires restriction of gene expression to subsynaptic nuclei, efficient internalization and degradation of extrasynaptic receptors, synaptic clustering by rapsyn, and slowing of the turnover of synaptically accumulated nAChRs (1, 2). Inversely, muscle denervation (2) or blockade of neurotransmission by α-bungarotoxin (3) causes a loss of nAChRs from the postsynaptic membrane because of an increased rate of protein turnover (4). Because nAChR degradation occurs only after internalization and lysosomal targeting of the receptor protein (4, 5), endocytosis is considered to be of crucial importance in the control of postsynaptic receptor density. An unexpectedly dynamic role of exo- and endocytosis in regulating synaptic efficacy has emerged recently from studies on glutamatergic synapses in the central nervous system (6, 7). High frequency stimulation of hippocampal neurons has been shown to trigger the plasma membrane insertion of AMPA subtype glutamate receptors in dendritic spines during long term potentiation (8), whereas receptor removal by clathrin-mediated internalization may be essential for inducing long term depression in the cerebellum (9, 10). In summary, developmental and electrical activity-driven changes in LGIC numbers appear to be based on a tight regulation of the surface incorporation and endocytotic recycling of these membrane proteins.

Another LGIC in the central nervous system known to undergo efficient endocytosis is the inhibitory glycine receptor (GlyR), a pentameric membrane protein (11, 12) that mediates postsynaptic inhibition in spinal cord and other regions of the mammalian central nervous system. Addition of the antagonist strychnine to cultured spinal neurons has been shown to cause internalization of GlyRs into an endosomal compartment (13, 14). Concomitantly, the blocked GlyRs fail to co-localize with gephyrin, a peripheral membrane protein that anchors GlyRs and $GABA_A$ receptors in the postsynaptic membrane (for review, see Ref. 15). This may indicate that anchoring to postsynaptic gephyrin protects synaptically localized GlyRs against endocytosis. Consistent with this view, in neurons from gephyrin-deficient mice a loss of $GABA_A$ receptor localization at synapses is accompanied by increased levels of intracellular receptor immunoreactivity (16).

In conclusion, there is a variety of processes in which regulated endocytosis appears to contribute significantly to the control of postsynaptic LGIC density. The mechanisms that trigger internalization are, however, not well understood. Here, we have used a recombinant homo-oligomeric GlyR generated in *Xenopus* oocytes as a model system to search for reactions involved in receptor endocytosis. The GlyR appeared to be particularly suited for such an analysis because its molecular structure, subunit assembly, and cell surface incorporation have been analyzed in detail. Presently, four GlyR genes encoding ligand-binding α subunits (α1–α4) and a single gene for

* This work was supported by Deutsche Forschungsgemeinschaft Grants SFB 474 and Schm536/2-3, the Fonds der Chemischen Industrie, and BIOMED 2 Contract BMH4-CT-97-2374. The costs of publication of this article were defrayed in part by the payment of page charges. This article must therefore be hereby marked "*advertisement*" in accordance with 18 U.S.C. Section 1734 solely to indicate this fact.

We dedicate this paper to the memory of the late Prof. Helmut Holzer and to Prof. Nobuhiko Katunuma.

¶ Present address: Unité de Neurobiologie et Pharmacologie Moléculaire, INSERM U109, Center Paul Broca, 2ter rue d'Alesia, Paris 75014, France.

‖ Present address: Dept. of Molecular Pharmacology, Technical University of Aachen, Wendlingweg 2, Aachen D-52074, Germany. To whom correspondence should be addressed. Tel.: 49-241-808-9130; Fax: 49-241-888-8433; E-mail: gschmalzing@post.klinikum.rwth-aachen.de.

[1] The abbreviations used are: LGIC(s), ligand-gated ion channel(s); nAChR(s), nicotinic acetylcholine receptor(s); AMPA, α-amino-3-hydroxy-5-methyl-4-isoxazole propionic acid; GlyR(s), inhibitory glycine receptor(s); $GABA_A$ and $GABA_C$, γ-aminobutyric acid types A and C, respectively; BN, blue native; PAGE; polyacrylamide gel electrophoresis; sulfo-SHPP, sulfosuccinimidyl-3-(4-hydroxyphenyl)proprionate; Ni^{2+}-NTA, nickel-nitrilotriacetic acid; Tricine, *N*-[2-hydroxy-1,1-bis(hydroxymethyl)ethyl]glycine; ER, endoplasmic reticulum; Endo H, endoglycosidase H; PNGase F, peptide *N*-glycosidase F.

the structural β subunit are known in vertebrates (for review, see Refs. 17 and 18). These subunits form homo-oligomeric and hetero-oligomeric chloride channels in different regions of the mammalian central nervous system. Each subunit shares with the other members of the nAChR superfamily a large glycosylated N-terminal ectodomain and four membrane-spanning regions (M1–M4), which, between M1 and M3, are separated by short hydrophilic stretches, and between M3 and M4 by a loop of ~85 amino acids (β subunit 124 amino acids) which faces the cytosol. All α subunit isoforms assemble into functional homopentameric GlyR upon heterologous expression in *Xenopus* oocytes or mammalian cells (19–21). This assembly occurs soon after polypeptide synthesis in the endoplasmic reticulum and is a prerequisite for efficient export to the cell surface (21). By using affinity purification combined with selective cell surface labeling and blue native (BN) polyacrylamide gel electrophoresis (PAGE), we now show that the recombinant GlyR is targeted to internalization and degradation after selective ubiquitination at the plasma membrane. Conjugation to ubiquitin is known to serve as an internalization signal for other receptor and ion channel proteins (22, 23). Our data thus suggest that ubiquitin-conjugating enzymes may have a crucial role in regulating postsynaptic LGIC densities.

EXPERIMENTAL PROCEDURES

Materials and Antibodies—Sulfosuccinimidyl-3-(4-hydroxyphenyl) proprionate (sulfo-SHPP) was from Pierce. Concanamycin and lactacystin were from Alexis Biochemicals (San Diego, CA). A rabbit antiserum and a monoclonal antibody to ubiquitin were purchased from Santa Cruz Biotechnologies (La Jolla, CA) and Chemicon (Temecula, CA), respectively.

cDNA Constructs—All amino acids were numbered according to their position in the mature protein sequence. cDNA constructs encoding α1-His with a C-terminal hexahistidyl tag (His) have been described before (21). Lysine 411 was mutated to arginine (mutant K411R) using the QuikChange site-directed mutagenesis kit (Stratagene), and the mutation was confirmed by sequencing. cDNA encoding human ubiquitin (24) was amplified by reverse transcription-polymerase chain reaction from a human brain cDNA library (Life Technologies, Inc.) using gene-specific primers (forward, 5′-AAAgacgtcGAAGTAGCCA-GAATGCAGATCTTCGTGAAGACTCTGACTGGTAA; reverse, 5′-TT-GAATTCTGCCCATTATCAACCCCCCCTCAAGCGCA) cloned into the vector pNKS2 (25) and sequenced. The forward polymerase chain reaction primer contained unique restriction sites for *Aat* II (lower case letters) and *Bsm* I (underlined) at the start codon. Taking advantage of these sites, codons for a N-terminal hexahistidyl tag were inserted to generate His-ubiquitin (His tag at the N terminus).

cRNA Synthesis and Oocyte Expression—Capped cRNAs were synthesized from linearized templates with SP6 RNA polymerase (Amersham Pharmacia Biotech) and purified as described (26). For oocyte injection, the cRNAs were dissolved in 5 mM Tris/HCl, pH 7.5, at 0.5 μg/μl, using the absorbance reading at 260 nm for quantitation (*A* 1.0 = 40 μg/μl). Defolliculated *Xenopus* oocytes of oogenesis stage V or VI (26) were injected with about 50-nl aliquots of cRNAs. Oocytes were kept at 19 °C in sterile frog Ringer's solution (90 mM NaCl, 1 mM KCl, 1 mM $CaCl_2$, 1 mM $MgCl_2$, and 10 mM Hepes, pH 7.4) supplemented with 50 mg/liter gentamycin. One to 3 days after cRNA injection, macroscopic glycine responses were measured by two-electrode voltage clamp recording at a holding potential of −70 mV as described previously (12).

Protein Purification, BN-PAGE, and SDS-PAGE—cRNA-injected oocytes and noninjected controls were labeled metabolically by overnight incubation with L-[^{35}S]methionine (>40 TBq/mmol, Amersham Pharmacia Biotech) at about 100 MBq/ml (0.1 MBq/oocyte) in frog Ringer's solution at 19 °C and chased with 1 mM unlabeled methionine as indicated. Oocytes expressing His-ubiquitin were preincubated at 10 mM *N*-ethylmaleimide to inactivate ubiquitin proteases prior to cell lysis. His-tagged proteins were then purified by Ni^{2+}-NTA-agarose (Qiagen) chromatography from digitonin (1%, w/v) extracts of oocytes as detailed previously (27) with the following modification. Iodoacetamide was routinely included at 10 mM and 1 mM in the lysis and washing buffers, respectively, to prevent artificial cross-linking of polypeptides by disulfide bonds. Bound proteins were released from the Ni^{2+}-NTA-agarose with nondenaturing elution buffer consisting of 0.5% (w/v) digitonin and 250 mM imidazole HCl, pH 7.6 (equivalent to 50 mM Cl^-), and kept at 0 °C until analyzed by PAGE. For selective labeling of plasma membrane receptors, the injected oocytes were incubated for 3 days at 19 °C and then labeled with freshly radioiodinated ($Na^{125}I$, Amersham Pharmacia Biotech) sulfo-SHPP (^{125}I-sulfo-SHPP), a membrane-impermeant derivative of the Bolton-Hunter reagent (28), exactly as described (27). Where indicated, surface radioiodinated oocytes were incubated for another 20 h at 19 °C after removal of unbound ^{125}I-sulfo-SHPP by washing in frog Ringer's solution. Proteins were then purified from digitonin extracts of the oocytes by Ni^{2+}-NTA-agarose chromatography as detailed above.

BN-PAGE (29) was performed as described (27). Before loading, purified proteins were supplemented with BN sample buffer to final concentrations of 10% (v/v) glycerol, 0.2% (w/v) Serva blue G, and 20 mM sodium 6-amino-*n*-caproate, and applied onto polyacrylamide gradient slab gels. Molecular mass markers (Combithek II, Roche Molecular Biochemicals) were visualized by Coomassie staining. For SDS-PAGE or Tricine-SDS-PAGE (30), proteins were supplemented with the appropriate SDS sample buffer containing 20 mM dithiothreitol (DTT) and electrophoresed in parallel with ^{14}C-labeled molecular mass markers (Rainbow, Amersham Pharmacia Biotech) on SDS-polyacrylamide gels. Where indicated, samples were treated prior to SDS-PAGE with either endoglycosidase H (Endo H) or PNGase F (New England Biolabs) in the presence of 1% (w/v) octyl glucoside to reduce inactivation of PNGase F. Gels were fixed, dried, and exposed to BioMax MR or MS film (Kodak) at −80 °C. In some experiments, radioactive bands were quantified with an image analyzer (PhosphorImager Storm 820, Molecular Dynamics).

RESULTS

Post-ER Cleavage of α1-His Subunits into Fragments of 35 and 13 kDa—After removal of the 28 amino acids of the signal peptide, the native human α1-His subunit encompasses 421+6 amino acid residues, corresponding to a calculated protein core of 49.2 kDa. The α1-His subunit migrated at an apparent mass of 48 kDa when isolated by Ni^{2+}-NTA-agarose chromatography under nondenaturing conditions from *Xenopus* oocytes and analyzed by reducing Tricine-SDS-PAGE after a 6-h [^{35}S]methionine pulse. Subsequent to a 20-h chase interval, an additional 35-kDa protein was isolated which was not present immediately after the pulse. To identify smaller fragments generated during cleavage of the 48-kDa full-length α1-His subunit, we used Tricine-SDS-polyacrylamide gels appropriate for resolution of low mass polypeptides. Fig. 1*A* shows that a 13-kDa polypeptide was detected consistently when α1-His GlyR was isolated after a 20-h chase interval, but not directly after the [^{35}S]methionine labeling pulse. These data indicate that the α1-His subunit is cleaved proteolytically into two defined fragments of 35 and 13 kDa during the chase period.

To determine the regions from which the two fragments originated, we exploited the fact that the α1-His subunit harbors a single *N*-linked oligosaccharide side chain at position 38 (^{38}NVS; see Fig. 7). Hence, the fragment derived from the N-terminal portion must include this unique *N*-glycan. Fig. 1*B* shows that PNGase F, which is capable of releasing complex-type carbohydrates, reduced the molecular masses of both the 48-kDa subunit and its 35-kDa fragment by ~3 kDa; this corresponds to the mass of one single *N*-linked oligosaccharide chain (21). In contrast, the mobility of the 13-kDa fragment did not increase upon PNGase F treatment. We conclude from these data that the sole *N*-glycan is located on the 35-kDa fragment, whereas the 13-kDa fragment originates from the nonglycosylated C-terminal portion of the α1-His subunit and thus carries the hexahistidyl tag.

Fig. 1*B* also shows that after a 20-h chase period none of the polypeptides was reduced in molecular mass by Endo H, which removes high mannose-type sugars characteristic for proteins that have not yet left the ER. The acquisition of Endo H resistance of virtually all full-length 48-kDa α1-His subunits during the chase is consistent with an efficient ER exit of the homopentameric receptor (21). The 35-kDa cleavage product appeared during the chase interval and existed in the complex-

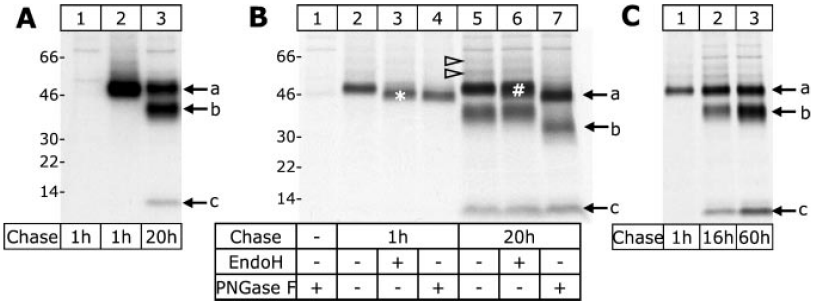

FIG. 1. **The α1-His subunit of the GlyR is cleaved outside the ER into a glycosylated 35-kDa fragment and a nonglycosylated 13-kDa fragment.** Oocytes were injected with α1-His GlyR cRNA, labeled with [^{35}S]methionine, and extracted with digitonin after the indicated chase interval. Proteins were natively purified by Ni^{2+}-NTA-agarose chromatography, denatured with Tricine-SDS sample buffer, and resolved by reducing Tricine-SDS-PAGE (4/10/13% acrylamide). The autoradiographs of the gels are shown. *Panel A*, during a 20-h chase interval, α1-His subunits within the homopentameric GlyR were cleaved into fragments of 35 and 13 kDa. *Lane 1*, noninjected control oocytes. *Panel B*, GlyRs were incubated in the presence of Tricine-SDS sample buffer, DTT, and octyl glucoside with Endo H or PNGase F for 2 h as indicated. Shortly after the pulse, α1-His subunits are largely in the Endo H-sensitive form (*) but become entirely Endo H-resistant during the chase (#). Deglycosylation with PNGase F reveals that the sole *N*-glycan of the α1-His subunit at Asn-38 is located on the 35-kDa fragment. *Lane 1*, noninjected control oocytes. *Panel C*, fragments are not degraded further upon extension of the chase interval. *a*, full-length α1-His; *b*, truncated α1-His; *c*, corresponding 13-kDa fragment.

glycosylated form only (Fig. 1*B*), indicating that the proteolytic cleavage took place outside the ER, *i.e.* within or beyond the Golgi. During prolonged chase intervals, there was a further increase in the amounts of both the 35- and 13-kDa fragments at the expense of the 48-kDa polypeptide (Fig. 1*C*). A significant fraction of the α1-His subunit remained at 48 kDa, however, even after a 60-h chase period.

The α1-His GlyR Complex Remains Assembled after Cleavage—GlyR α1 subunits assemble into a homopentamer rapidly after their synthesis while still in the ER (21). The isolation of two fragments of the full-length α1-His subunit suggested that these fragments remain associated during purification because only the 13-kDa C-terminal fragment carries the hexahistidyl tag that interacts with the Ni^{2+}-NTA beads. To examine directly whether the 13-kDa fragment is an integral part of the pentameric α1-His GlyR complex, we analyzed the natively isolated receptor by BN-PAGE before and after a 48-h chase interval, *i.e.* before and after partial cleavage. Under nondenaturing conditions, the α1-His GlyR migrated as a single protein with an apparent mass of 400 kDa irrespective of the length of the chase interval (Fig. 2*A*, *lanes 3* and *5*). The 13-kDa fragment in particular could not be detected.

Treatment of the α1-His GlyR isolated shortly after the pulse with urea and DTT to weaken noncovalent subunit interactions produced five distinct bands (Fig. 2*A*, *lane 4*), consistent with the pentameric nature of this receptor (21). If, however, the α1-His GlyR isolated after a 48-h chase interval was subjected to the same treatment, up to nine distinct bands were resolved by BN-PAGE (Fig. 2*A*, *lane 6*). To identify the individual polypeptides of which these bands were composed, the corresponding lane developed in the first dimension by BN-PAGE was excised, soaked with SDS and β-mercaptoethanol, and reanalyzed in the second dimension by reducing Tricine-SDS-PAGE (Fig. 2*B*). This analysis revealed that the 13-kDa fragment was released entirely by treatment with DTT/urea and corresponded to band 9 on the BN-polyacrylamide gel (Fig. 2*A*). In addition, the 35-kDa and 48-kDa polypeptides could be clearly attributed to bands 8 and 7, respectively, on the BN-polyacrylamide gel. Notably, the assembly intermediates consisted of multiples of either 48-kDa subunits or truncated 35-kDa subunits (Fig. 2*B*) but not a mixture of both. In other words, either the five subunits that constitute the native α1-His GlyR were all intact or all proteolytically nicked.

Truncated Forms of the α1-His GlyR Are Exclusively Intracellular—To visualize selectively the plasma membrane-bound α1-His GlyR, we radioiodinated the outer cell surface of oocytes with ^{125}I-sulfo-SHPP, a membrane-impermeant Bolton-Hunter derivative (28). Three days after cRNA injection, *i.e.* at a time when a large portion of the metabolically labeled α1-His subunits were already proteolytically nicked (Fig. 3*A*, *lane 1*), the plasma membrane contained only the full-length 48-kDa polypeptide (Fig. 3*A*, *lane 2*). This indicated that the 35-kDa product was either not routed to the cell surface or that cleavage occurred in a compartment distal from the plasma membrane (see below). Unexpectedly, however, two polypeptides of 55 and 62 kDa, and occasionally a third band of 69 kDa, were resolved by Tricine-SDS-PAGE in addition to the 48-kDa full-length α1-His subunit. Upon treatment with glycosidases, the 55- and 62-kDa polypeptides behaved exactly like authentic α1-His subunits: they were Endo H-resistant but reduced by 3 kDa upon PNGase F treatment, indicating that they all carried a single complex-type *N*-glycan (data not shown). BN-PAGE analysis of the surface radioiodinated GlyR combined with Tricine-SDS-PAGE in the second dimension revealed that the 55- and the 62-kDa polypeptides were integral parts of the α1-His pentamer (Fig. 3*B*) and not co-isolated accessory proteins. We conclude from these results that the 55- and the 62-kDa poylpeptides represent α1-His subunits of the homopentameric GlyR which were conjugated with a 7-kDa molecule en route to the plasma membrane or at the plasma membrane itself. Retrospectively, small amounts of these additional polypeptides could also be detected on autoradiographs of α1-His GlyR purified from [^{35}S]methionine-labeled oocytes (Fig. 1*B*, *open arrowheads*).

The α1 GlyR Can Be Isolated from the Cell Surface through Hexahistidyl-tagged Ubiquitin—Because the ladder of plasma membrane α1 subunit bands differing from each other by ~7 kDa was reminiscent of that of other polypeptides conjugated to one, two, and three molecules of ubiquitin, a protein of 76 amino acids, we examined whether a significant fraction of the α1-His GlyR indeed exists in ubiquitinated form at the plasma membrane. Using antibodies to ubiquitin, we were unable to detect the presence of ubiquitin in affinity-purified GlyR preparations by Western blotting; this presumably reflects the low abundance of this membrane receptor in our purified preparations. We therefore co-expressed human His-ubiquitin together with the nonhistidyl-tagged GlyR α1 subunit to examine whether GlyRs can be isolated through covalently attached His-ubiquitin. Control purifications from [^{35}S]methionine-labeled oocytes confirmed that His-ubiquitin was synthesized efficiently in oocytes (see Fig. 4*C*). Using this co-expression approach, nontagged α1 GlyR was purified through His-tagged

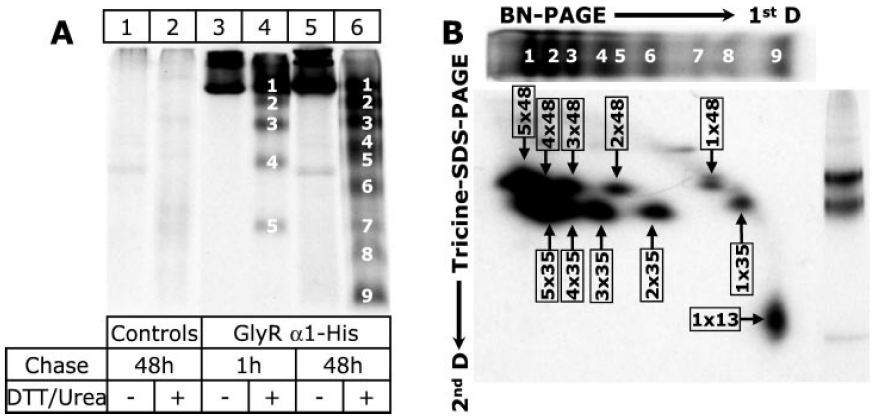

FIG. 2. **Analysis of proteolytically nicked α1-His GlyR by two-dimensional PAGE.** Oocytes injected with α1-His GlyR cRNA and labeled with [^{35}S]methionine were extracted with digitonin after the indicated chase interval. Autoradiographs of the gels are shown. *Panel A*, GlyR was natively purified by Ni^{2+}-NTA-agarose chromatography and resolved by BN-PAGE either without further treatment or after a 1-h incubation at 37 °C and 100 mM DTT, 8 M urea as indicated. Incubation with DTT and urea of GlyR isolated after a 1-h chase, *i.e.* prior to intracellular cleavage, leads to five bands (numbered *1–5*, *lane 4*), whereas nine bands (numbered *1–9*, *lane 6*) are produced when the proteolytically nicked GlyR is subjected to treatment with DTT and urea. *Lanes 1* and *2* refer to noninjected oocytes that were used as controls. *Panel B*, an aliquot of the same α1-His GlyR isolated after a 48 h chase as in *panel A* was treated with DTT and urea to generate dissociation intermediates and then resolved by BN-PAGE (4–16% acrylamide) and reducing Tricine-SDS-PAGE (4/10/13% acrylamide) in the first and second dimensions, respectively. As in *panel A*, the protein bands resolved by BN-PAGE are numbered from *1* to *9*. Second dimension Tricine-SDS-PAGE identifies bands 7, 8, and 9 to correspond to monomers of 48, 35, and 13 kDa, respectively. The additionally resolved protein bands 1–6 represent homomultimers of either full-length 48-kDa α1-His subunits or truncated 35-kDa α1-His subunits. The *boxed* numbers denote the number of subunits × molecular mass/subunit of the protein resolved by BN-PAGE, which leads in the second dimension to the spot indicated by the *arrow*. Note that the 13-kDa fragment exists solely as a monomer after treatment with urea and DTT and not in a complex with any of the 35-kDa multimers, inferring that the interaction of the N-terminal 35-kDa fragments among themselves is much stronger than with the C-terminal 13-kDa fragment.

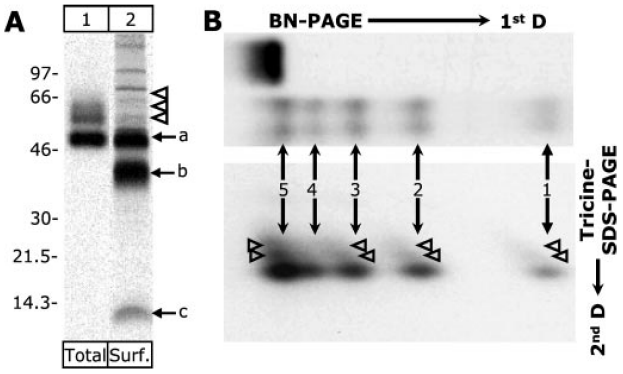

FIG. 3. **Surface GlyR lacks nicked α1-His subunits but contains 55- and 62-kDa α1-His subunits.** Three days after injection of the indicated cRNAs, oocytes were surface labeled with ^{125}I-sulfo-SHPP and extracted with digitonin. *Panel A*, proteins were purified under nondenaturing conditions by Ni^{2+}-NTA-agarose chromatography, denatured with SDS, and resolved by reducing Tricine-SDS-PAGE. For direct comparison, α1-His subunits isolated after a 6-h [^{35}S]methionine pulse and a 40-h chase are also shown (*lane 1*). *Total* and *Surf.* refer to the [^{35}S]methionine-labeled total form of the α1-His subunit and the ^{125}I-labeled surface GlyR α1-His subunit, respectively. *a*, full-length 48-kDa α1-His subunit; *b* and *c*, positions of α1-His cleavage products of 35 and 13 kDa, respectively. *Open arrowheads*, mono-, di-, and triubiquitinated α1-His subunits. *Panel B*, ^{125}I-labeled surface GlyR was treated with DTT and urea to generate assembly intermediates and then resolved by BN-PAGE (4–10% acrylamide) and reducing Tricine-SDS-PAGE (4/10/13% acrylamide) in the first and second dimensions, respectively. *Numbered arrows* indicate positions of monomeric, dimeric, trimeric, tetrameric, and pentameric GlyR α1-His displayed by first dimension BN-PAGE. In addition, the *arrows* assign the multimers and the monomer to the corresponding polypeptides resolved by second dimension Tricine-SDS-PAGE. *Open arrowheads* mark positions of 55- and 62-kDa polypeptides representing mono- and di-ubiquitinated α1-His subunits.

ubiquitin from surface-radioiodinated oocytes (Fig. 4*A*). Tricine-SDS-PAGE analysis revealed the presence of polypeptides of 55 and 62 kDa, corresponding to mono- and di-ubiquitinated forms of the 48 kDa α1 subunit (Fig. 4*A*). A major fraction of the α1 subunit existed also in the nonubiquitinated 48-kDa form and was apparently co-isolated with the ubiquitinated receptor polypeptides. This argues that not all α1 subunits within the homopentamer carried ubiquitin chains, whereas some were evidently multiply ubiquitinated. Nonhistidyl-tagged GlyR α1 subunits could also be purified from oocytes injected with a commercially available recombinant His-ubiquitin protein together with GlyR α1 cRNA (Fig. 4*B*).

From oocytes synthesizing nontagged GlyR α1 subunits without recombinant His-ubiquitin, only small amounts of GlyR protein were purified on the Ni^{2+}-NTA beads, which consistently accounted for ≤ 5% of that obtained after coinjection of His-ubiquitin. Notably, we could not co-isolate significant amounts of GlyR α1 subunits with His-ubiquitin when using this co-expression approach with [^{35}S]methionine-labeled oocytes (Fig. 4*C*). Thus, only a minor fraction of the total cellular pool of the α1 GlyR is ubiquitinated, and this ubiquitination occurs predominantly or exclusively at the plasma membrane (see Fig. 3).

The α1-His GlyR Is Cleaved after Internalization—To characterize the membrane trafficking step at which proteolysis of the α1 GlyR occurs, we first surface labeled oocytes with ^{125}I-sulfo-SHPP and then incubated these oocytes for 20 h at either 0 °C or 19 °C. Fig. 5 shows that surface α1-His subunits migrated entirely in their full-length form and as respective ubiquitin conjugates when isolated after incubation at 0 °C. However, when the oocytes were kept for 20 h at 19 °C subsequent to surface radioiodination, both the truncated 35-kDa form and the cleaved 13-kDa fragment appeared. Because these fragments were never detected at the plasma membrane directly after surface radioiodination (Fig. 4*A*), this suggests that cleavage does not take place *en route* to or at the plasma membrane itself, but in a later compartment, *i.e.* in the endocytotic pathway.

The intense radiolabeling of the 13-kDa fragment found in these surface labeling experiments was surprising in view of the presence of only a single extracellular lysine residue (Lys-411) that is located in the short tail region just behind the fourth transmembrane domain (see Fig. 7). In contrast, the extracellularly exposed N-terminal half of the α1-His subunit

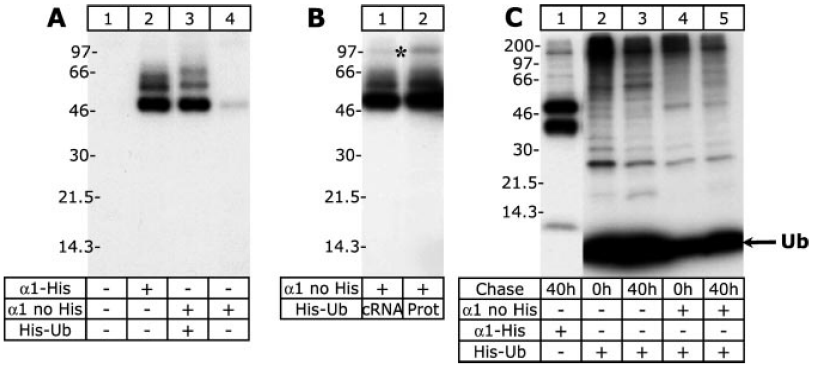

FIG. 4. **GlyR α1 is ubiquitinated at the plasma membrane.** Autoradiographies of reducing Tricine-SDS-polyacrylamide gels are shown. *Panels A* and *B*, 3 days after injection of the indicated cRNAs, oocytes were surface labeled for 1 h at 0 °C with ^{125}I-sulfo-SHPP. Oocytes were immediately extracted with digitonin, and proteins were purified under nondenaturing conditions by Ni^{2+}-NTA-agarose chromatography. The nontagged GlyR α1 subunit (*α1 no His*) could be isolated in large amounts in both His-ubiquitinated and nonubiquitinated form upon co-expression of His-ubiquitin (*panels A* and *B*) or co-injection of recombinant His-ubiquitin protein (*His-Ub prot*, *panel B*). * indicates a protein band that was also isolated from noninjected control oocytes in this particular experiment. *Panel C*, proteins were purified by Ni^{2+}-NTA-agarose chromatography from [^{35}S]methionine-labeled oocytes injected with the indicated cRNAs. Note that *lanes 4* and *5* show solely small amounts of nonubiquitinated GlyR α1 subunit but no His-ubiquitinated GlyR α1 subunit co-isolated with His-ubiquitin. *Ub*, His-ubiquitin.

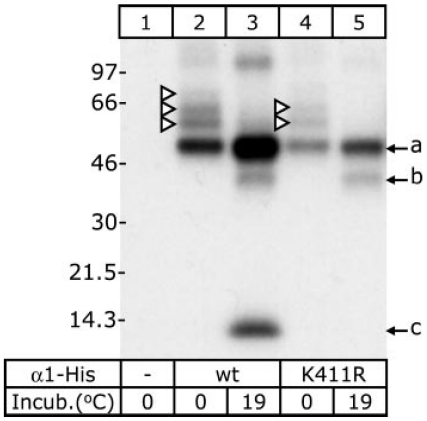

FIG. 5. **Ubiquitinated GlyR α1-His is proteolyzed after internalization.** Oocytes injected with GlyR α1-His cRNA and labeled 3 days later with ^{125}I-sulfo-SHPP were incubated further either at 0 °C or at 19 °C as indicated. After 20 h at either temperature, α1-His receptors were isolated under nondenaturing conditions by Ni^{2+}-NTA-agarose chromatography, denatured with Tricine-SDS sample buffer, and resolved by reducing Tricine-SDS-PAGE (4/10/13% acrylamide). *a*, full-length α1-His subunit of 48 kDa; *b* and *c*, positions of α1-His cleavage products of 35 and 13 kDa, respectively. Note that the 35- and 13-kDa fragments are not present at the plasma membrane of oocytes kept on ice, but appear when oocytes were kept for 20 h at 19 °C. The 13-kDa fragment remained invisible when Lys-411 of the α1-His subunit was replaced by Arg. This indicates that Lys-411 represents the sole residue at which ^{125}I-sulfo-SHPP labeling occurred at the C-terminal end of the α1-His subunit. *Open triangles* indicate ubiquitinated α1-His carrying one to three ubiquitin chains.

carries a total of 12 lysine residues that all might react with ^{125}I-sulfo-SHPP. To unravel whether Lys-411 is indeed a preferred site of iodination, we mutated this residue to arginine and purified the resulting mutant GlyR after surface radioiodination. Fig. 5 (*lane 5*) shows that the K411R mutation did not prevent the cleavage of the surface-radioiodinated full-length α1-His subunit upon subsequent incubation of the oocytes at 19 °C, as the 35-kDa band was clearly detected. The corresponding 13-kDa fragment, however, remained invisible, evidently as a result of Lys-411 elimination. Functionally, the Arg-411 α1-His GlyR was indistinguishable from its parent α1-His GlyR as assessed by two-electrode voltage clamp measurements (results not shown). These data confirm that Lys-411 is particularly accessible to covalent modification.

Cleavage of α1-His GlyR Is Blocked by Elevation of Vesicular pH but Not by a Proteasome Inhibitor—The role of endosomal or lysosomal compartments in the cleavage of α1-His GlyR was assessed further by using chemical inhibitors. Concanamycin, a specific inhibitor of vesicular H^+-ATPases similar to bafilomycin A1, has been reported to block the acidification of endosomes and lysosomes and to interfere with early to late endosomal transport (31). Incubation of oocytes in the presence of concanamycin greatly reduced the formation of the 35- and 13-kDa cleavage products (Fig. 6*A*), corroborating the view that cleavage occurs in the endocytotic pathway. Likewise, cleavage of α1-His was abolished upon addition of the lysosomotropic amine NH_4Cl (Fig. 6*A*), which dissipates transmembrane H^+ gradients of acidic organelles (32), thereby inhibiting the activity of lysosomal enzymes (33). The routing of α1-His GlyR toward the cell surface was not affected notably by concanamycin or NH_4Cl, as assessed by the unimpaired acquisition of complex-type carbohydrates in the presence of either compound (results not shown). A complete inhibition of α1-His cleavage was also seen in the presence of the serine protease inhibitor phenylmethylsulfonyl fluoride (Fig. 6*B*), which, unlike conventional lysosomal inhibitors such as NH_4Cl, does not raise lysosomal pH values. Together these data show that lysosomal serine protease activity is required for efficient cleavage of the α1-His GlyR.

Certain mammalian membrane proteins that become ubiquitinated at the plasma membrane appear to be subsequently degraded by both the lysosome and the proteasome system (34). Proteasome activity seems to be required even for endocytosis and subsequent lysosomal degradation of proteins that do not become ubiquitinated, such as the growth factor receptor (35) and the cytokine interleukin-2 receptor (36). To examine whether proteasomes contribute to the degradation of GlyR α1-His, we employed the proteasome inhibitor lactacystin. Even in the continued presence of 5 μM lactacystin, the absolute amounts of the full-length subunit and of its 35- and 13-kDa cleavage products remained unchanged (Fig. 6*C*). PhosphorImaging analysis indicated that 26 and 24% of the total α1-His were in the uncleaved 48-kDa form in the absence and presence of lactacystin, respectively. These data argue against an involvement of the proteasome in the proteolytic cleavage of the α1-His receptor.

DISCUSSION

In this paper, we show that recombinant GlyRs generated in *Xenopus* oocytes are internalized and cleaved proteolytically into defined fragments after ubiquitination at the plasma membrane. Based on these data we propose that ubiquitin

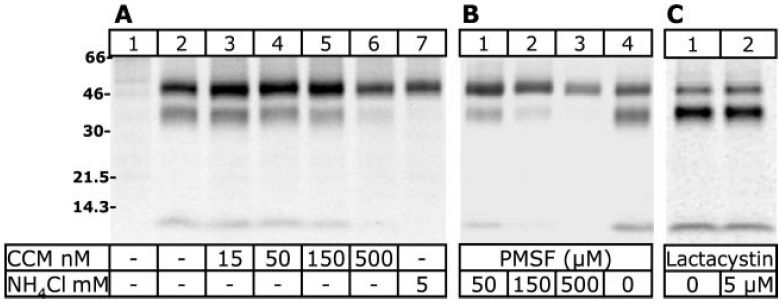

FIG. 6. **GlyR α1-His proteolysis is blocked by concanamycin, NH_4Cl, and phenylmethylsulfonyl fluoride, but not by lactacystin.** α1-His cRNA-injected oocytes were labeled with [^{35}S]methionine for 4 h and chased for 20 h in the absence and presence of the indicated concentrations of concanamycin A (*CCM*) or NH_4Cl (*panel A*), phenylmethylsulfonyl fluoride (*PMSF*, *panel B*), or lactacystin (*panel C*). Proteins were natively purified by Ni^{2+}-NTA-agarose chromatography, denatured with Tricine-SDS sample buffer, and resolved by reducing Tricine-SDS-PAGE (4/10/13% acrylamide). Autoradiographs of the gels are shown.

conjugation reactions may play a key role in the regulation of LGIC dynamics underlying synaptic development and plasticity. Although this suggestion relies at the moment entirely on *Xenopus* oocytes as host cells, it should be mentioned that an apparently identical and developmentally regulated truncation of the GlyR α1 subunits has been previously observed to occur in native neural tissue as well (37). This indicates that the oocyte system represents a useful model system to examine this particular aspect of GlyR regulation. Data obtained with oocytes will therefore be helpful to tackle questions of receptor metabolism in intact neurons.

Ubiquitination of the α1 GlyR: A Targeting Signal for Internalization and Lysosomal Degradation?—The results presented in this study show that the recombinant human α1 GlyR is ubiquitinated at the plasma membrane of *Xenopus* oocytes. Ubiquitination could be demonstrated by co-isolation of the nontagged α1 GlyR through hexahistidyl-tagged ubiquitin and by the identification of α1 subunit conjugates that differed in apparent molecular mass by ~7 kDa from each other. Mono-, di-, and tri-ubiquitinated α1 subunits within the GlyR homopentamer as visualized by surface radioiodination were prominent at the cell surface but hardly detected in total cell homogenates. Thus, ubiquitination of α1 GlyRs occurs largely or exclusively at the plasma membrane and not during intracellular routing of the receptor. Subsequent to internalization, the α1 subunits within the homopentameric GlyR complex were proteolytically nicked into an N-terminal glycosylated fragment of 35 kDa and a C-terminal fragment of 13 kDa. This nicking did, however, not impair affinity purification of the homopentameric GlyR complex, indicating that cleavage of the α1 subunits distal to M3 does not cause dissociation of fragments from the assembled receptor prior to treatment with urea or SDS. This observation agrees well with previous results showing that the extracellular N-terminal domains of GlyR subunits harbor crucial determinants of subunit assembly (12). The importance of the extracellular portion of LGIC subunits for receptor assembly has similarly been demonstrated for $GABA_A$ and $GABA_C$ receptors (38) as well as for the muscle nAChR (39). Also, the proteolytically nicked nAChR has been shown to be remarkably resistant to disassembly. Fragments produced by papain treatment of intact nAChR remained physically and functionally associated (40, 41). Even extensive proteolysis had no dramatic effect on sedimentation characteristics, toxin binding, the doughnut-like appearance in transmission electron microscopy, or cation channel function. By analogy, the nicked α1 GlyR may be able to function as a glycine-gated Cl^- channel, but apparently it is not localized in the plasma membrane. Collectively, our findings place the α1 GlyR into an abundant class of mammalian and yeast membrane proteins that, upon ubiquitination at the cell surface, are targeted into the endocytotic pathway; usually, endocytosis is followed by lysosomal or lysosomal-like vacuolar degradation (for review, see Ref. 42). This is consistent with growing evidence that ubiquitination at the plasma membrane may function as a general internalization signal to trigger the down-regulation of different receptor and channel proteins (22, 42).

Ubiquitination is well established as a major targeting signal for the recognition and degradation of short lived cytosolic proteins by the 26 S proteasome (43). In addition, ubiquitination followed by proteasomal destruction provides for degradation of many luminal and transmembrane ER proteins that, when abnormally folded or incompletely assembled, are translocated back into the cytosol (42). Among the proteins undergoing ER-associated proteasomal degradation are also unassembled subunits of multiprotein complexes. Hence, the ubiquitination of GlyR α1 subunits observed here could be a consequence of overexpression and ensuing retention of large amounts of unassembled α1 subunits in the ER. However, several lines of evidence argue against this view. First, our pulse-chase experiments clearly show that newly synthesized GlyR α1 subunits homo-oligomerize with high efficiency in the ER of *Xenopus* oocytes and, once assembled, are translocated efficiently to the Golgi, as judged from the rapid and complete acquisition of complex-type carbohydrates. Second, the homopentameric α1 GlyR is metabolically stable in *Xenopus* oocytes (half-life in the range of days) compared with incompletely folded or unassembled proteins that are targeted to the proteasome and have in general a very short half-life of <1 h. Third, we have shown that the ubiquitin-conjugated α1 subunits are contained within the assembled homopentameric GlyR complex and carry a complex-type carbohydrate chain indicative of a localization in the Golgi or later compartments. Moreover, our differential labeling experiments indicate that ubiquitination of the α1 GlyR is topologically restricted to the plasma membrane rather than occurring *en route* to the cell surface. Fourth, the proteasome inhibitor lactacystin did not increase α1-His subunit levels or inhibit α1-His cleavage. In contrast, cleavage appears to be mediated by lysosomal serine proteases because phenylmethylsulfonyl fluoride blocked processing almost as efficiently as NH_4Cl. In this respect, degradation of GlyR α1 also differs from degradation of the epithelial Na^+ channel ENaC, which involves the proteasome, but not lysosomes (44). Finally, the ubiquitinated GlyR carries only one to three ubiquitin molecules per α1 subunit; this contrasts the polyubiquitinated high molecular weight adducts routinely seen with proteins targeted for proteasomal degradation. To account for the addition of up to three ubiquitin molecules per α1 subunit, we assume that multiple lysine residues within the large cytoplasmic loop of the α1 subunit (Fig. 7) are mono-ubiquitinated, rather than that a single lysine residue carries a

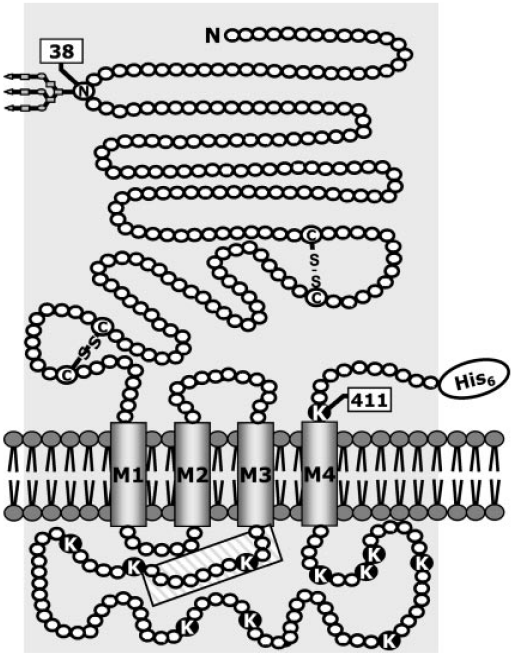

FIG. 7. **Membrane topology of the GlyR α1 subunit.** The sole *N*-glycosylation site at asparagine 38 (*N38*) and the approximate position of the cytoplasmic α1-His cleavage site (*boxed*) within the endodomain (85 amino acids) are indicated. Mutation of the extracellularly located uttermost C-terminal lysine residue (*K411*) to arginine prevents labeling of the 13-kDa C-terminal fragment by ^{125}I-sulfo-SHPP. The 10 lysine residues (*K*) within the endodomain represent putative sites for ubiquitination. *M1–M4*, membrane-spanning segments; *His$_6$*, C-terminal hexahistidyl tag.

branched multiubiquitin chain. Mono-ubiquitination has been shown to be sufficient for internalization of yeast membrane proteins, such as Ste2p, a G protein-coupled receptor (45), or the maltose transporter, a protein with 12 transmembrane segments (46). Also, ubiquitin conjugation has been shown to promote endocytosis in the absence of any other internalization signal (47). Conversely, modification by a single ubiquitin molecule or by multiple single ubiquitins on multiple distinct lysine residues is not sufficient to serve as a proteasomal targeting signal because recognition by the proteasome requires branched multiubiquitin chains containing at least four copies of ubiquitin (48). We therefore conclude that the ubiquitination reactions identified here serve exclusively in labeling GlyRs for removal from the plasma membrane.

The human GlyR α1 subunit harbors 10 cytoplasmic lysine residues, which are all located in the large intracellular loop between transmembrane segments M3 and M4 (Fig. 7). These 10 lysine residues are exposed to the cytosol not only at the plasma membrane, but also during intracellular trafficking of the GlyR. The enzymes of the ubiquitin system evidently are able to discriminate structurally the cytoplasmic GlyR loop from the many other substrates that are ubiquitinated in the same cellular compartment and to distinguish topologically GlyRs present at the cell surface from those *en route* to the plasma membrane. Ubiquitin can be transferred directly from a ubiquitin-charged ubiquitin-conjugation enzyme (denoted E2) to a substrate protein, with specificity in substrate recognition being provided by a large number of E3 ubiquitin-protein ligases. A candidate E3 molecule for ubiquitination of neuronal plasma membrane proteins including the GlyR is Nedd4 (neuronal precursor cells expressed developmentally down-regulated 4; for review, see Ref. 23), which upon overexpression in *Xenopus* oocytes, has been shown to decrease epithelial Na^+ channels numbers in the plasma membrane efficiently (49).

Potential Roles of Receptor Ubiquitination in Synaptic Development and Remodeling—Ubiquitination may serve as a general mechanism for targeting GlyRs and related LGICs to endocytosis and lysosomal degradation and thus for regulating surface receptor numbers during development and at the adult synapse. In developing muscle, extrasynaptic nAChRs are removed from the noninnervated sarcolemmal membrane rapidly, whereas synaptic receptors become metabolically stable upon further development of the neuromuscular junction (2). In contrast, during withdrawal of nerve terminals from the motor endplate the postsynaptic membrane is depleted of nAChRs before there is any obvious loss of membrane in the overlying motor nerve ending (50). A similar early loss of postsynaptic nAChRs also takes place during synapse elimination in reinnervated adult muscle (51). Notably, ubiquitin has been reported to be highly concentrated in postsynaptic membranes of neuromuscular junctions with a distribution identical to that of nAChR (52). Moreover, a rise in cytosolic ubiquitin occurs early in response to axonal injury (53). These data are consistent with ubiquitination being important in synaptic processes that require enhanced rates of receptor internalization and/or degradation.

Another process in which regulation of endocytosis by ubiquitination could play a crucial role is that of changes in receptor isoforms during development. At the neuromuscular junction, the γ subunit of the embryonic nAChR is replaced postnatally by the ϵ subunit of the adult receptor (54). Similar isoform switches occur also with glutamate, $GABA_A$, and glycine receptors in the developing central nervous system (for references, see 55). At glycinergic synapses in spinal cord, replacement of α2 homo-oligomeric neonatal GlyRs by $\alpha1\beta$ adult-type receptors accounts for the shortening of the decay of inhibitory postsynaptic currents during the first 2 postnatal weeks (56, 57). Also, electrical silencing of embryonic GlyRs by the selective antagonist strychnine causes internalization of the receptors into an endosomal compartment by an as yet unidentified pathway (13). This is consistent with an activity-dependent regulation of GlyR numbers via an endocytotic mechanism. A similar regulation of receptor internalization by synaptic activity may also be important in long term depression of excitatory synapses. In the cerebellum (9, 58) and in hippocampal neurons (10), long term depression is known to be accompanied by a reduction in AMPA receptor numbers at synaptic sites.

An important consequence of ubiquitin additions to LGIC subunits may be the disruption of protein-protein interactions at the synapse. The GlyR β subunit is known to bind the receptor-anchoring protein gephyrin via the hydrophobic side of an amphipathic sequence (amino acids 395–411) within its large cytoplasmic loop (59, 60), and this interaction is thought to be crucial for the postsynaptic localization of the receptor (15, 60, 61). Recruitment of an E3 ligase to one or several α1 subunits within an $\alpha1_3\beta_2$ heteropentameric GlyR (11) may sterically affect GlyR-gephyrin interactions and even result in ubiquitination of one or several of the 13 lysine residues within the large cytoplasmic loop of a neighboring β subunit. Conceivably, such modification might interfere with GlyR anchoring to postsynaptic gephyrin and thus facilitate receptor internalization by endocytosis. Conversely, immobilization of plasma membrane-bound heteromeric GlyRs on a preassembled gephyrin scaffold (15, 62) could protect receptors against ubiquitination and thus stabilize the postsynaptic receptor pool at the synapse (63). This hypothesis is consistent with results obtained on cultured hippocampal neurons from gephyrin-deficient mice, in which the intracellular immunoreactivities of subunits of another gephyrin-anchored receptor, the $GABA_A$ receptor, were found to be strikingly increased compared with

wild-type cells (16). Similarly, the reduction of synaptic AMPA receptor numbers seen upon induction of long term depression in cerebellar neurons is thought to involve release from the postsynaptic anchoring protein GRIP and subsequent clathrin-dependent endocytosis (58, 64).

In conclusion, all presently available data can be reconciled with the view that ubiquitination of plasma membrane LGICs constitutes an important signal in targeting receptors to intracellular compartments for proteolytic degradation and that receptor-protein interactions at the synapse may regulate receptor turnover by affecting ubiquitination reactions. The observation that multiple membrane proteins of unknown identity are conjugated with ubiquitin in brain synaptic membranes and postsynaptic densities lends further support to the idea that ubiquitination of membrane proteins is a widespread phenomenon in the mammalian brain (65).

REFERENCES

1. Colledge, M., and Froehner, S. C. (1998) *Curr. Opin. Neurobiol.* **8,** 357–363
2. Sanes, J. R., and Lichtman, J. W. (1999) *Annu. Rev. Neurosci.* **22,** 389–442
3. Akaaboune, M., Culican, S. M., Turney, S. G., and Lichtman, J. W. (1999) *Science* **286,** 503–507
4. Xu, R., and Salpeter, M. M. (1999) *J. Cell. Physiol.* **181,** 107–112
5. Pumplin, D. W., and Fambrough, D. M. (1982) *Annu. Rev. Physiol.* **44,** 319–335
6. Turrigiano, G. G. (2000) *Neuron* **26,** 5–8
7. Lüscher, C., Nicoll, R. A., Malenka, R. C., and Muller, D. (2000) *Nat. Neurosci.* **3,** 545–550
8. Shi, S. H., Hayashi, Y., Petralia, R. S., Zaman, S. H., Wenthold, R. J., Svoboda, K., and Malinow, R. (1999) *Science* **284,** 1811–1816
9. Wang, Y. T., and Linden, D. J. (2000) *Neuron* **25,** 635–647
10. Man, Y. H., Lin, J. W., Ju, W. H., Ahmadian, G., Liu, L., Becker, L. E., Sheng, M., and Wang, Y. T. (2000) *Neuron* **25,** 649–662
11. Langosch, D., Thomas, L., and Betz, H. (1988) *Proc. Natl. Acad. Sci. U. S. A.* **85,** 7394–7398
12. Kuhse, J., Laube, B., Magalei, D., and Betz, H. (1993) *Neuron* **11,** 1049–1056
13. Kirsch, J., and Betz, H. (1998) *Nature* **392,** 717–720
14. Levi, S., Vannier, C., and Triller, A. (1998) *J. Cell Sci.* **111,** 335–345
15. Kneussel, M., and Betz, H. (2000) *Trends Neurosci.* **23,** 429–435
16. Kneussel, M., Brandstätter, J. H., Laube, B., Stahl, S., Müller, U., and Betz, H. (1999) *J. Neurosci.* **19,** 9289–9297
17. Kuhse, J., Betz, H., and Kirsch, J. (1995) *Curr. Opin. Neurobiol.* **5,** 318–323
18. Harvey, R. J., and Betz, H. (2000) *Handb. Exp. Pharmacol.* **147,** 479–497
19. Schmieden, V., Grenningloh, G., Schofield, P. R., and Betz, H. (1989) *EMBO J.* **8,** 695–700
20. Akagi, H., Hirai, K., and Hishinuma, F. (1991) *FEBS Lett.* **281,** 160–166
21. Griffon, N., Büttner, C., Nicke, A., Kuhse, J., Schmalzing, G., and Betz, H. (1999) *EMBO J.* **18,** 4711–4721
22. Hicke, L. (1999) *Trends Cell Biol.* **9,** 107–112
23. Staub, O., Abriel, H., Plant, P., Ishikawa, T., Kanelis, V., Saleki, R., Horisberger, J. D., Schild, L., and Rotin, D. (2000) *Kidney Int.* **57,** 809–815
24. Wiborg, O., Pedersen, M. S., Wind, A., Berglund, L. E., Marcker, K. A., and Vuust, J. (1985) *EMBO J.* **4,** 755–759
25. Gloor, S., Pongs, O., and Schmalzing, G. (1995) *Gene (Amst.)* **160,** 213–217
26. Schmalzing, G., Gloor, S., Omay, H., Kröner, S., Appelhans, H., and Schwarz, W. (1991) *Biochem. J.* **279,** 329–336
27. Nicke, A., Bäumert, H. G., Rettinger, J., Eichele, A., Lambrecht, G., Mutschler, E., and Schmalzing, G. (1998) *EMBO J.* **17,** 3016–3028
28. Thompson, J. A., Lau, A. L., and Cunningham, D. D. (1987) *Biochemistry* **26,** 743–750
29. Schägger, H., Cramer, W. A., and von Jagow, G. (1994) *Anal. Biochem.* **217,** 220–230
30. Schägger, H., and von Jagow, G. (1987) *Anal. Biochem.* **166,** 368–379
31. Woo, J. T., Shinohara, C., Sakai, K., Hasumi, K., and Endo, A. (1992) *Eur. J. Biochem.* **207,** 383–389
32. Maxfield, F. R. (1982) *J. Cell Biol.* **95,** 676–681
33. Seglen, P. O., and Gordon, P. B. (1980) *Mol. Pharmacol.* **18,** 468–475
34. Strous, G. J., and Govers, R. (1999) *J. Cell Sci.* **112,** 1417–1423
35. Strous, G. J., van Kerkhof, P., Govers, R., Rotwein, P., and Schwartz, A. L. (1997) *J. Biol. Chem.* **272,** 40–43
36. Yu, A., and Malek, T. R. (2001) *J. Biol. Chem.* **276,** 381–385
37. Becker, C. M., Hoch, W., and Betz, H. (1988) *EMBO J.* **7,** 3717–3726
38. Hackam, A. S., Wang, T. L., Guggino, W. B., and Cutting, G. R. (1997) *Neuroreport* **8,** 1425–1430
39. Verrall, S., and Hall, Z. W. (1992) *Cell* **68,** 23–31
40. Lindstrom, J., Gullick, W., Conti-Tronconi, B., and Ellisman, M. (1980) *Biochemistry* **19,** 4791–4795
41. Huganir, R. L., and Racker, E. (1980) *J. Supramol. Struct.* **14,** 13–19
42. Bonifacino, J. S., and Weissman, A. M. (1998) *Annu. Rev. Cell Dev. Biol.* **14,** 19–57
43. Hershko, A., and Ciechanover, A. (1998) *Annu. Rev. Biochem.* **67,** 425–479
44. Malik, B., Schlanger, L., Al Khalili, O., Bao, H. F., Yue, G., Price, S. R., Mitch, W. E., and Eaton, D. C. (2001) *J. Biol. Chem.* **276,** 12903–12910
45. Terrell, J., Shih, S., Dunn, R., and Hicke, L. (1998) *Mol. Cell* **1,** 193–202
46. Lucero, P., Penalver, E., Vela, L., and Lagunas, R. (2000) *J. Bacteriol.* **182,** 241–243
47. Shih, S. C., Sloper-Mould, K. E., and Hicke, L. (2000) *EMBO J.* **19,** 187–198
48. Thrower, J. S., Hoffman, L., Rechsteiner, M., and Pickart, C. M. (2000) *EMBO J.* **19,** 94–102
49. Staub, O., Gautschi, I., Ishikawa, T., Breitschopf, K., Ciechanover, A., Schild, L., and Rotin, D. (1997) *EMBO J.* **16,** 6325–6336
50. Balice-Gordon, R. J., and Lichtman, J. W. (1993) *J. Neurosci.* **13,** 834–855
51. Rich, M. M., and Lichtman, J. W. (1989) *J. Neurosci.* **9,** 1781–1805
52. Serdaroglu, P., Askanas, V., and Engel, W. K. (1992) *Neuropathol. Appl. Neurobiol.* **18,** 232–236
53. De Stefano, M. E., Squitti, R., and Toschi, G. (1998) *J. Neuropathol. Exp. Neurol.* **57,** 1000–1012
54. Mishina, M., Takai, T., Imoto, K., Noda, M., Takahashi, T., Numa, S., Methfessel, C., and Sakmann, B. (1986) *Nature* **321,** 406–411
55. Missias, A. C., Mudd, J., Cunningham, J. M., Steinbach, J. H., Merlie, J. P., and Sanes, J. R. (1997) *Development* **124,** 5075–5086
56. Hoch, W., Betz, H., and Becker, C. M. (1989) *Neuron* **3,** 339–348
57. Takahashi, T., Momiyama, A., Hirai, K., Hishinuma, F., and Akagi, H. (1992) *Neuron* **9,** 1155–1161
58. Matsuda, S., Launey, T., Mikawa, S., and Hirai, H. (2000) *EMBO J.* **19,** 2765–2774
59. Meyer, G., Kirsch, J., Betz, H., and Langosch, D. (1995) *Neuron* **15,** 563–572
60. Kneussel, M., Hermann, A., Kirsch, J., and Betz, H. (1999) *J. Neurochem.* **72,** 1323–1326
61. Kirsch, J., Meyer, G., and Betz, H. (1996) *Mol. Cell Neurosci.* **8,** 93–98
62. Sola, M., Kneussel, M., Heck, I. S., Betz, H., and Weissenhorn, W. (2001) *J. Biol. Chem.* **276,** 25294–25301
63. Changeux, J. P., and Danchin, A. (1976) *Nature* **264,** 705–712
64. Xia, J., Chung, H. J., Wihler, C., Huganir, R. L., and Linden, D. J. (2000) *Neuron* **28,** 499–510
65. Chapman, A. P., Smith, S. J., Rider, C. C., and Beesley, P. W. (1994) *Neurosci. Lett.* **168,** 238–242

THE JOURNAL OF BIOLOGICAL CHEMISTRY
Vol. 278, No. 19, Issue of May 9, pp. 16782–16790, 2003
Printed in U.S.A.

A Basic Cluster Determines Topology of the Cytoplasmic M3-M4 Loop of the Glycine Receptor α1 Subunit*

Received for publication, December 23, 2002, and in revised form, February 21, 2003
Published, JBC Papers in Press, February 28, 2003, DOI 10.1074/jbc.M213077200

Sven Sadtler‡, Bodo Laube§, Alhassan Lashub§, Annette Nicke‡, Heinrich Betz§, and Günther Schmalzing‡¶

From the ‡Department of Molecular Pharmacology, Medical School of the Technical University of Aachen, Wendlingweg 2, D-52074 Aachen, Germany and §Department of Neurochemistry, Max Planck Institute for Brain Research, Deutschordenstrasse 46, D-60528 Frankfurt am Main, Germany

The inhibitory glycine receptor is a member of the ligand-gated ion channel superfamily of neurotransmitter receptors, which are composed of homologous subunits with four transmembrane segments (M1-M4), each. Here, we demonstrate that the correct topology of the glycine receptor α1 subunit depends critically on six positively charged residues within a basic cluster, RFRRKRR, located in the large cytoplasmic loop (designated M3-M4 loop) following the C-terminal end of M3. Neutralization of one or more charges of this cluster, but not of other charged residues in the M3-M4 loop, led to an aberrant translocation into the endoplasmic reticulum lumen of the M3-M4 loop. However, when two of the three basic charges located in the ectodomain linking M2 and M3 were neutralized, in addition to two charges of the basic cluster, endoplasmic reticulum disposition of the M3-M4 loop was prevented. We conclude that a high density of basic residues C-terminal to M3 is required to compensate for the presence of positively charged residues in the M2-M3 ectodomain, which otherwise impair correct membrane integration of the M3 segment.

The anion-conductive inhibitory glycine receptor (GlyR)[1] is a member of the ligand-gated ion channel superfamily of neurotransmitter receptors that includes the closely related inhibitory γ-aminobutyric acid, type A receptors, as well as the cation-permeable nicotinic acetylcholine receptors and 5-hydroxytryptamine type 3 receptors. Four GlyR genes encoding ligand binding α subunits (α1-α4) and a single gene for the structural β subunit are known in vertebrates (for review see Refs. 1 and 2). These subunits form homopentameric and heteropentameric chloride channels (3, 4), which mediate postsynaptic inhibition in the spinal cord and other regions of the mammalian central nervous system, thus controlling motor and sensory pathways. All α subunit isoforms assemble into functional homopentameric GlyRs upon heterologous expression in *Xenopus* oocytes or mammalian cells (5–8).

* This work was supported by grants from the Deutsche Forschungsgemeinschaft (Schm536/2-3 and La1086/2-2) and Fonds der Chemischen Industrie. The costs of publication of this article were defrayed in part by the payment of page charges. This article must therefore be hereby marked "*advertisement*" in accordance with 18 U.S.C. Section 1734 solely to indicate this fact.

¶ To whom correspondence should be addressed: Dept. of Molecular Pharmacology, Wendlingweg 2, D-52074 Aachen, Germany. Tel.: 49-241-8089130; Fax: 49-241-8082433; E-mail: gschmalzing@ukaachen.de.

[1] The abbreviations used are: GlyR, glycine receptor; ER, endoplasmic reticulum; BN-PAGE, blue native-PAGE; Ni^{2+}-NTA, nickel-nitrilotriacetic acid; Endo H, endoglycosidase H; PNGase F, peptide-*N*-glycosidase F; Tricine, *N*-[2-hydroxy-1,1-bis(hydroxymethyl)ethyl]glycine.

Like other proteins of the ligand-gated ion channel superfamily, GlyR subunits are multispanning (polytopic) type I membrane proteins with an N-terminal cleavable signal sequence, which targets the nascent polypeptide to the ER and drives its insertion into the lipid bilayer. Mature GlyR subunits as released by signal peptidase cleavage are modular polypeptides, composed of 1) a large glycosylated N-terminal ectodomain that forms the agonist binding site; 2) four transmembrane segments (M1-M4), which between M1 and M3 are connected by short hydrophilic loops and between M3 and M4 by a large cytoplasmic loop of ~85 amino acids (designated M3-M4 loop in this paper); and 3) a short extracellular C-terminal tail.

The classic model of how multispanning membrane proteins insert cotranslationally into the ER membrane assumes that the overall topology of the mature protein is determined by the orientation of the signal sequence, which is inserted first and initiates the translocation of the following peptide segments (9, 10). Accordingly, downstream hydrophobic sequences simply serve as alternate stop transfer and signal anchor sequences, which cause the nascent polypeptide to passively follow the lead of the preceding transmembrane segment and thereby direct the sequential insertion of polytopic proteins. In prokaryotes, the transmembrane orientation of the most N-terminal hydrophobic sequence, *i.e.* the cleavable signal sequence in case of type I proteins, has been found to depend on the flanking charged residues; the more positively charged end is retained on the cytoplasmic (Cis) side of the membrane, as described by the "inside- or Cis-positive rule" (11). Electrostatic interaction of arginine and lysine residues with negatively charged head groups of phospholipids (12), and, at least in prokaryotes, the negative-inside transmembrane potential (13) determines the transmembrane orientation. Because of their low average degree of ionization at physiological pH, histidines have almost no effect on peptide topology (14). Negatively charged residues affect the topology of prokaryotic proteins only when present in high numbers (15). In contrast, the orientation of the first transmembrane segment of eukaryotic proteins correlates best with the charge difference hypothesis, which considers both positively and negatively charged amino acids by proposing that a net negative cytoplasmic charge dictates a luminal disposition (16). Besides charges, the length and hydrophobicity of the signal sequence (17, 18), as well as glycosylation at sites near the signal sequence (19), have all been documented to affect transmembrane topology. Experimental support for the classical insertion model has been provided for a variety of membrane proteins (20–23). There is, however, increasing evidence that the initial translocation events may not necessarily dictate the topology of the entire mature protein (24–26). Rather, additional topogenic sequence

information in subsequent transmembrane segments or internal loops appears to be required for the correct positioning of some transmembrane segments of multispanning proteins (for a recent review see Ref. 27).

In this paper, we show that a cluster of basic residues located in the cytoplasmic loop of the GlyR α1 subunit approximately eight residues C-terminal to the transmembrane segment M3 constitutes an important determinant of proper membrane insertion. Based on the usage of three naturally occurring, though normally inaccessible *N*-glycosylation sites of the M3-M4 loop, we demonstrate that the unbiased orientation of M3 and the ensuing hydrophilic loop depends on the presence of these positively charged residues. The other positively charged amino acids of the M3-M4 loop located outside of this basic cluster exert little or no effect, indicating that a high density of positive charges rather than a net charge difference determines topology.

EXPERIMENTAL PROCEDURES

cDNA Constructs—The cDNA construct encoding α1-His with a C-terminal hexahistidyl tag (His) has been described previously (8). Mutations were inserted using the QuikChange™ site-directed mutagenesis kit (Stratagene) and confirmed by sequencing. All amino acids were numbered according to their position in the mature protein sequence.

Oocyte Expression—Defolliculated *Xenopus* oocytes were injected with ~50-nl aliquots of capped cRNAs (0.5 μg/μl) and kept at 19 °C in sterile frog Ringer's solution (90 mM NaCl, 1 mM KCl, 1 mM $CaCl_2$, 1 mM $MgCl_2$, and 10 mM Hepes, pH 7.4) supplemented with 50 mg/liter gentamycin as described (28). One to three days after cRNA injection, glycine responses were measured by two-electrode voltage-clamp recording at a holding potential of −70 mV as described previously (4).

Protein Purification, SDS-PAGE and BN-PAGE—cRNA-injected and non-injected control oocytes were metabolically labeled by overnight incubation with L-[^{35}S]methionine (>40 TBq/mmol; Amersham Biosciences) at about 100 MBq/ml (0.1 MBq per oocyte) in frog Ringer's solution at 19 °C and chased with 1 mM unlabeled methionine as indicated. His-tagged proteins were then purified by Ni^{2+}-NTA-agarose (Qiagen) chromatography from digitonin (1%) (w/v) extracts of oocytes as detailed previously (29) with the following modification. Iodoacetamide was routinely included at 10 and 1 mM in the lysis and washing buffers, respectively, to prevent artificial cross-linking of polypeptides by disulfide bonds. Bound proteins were released from the Ni^{2+}-NTA-agarose with non-denaturing elution buffer consisting of 0.5% (w/v) digitonin and 250 mM imidazole/HCl, pH 7.6, and kept at 0 °C until analyzed by PAGE.

For SDS-PAGE or Tricine-PAGE (30), proteins were supplemented with the appropriate SDS sample buffer containing 20 mM dithiothreitol and electrophoresed in parallel with [^{14}C]labeled molecular mass markers (Rainbow; Amersham Biosciences) on linear SDS-polyacrylamide gels. Where indicated, samples were treated prior to SDS-PAGE with either endoglycosidase H (Endo H) or peptide-*N*-glycosidase F (PNGase F; both enzymes were purchased from New England Biolabs) in the presence of 1% (w/v) Nonidet P-40 to counteract SDS inactivation of PNGase F.

BN-PAGE (31) was performed as described previously (29) immediately after protein purification. Purified proteins were supplemented with blue native sample buffer to final concentrations of 10% (v/v) glycerol, 0.2% (w/v) Serva blue G, and 20 mM sodium 6-amino-*n*-caproate and applied onto polyacrylamide gradient slab gels. Where indicated, samples were treated prior to BN-PAGE with 8 M urea to induce partial dissociation of receptor complexes into lower order intermediates. Both SDS- and BN-polyacrylamide gels were fixed, dried, and exposed to BioMax MS film (Eastman Kodak Co.) at −80 °C. For quantification, the dried gels were exposed to a PhosphorImager screen and scanned using a Storm 820 PhosphorImager (Amersham Biosciences). Individual bands were quantified with the ImageQuant software.

RESULTS

Alanine Substitution of Basic Residues of the α1-His Chain Downstream to M3 Results in a Mixed Orientation of the M3-M4 Loop—Between the M3 and M4 segments, the GlyR α1 polypeptide contains a cytoplasmic loop of ~85 amino acids that includes a total of 23 basic (ten Lys, ten Arg, three His) and nine acidic (three Asp, six Glu) residues (Fig. 1*A*). Particularly remarkable is a cluster of basic amino acids, ^{316}RFRRKRRHHK, a few residues downstream to M3. To examine a possible functional role of this sequence motif, we replaced four or seven of its basic residues by alanines, yielding ^{316}AAAAARRHHK ($^{316–320}$A-α1-His mutant) or ^{316}AAAAAAAHHA ($^{316–322,325}$A-α1-His mutant), respectively (Fig. 1*B*). Two-electrode voltage-clamp analysis of *Xenopus* oocytes injected with the respective mutant cRNAs revealed no effect of these alanine replacements on the shape of the glycine-induced currents or on glycine potency (results not shown). However, a statistically significant reduction of the amplitude of the maximal current elicited by glycine from 4.7 ± 1.2 to 2.3 ± 0.8 μA was observed for the $^{316–320}$A-α1-His receptor as compared with the parent α1-His receptor, respectively, in three independent experiments, each with five to ten oocytes.

Next we compared the synthesis and post-translational processing of the parent α1-His GlyR and the charge neutralization mutants. The parent α1-His polypeptide isolated as a control migrated as a single band at 48 kDa when analyzed by reducing Tricine-PAGE subsequent to isolation by Ni^{2+}-NTA-agarose chromatography from [^{35}S]methionine-labeled *Xenopus* oocytes (Fig. 2, *A* and *B*, *lane 1*). Treatment with Endo H reduced the mass of the α1-His subunit isolated directly after the pulse by 3 kDa to the 45-kDa protein core (Fig. 2*B*, *lane 2*). This mass shift is consistent with the presence of a single *N*-glycan, resulting from usage of the sole *N*-glycosylation motif, ^{38}NVS, in the N-terminal extracellular domain of the α1 polypeptide (Fig. 1*A*) (8). After replacement of the acceptor Asn^{38} by glutamine, the α1-His polypeptide migrated at 45 kDa, and no mass shift upon Endo H treatment was observed (results not shown).

In contrast to the parent α1-His polypeptide, both the $^{316–320}$A-α1-His and the $^{316–322,325}$A-α1-His mutants migrated as double bands of apparent masses of 48 and 54 kDa when analyzed under the same conditions (Fig. 2*A*, *lanes 2* and *3*). Strikingly, Endo H treatment of the $^{316–320}$A-α1-His (Fig. 2*B*, *lane 5*) and the $^{316–322,325}$A-α1-His (not shown) mutants shifted both the 48- and the 54-kDa polypeptides to the 45-kDa α1-His protein core. The same result was obtained with PNGase F (Fig. 2*B*, *lane 6*). This indicates that the 48- and the 54-kDa polypeptides possess the same protein mass but differ in their number of *N*-glycans.

To determine the number of *N*-glycans that give rise to the 54-kDa polypeptide, the $^{316–320}$A-α1-His mutant was incubated with increasing concentrations of Endo H (Fig. 2*C*, *lanes 7–12*). Because of partial deglycosylation at intermediate Endo H concentrations, a ladder-like pattern of four bands was generated (*lanes 8* and *9*). Neighboring bands differ in mass by 3 kDa, the mass of an *N*-linked oligosaccharide side chain. The 45-kDa band represents the core protein, whereas the 48-, 51-, and 54-kDa bands correspond to polypeptides with one, two, and three *N*-glycans, respectively. Because ^{38}NVS is the only potential acceptor site for *N*-linked glycosylation on the extracellular part of the α1-His polypeptide, the two additional *N*-glycans must originate from usage of other endogenous sequons that are topologically inaccessible in the non-mutated GlyR α1 polypeptide. Indeed, the GlyR α1 subunit sequence carries a total of four consensus *N*-glycosylation sites, three of which reside on the cytoplasmic M3-M4 loop, ^{335}NFS, ^{358}NNS, and ^{361}NTT (*cf.* Fig. 1*A*). These sites should be glycosylated only when the M3-M4 loop translocates into the ER lumen, thus allowing for formation of the hyperglycosylated 54-kDa form.

The glycosylation of only two of the three sequons of the

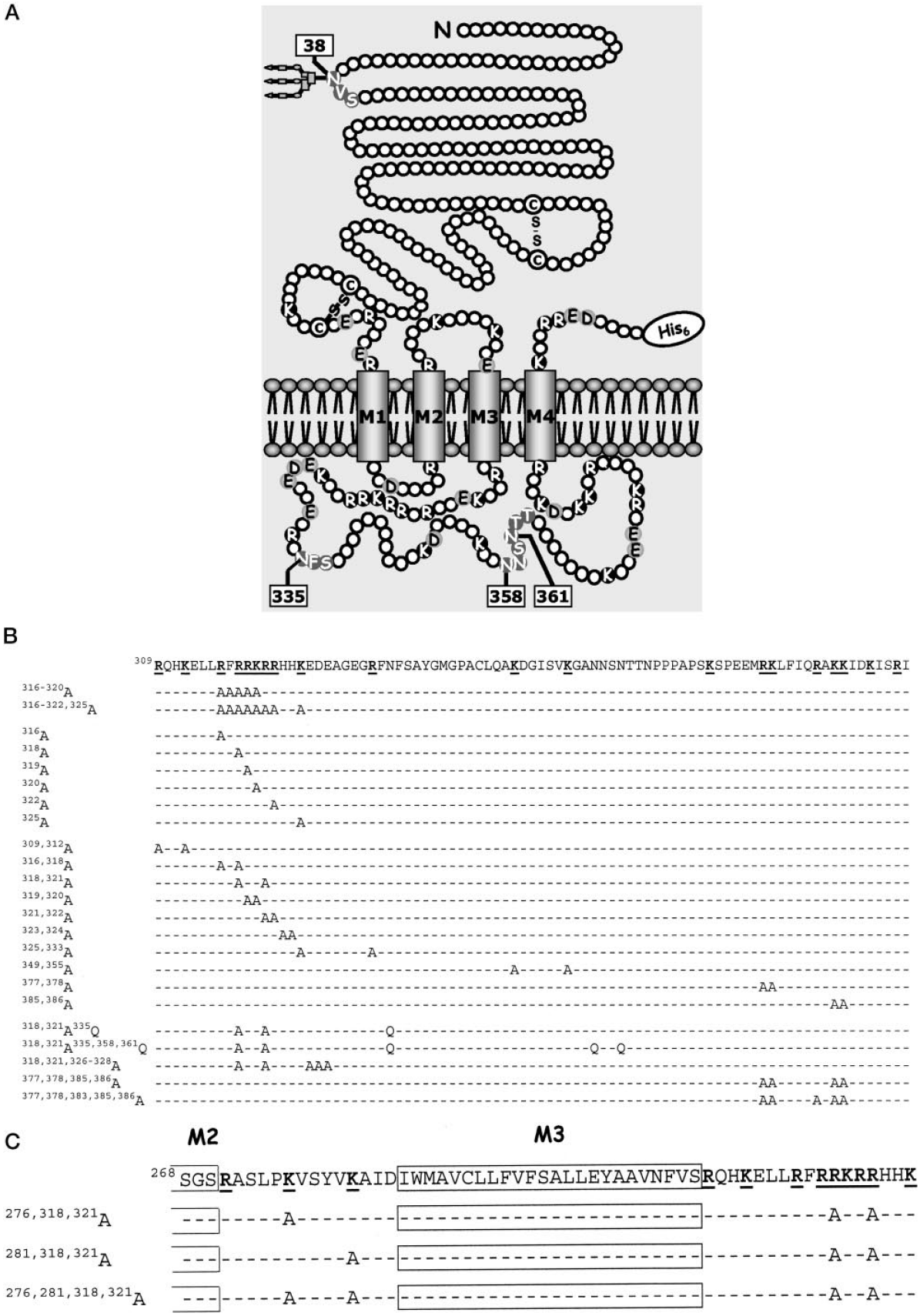

FIG. 1. **Sequence and topology of the human GlyR α1 subunit.** *A*, the membrane topology and predicted boundaries of the transmembrane segments are based on the original model (see Ref. 2). N*X*(T/S) sequons are indicated with *gray symbols* combined with *white lettering*. Notably, only one of the sequons (^{38}NVS) is located on the predicted ectodomain, whereas the three others (^{335}NFS, ^{358}NNS, ^{361}NTT) are located on the

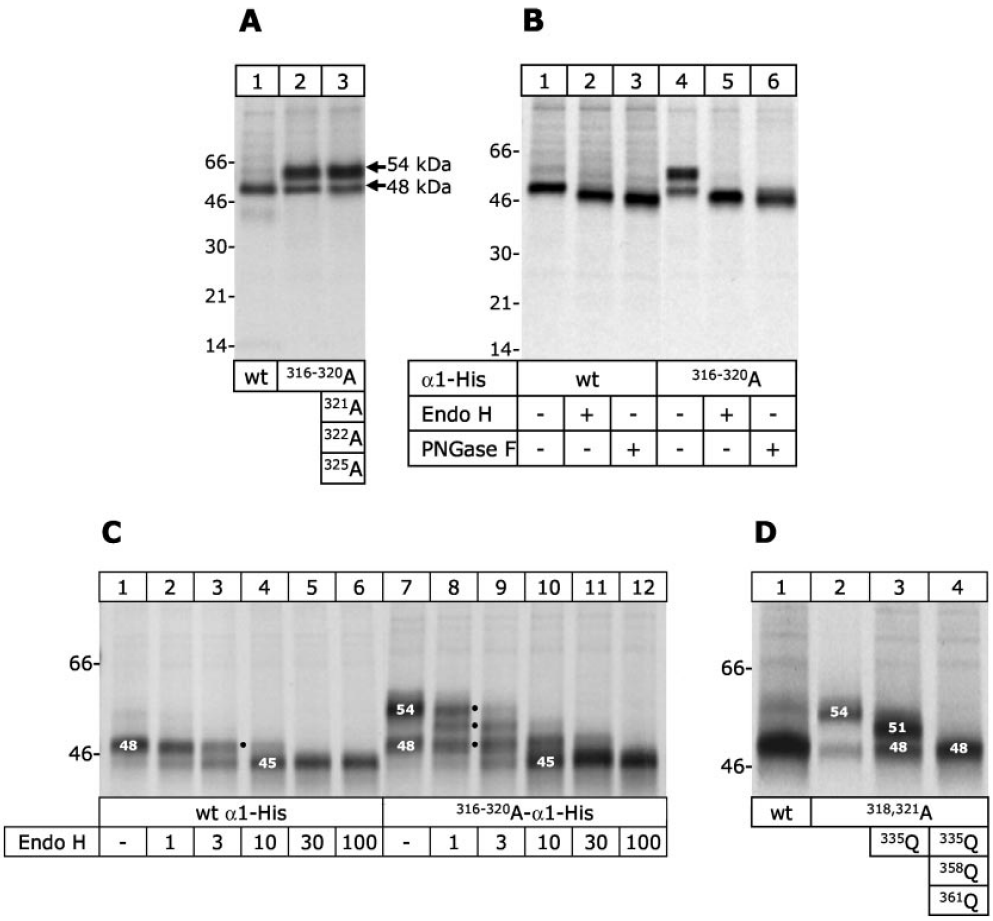

FIG. 2. ***N*-Glycan status of GlyR α1-His subunits with neutralized basic charges downstream to M3.** Oocytes were injected with indicated cRNAs, labeled overnight with [^{35}S]methionine, and extracted with digitonin. Proteins were natively purified by Ni^{2+}-NTA-agarose chromatography, denatured with Tricine-SDS sample buffer, and resolved by reducing Tricine-SDS-PAGE (4%/10%/13% acrylamide). Autoradiographs of the gels are shown. *A*, the wild-type GlyR α1-His subunit migrates as a 48-kDa polypeptide. Neutralization of positively charged amino acids leads to the appearance of an additional 54-kDa polypeptide. *B*, the same samples as in *A* were denatured with reducing Tricine-SDS sample buffer and then incubated for 2 h with Endo H or PNGase F as indicated. The 54-kDa form of the $^{316-320}$A-α1-His mutant was reduced to the 45-kDa protein core by deglycosylation with Endo H or PNGase F. *C*, the indicated polypeptides were incubated with increasing amounts of Endo H (in percent of maximum amount of enzyme used). *D*, elimination of *N*-glycosylation sequons located in the M3-M4 loop results in mass shifts, which corroborate that the misfolded 54-kDa polypeptides carries *N*-glycans at Asn^{335} and Asn^{358} (or Asn^{361}).

M3-M4 loop could signify either that one of the closely adjacent sequons ^{358}NNS and ^{361}NTT remains unused for steric or other reasons or that acceptor Asn^{335} is exposed to the cytoplasm. To discriminate between these possibilities, we substituted Asn^{335} of the ^{318,321}A-α1-His mutant with glutamine. The ^{318,321}A-α1-His mutant behaved virtually identical to the $^{316-320}$A-α1-His mutant (Fig. 2*D*, *lane 2*) (see also below). Consistent with the occupancy of Asn^{335} of the 54-kDa form with an *N*-glycan, elimination of Asn^{335} resulted in a 3-kDa shift to 51 kDa (Fig. 2*D*, *lane 3*). After further 3-kDa shift was observed when ^{358}NNS and ^{361}NTT were simultaneously eliminated in addition to Asn^{335} (Fig. 2*D*, *lane 4*). This indicates that the two *N*-glycans of the M3-M4 loop of the 54-kDa α1-His mutant polypeptides are located at Asn^{335} and Asn^{358} (or Asn^{361}), each contributing a 3-kDa oligosaccharide side chain to the total mass of 54 kDa. Because of the highly polar nature of the amino acid residues between the end of M3 (position 307) and Asn^{335}, the simultaneous usage of both Asn^{335} and Asn^{358} (or Asn^{361}) further implies that virtually the entire M3-M4 loop was translocated into the ER lumen upon charge neutralization in mutants. Accordingly, the preceding lipophilic segment, M3, fails to integrate properly into the membrane upon neutralization of positive charges of the M3-M4 loop.

GlyRs with Mixed Topology of the M3-M4 Loop Have an Impaired Assembly Capacity and Are Unable to Leave the Endoplasmic Reticulum—To analyze the effect of a mixed topology of the M3-M4 loop on subunit assembly, we resolved natively purified α1-His mutants by BN-PAGE, a method which displays the oligomeric nature of receptor proteins (8, 32). Regardless of the number of basic charges neutralized downstream to M3, all mutants analyzed migrated as perfectly assembled homopentamers when the [^{35}S]methionine pulse was

cytoplasmic M3-M4 loop. Basic residues (Lys, Arg) are highlighted with *filled black symbols* and *white lettering*, whereas acidic residues (Glu, Asp) are highlighted in *gray*. *B* and *C*, survey about the GlyR α1 subunit mutants used in this study. Amino acid residues are designated by the single letter code with basic residues highlighted in *boldface*. *Numbers* indicated by indices correspond to positions of the mature α1 sequence, *i.e.* after cleavage of the 28-amino acid-long signal peptide. *B*, GlyR α1 subunit constructs carrying mutations solely in the M3-M4 loop. The entire sequence of the M3-M4 loop is shown without the flanking transmembrane segments M3 and M4. Charged residues were replaced by alanine, whereas asparagine was replaced by glutamine. *C*, the amino acid sequence of the hydrophobic stretches thought to represent the transmembrane segments M2 and M3 (*boxed*) are shown together with the linking sequence (M2-M3 ectodomain) and the N-terminal part of the M3-M4 loop encompassing the cluster of basic residues.

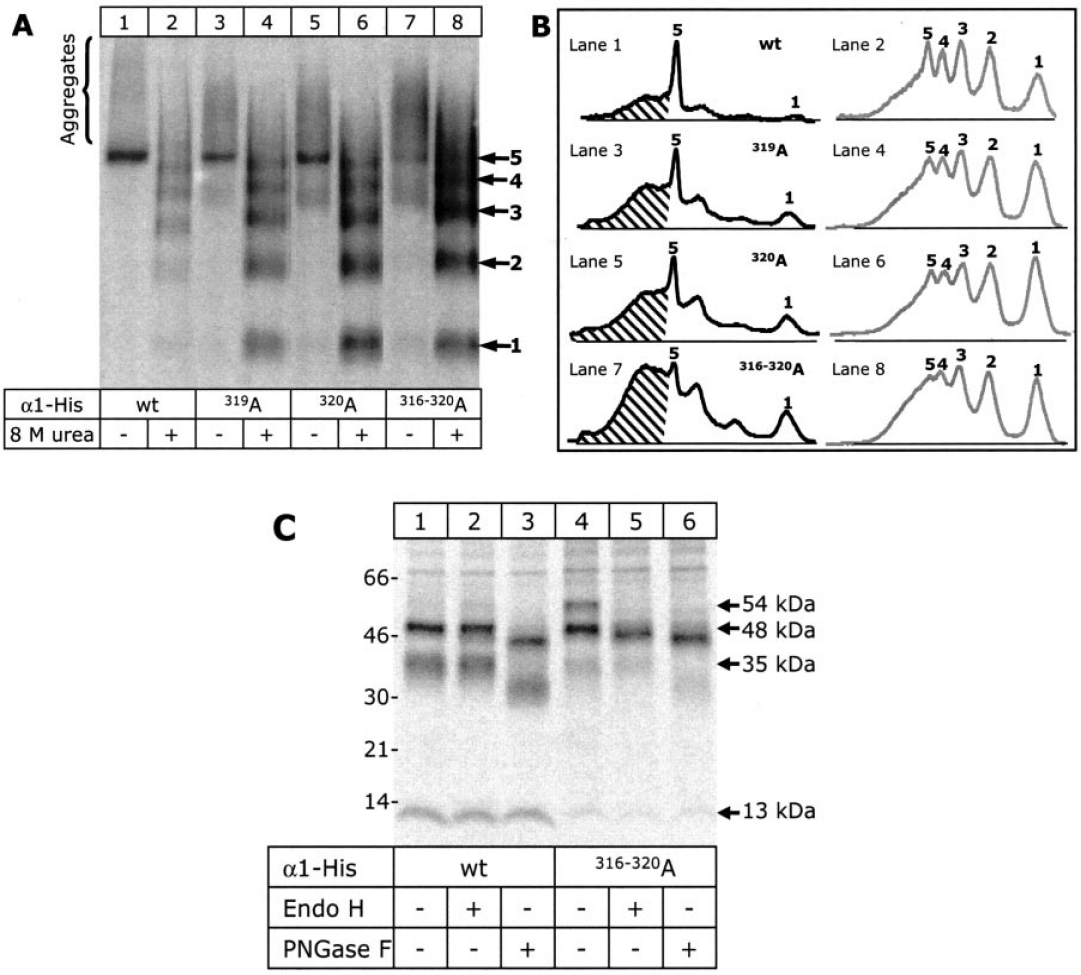

FIG. 3. **Assembly and ER exit of GlyR α1-His subunits with neutralized basic charges downstream to M3.** *A*, α1-His GlyRs natively purified from cRNA-injected oocytes immediately after a 4-h [^{35}S]methionine pulse were resolved by BN-PAGE (4–12% acrylamide). Where indicated, samples were partially denatured by a 1-h incubation at 8 M urea and 56 °C. *B*, quantitative profiles of the protein bands of the *lanes* shown in *A* obtained by PhosphorImager analysis reveal an increased propensity of the α1-His mutants to aggregate (*hatched areas*). *C*, α1-His GlyRs natively purified from cRNA-injected oocytes after a 4-h [^{35}S]methionine pulse and an additional 36-h chase interval were denatured with reducing Tricine-SDS sample buffer and then incubated for 2 h with Endo H or PNGase F as indicated. The monoglycosylated 48-kDa polypeptide was entirely Endo H-resistant, indicating that it had reached the Golgi apparatus. In contrast, the 54-kDa polypeptide persisted in the Endo H-sensitive form, consistent with retention in the ER.

followed by an overnight chase interval (results not shown). If, however, the GlyRs were purified directly after a 4-h [^{35}S]methionine pulse, a propensity of the mutants to aggregate became apparent, as indicated by the appearance of high molecular weight α1-His protein that migrated at a broad range of masses above that of the pentameric receptor (Fig. 3*A*). Quantitative scanning of the protein bands resolved by BN-PAGE showed also that the wild-type GlyR α1-His subunits existed partially in an aggregated form shortly after synthesis (Fig. 3*B*). However, the amount of aggregates was markedly higher when one charge of the basic cluster downstream of M3 was neutralized (R319A, K320A; see *lanes 3* and *5*) and increased further upon neutralization of four basic charges (RFRRK$^{316-320}$AFAAA; see *lane 7*). Most likely, these aggregates are formed primarily of α1 subunits with luminally exposed M3-M4 loop. The aggregates of both the wild-type and the mutant GlyR α1 subunits disappeared during a subsequent chase interval despite the continued presence of the hyperglycosylated 54-kDa form (not shown) (*cf.* Fig. 3*C*). Evidently, the luminally exposed M3-M4 loop delays but does not prevent proper GlyR assembly. The lack of a marked effect of the wrongly folded M3-M4 loop on assembly can be reconciled with the known location of the assembly domains of ligand-gated ion channel subunits in the N-terminal ectodomain (1).

To examine whether α1-His GlyRs with aberrantly folded M3-M4 loop are able to leave the ER, we exploited that *N*-glycans in general become complex-glycosylated and hence resistant to Endo H during passage of the Golgi apparatus *en route* to the cell surface. Accordingly, the glycosylation status of the 48- and the 54-kDa polypeptides was determined after a chase interval (Fig. 3*C*). Consistent with previous observations, the wild-type 48-kDa α1-His chain was entirely Endo H-resistant when isolated after a 24-h chase interval (Fig. 3*C*, *lane 2*). In contrast, the hyperglycosylated 54-kDa polypeptide generated from the $^{316-320}$A-α1-His construct persisted entirely in the Endo H-sensitive form, indicating that α1-His chains with aberrantly folded M3-M4 loop are incapable of leaving the ER. This view is supported by a relative decrease in the amounts of the additional 35- and 13-kDa polypeptides, which represent proteolytic cleavage products generated in a lysosomal compartment from GlyRs that are endocytotically retrieved from the cell surface, and hence are indicative of the plasma membrane insertion of

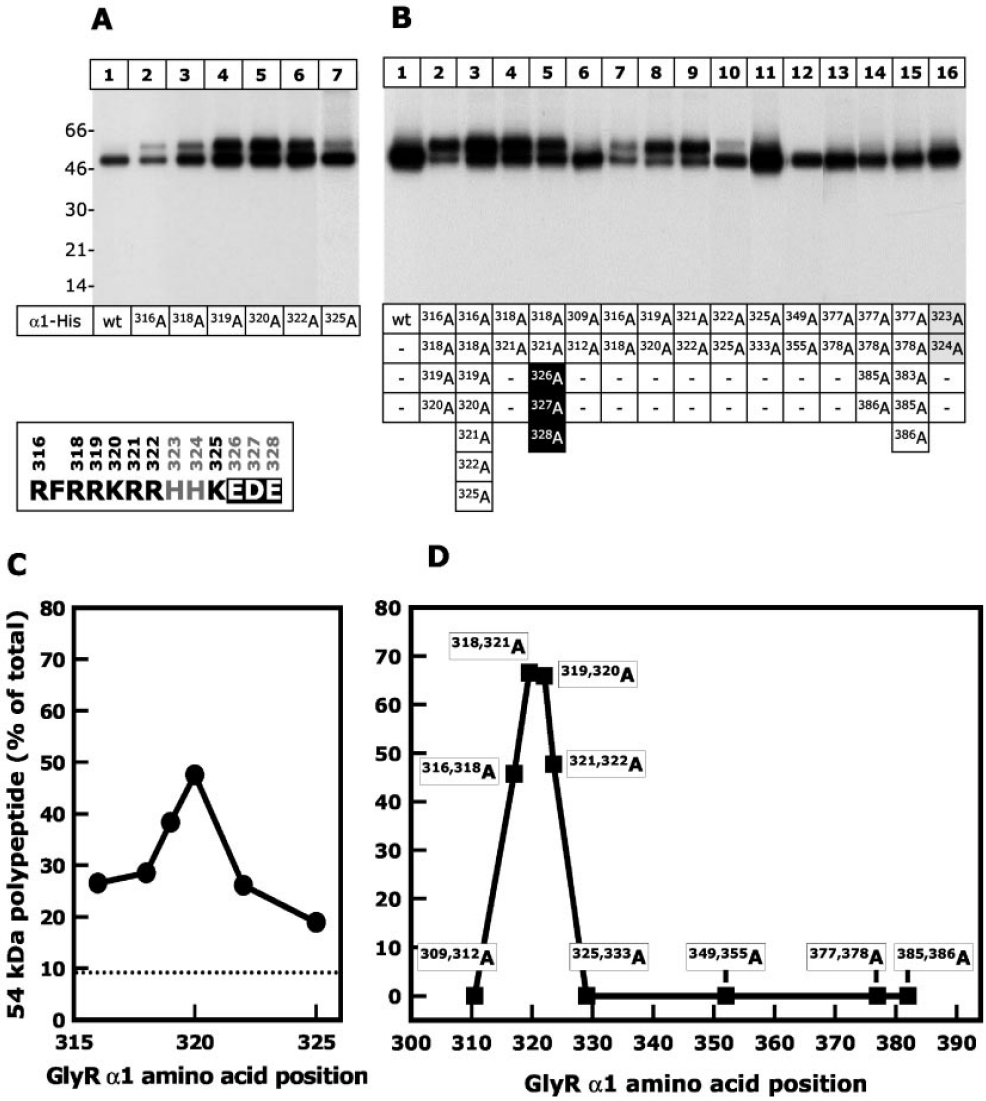

FIG. 4. **Positional effects of charged residues on M3-M4 loop topology of the GlyR α1 subunit revealed by alanine scanning mutagenesis.** cRNA injected oocytes were incubated with [^{35}S]methionine for 4 h (*A*) or 14 h (*B*) prior to extraction with digitonin. Proteins were resolved by reducing Tricine-SDS-PAGE. Autoradiographs of the gels are shown. *C* and *D*, protein bands shown in *A* or *B* were quantified by PhosphorImager analysis to determine the fraction of misfolded 54-kDa polypeptide of single mutants (*C*) and double mutants (*D*) as a function of the position of the neutralized basic residues. For the double mutants, the arithmetic mean of the amino acid position of the two mutations is plotted. The *dotted line* indicates the relative level of misfolded 54-kDa wild-type α1 subunit in these experiments.

GlyRs (33). Quantification by PhosphorImager analysis revealed that 57% of the wild-type α1-His subunit, but only 16% of the $^{316–320}$A-α1-His mutant, was proteolytically cleaved into the 35- and 13-kDa products. We conclude from these results that GlyRs with aberrantly folded M3-M4 loop are not exported to the cell surface.

Neutralization of a Single Basic Residue Downstream to M3 Is Sufficient to Disturb Topology of the M3-M4 Loop—To determine how many basic residues can be removed without disturbing membrane topology, GlyR α1 mutants with only one or two alanine substitutions in the ^{316}RFRRKRRHHK motif were generated. Surprisingly, substitution of only a single basic residue was already sufficient to create a mixed topology of the M3-M4 loop, as evidenced by the synthesis of the hyperglycosylated 54-kDa polypeptide (Fig. 4*A*). The faint 54-kDa band isolated with the parent GlyR α1-His subunit indicates that even a minor portion of the wild-type α1 subunit adopts the incorrectly folded conformation (Fig. 4*A*, *lane 1*; see also Fig. 2*D*, *lane 1*). Quantification by PhosphorImager analysis revealed that 5–10% wild-type α1 subunits possessed a luminally oriented M3-M4 loop shortly after synthesis.

Positional Effect of Basic Residues on M3-M4 Loop Topology—Quantification by PhosphorImager analysis of the 48- and 54-kDa bands revealed a striking positional effect of single charge neutralizations of the M3-M4 loop. Neutralization of Lys^{320}, located at a distance of ~12 residues from the end of the M3 domain (*cf.* Fig. 1), produced the largest effect among all single mutants investigated, with a fraction of 48% aberrantly folded 54-kDa polypeptide (Fig. 4*C*). To examine the effect of charge neutralization over the entire M3-M4 loop, a set of double mutants was generated in which two consecutive positively charged amino acids were systematically replaced by alanine. The aberrantly folded 54-kDa polypeptide was most abundant relative to the normal 48-kDa polypeptide when Arg^{318} and Arg^{321} or Arg^{319} and Lys^{320} were neutralized by alanine substitution (Fig. 4, *B* (*lane 8*) and *D*). Thus, the positive charges in the center of the basic cluster are of particular importance for the topology of the M3-M4 loop. Neutralization

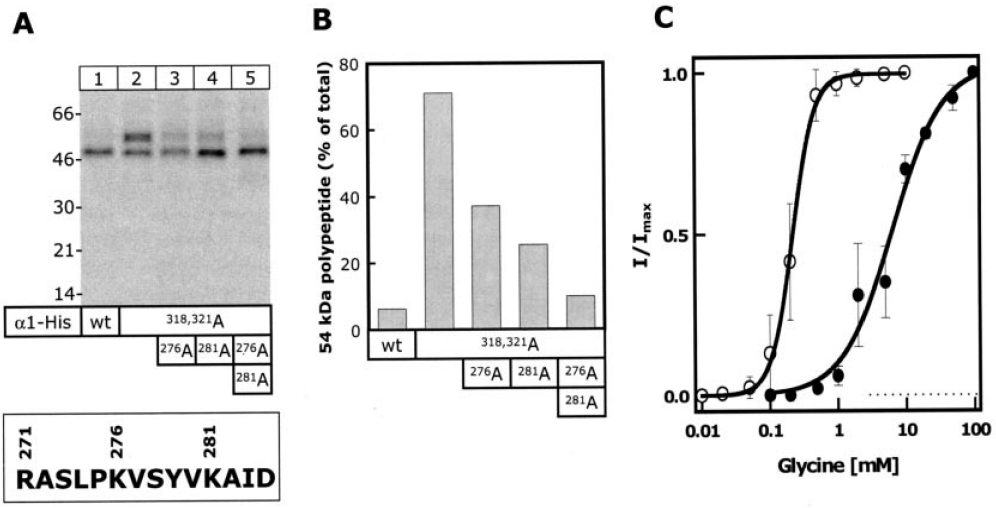

FIG. 5. **Effect of simultaneous neutralization of positive charges of the M2-M3 ectodomain and the basic cluster on the disposition of the M3-M4 loop.** *A*, cRNA-injected oocytes were pulse-labeled with [^{35}S]methionine for 4 h. Proteins were purified from digitonin extracts of these cells and resolved by reducing Tricine-SDS-PAGE. *B*, the relative amount of the misfolded 54-kDa polypeptide in *A* was quantified by PhosphorImager analysis. *C*, glycine dose-response curves. The *lines* drawn through *data points* represent non-linear fits of the Hill equation to the data, which yielded EC_{50} values of 0.22 mM (Hill coefficient of 2.7) and 6.4 mM (Hill coefficient of 1.2) for the parent ^{318,321}A-α1-His mutant (○) and the ^{276,281,318,321}A-α1-His mutant (●), respectively. *Error bars*, S.D. values of 11 (parent construct) and four (mutant) recordings in oocytes of different females.

of >two positive charges within the cluster (up to seven positive charges as in the $^{316-322,325}$A-α1-His mutant; see Fig. 4*B*, *lane 3*) did not further increase the relative amount of the 54-kDa polypeptide. Notably, charge neutralizations close to the M3 segment (Fig. 4*B*, *lane 6*) or in the C-terminal half of the M3-M4 loop (*lanes 11–14*) had only little or no effect. Even when a total of five basic residues was replaced by alanines in the C-terminal half of the M3-M4 loop, no 54-kDa polypeptide was formed (*lane 15*).

In a further attempt to assess the role of charges for the disposition of the M3-M4 loop, we used the ^{318,321}A-α1-His-mutant to also neutralize three negative charges, EDE, at positions 326–329 immediately downstream of the basic cluster. The resulting $^{318,321,326-328}$A-α1-His mutant displayed a mixed topology of the M3-M4 loop (Fig. 4*B*, *lane 5*). Quantification revealed a relative decrease of the misfolded 54-kDa polypeptide from 60% (parent ^{318,321}A-α1-His mutant) to 48% ($^{318,321,326-328}$A-α1-His mutant), indicating that increasing the net charge difference (positive charges minus negative charges) can only partially compensate for neutralization of residues within the basic cluster.

Neutralization of Basic Charges in the M2-M3 Ectodomain Rescues GlyR α1 Mutant Topology—The presence of several positive charges on both sides of a transmembrane segment can prevent its membrane insertion (34). We, therefore, considered that positively charged residues in the 14-amino acid-long hydrophilic loop connecting M2 and M3 may impede membrane insertion of M3 in our charge neutralization mutants. Indeed, alanine substitution of one of these charges, Lys^{276} or Lys^{281} (Fig. 1*C*), markedly reduced the fraction of newly synthesized ^{318,321}A-α1-His mutant with luminal M3-M4 loop orientation (Fig. 5, *A* (*lanes 3* and *4*) and *B*). Simultaneous neutralization of both Lys^{276} and Lys^{281} almost fully abolished formation of the 54-kDa polypeptide (*lane 5*), suggesting that the basic cytoplasmic cluster C-terminal to M3 is required to counteract the three basic charges in the M2-M3 ectodomain. Two-electrode voltage-clamp measurements in oocytes demonstrated that the K276A and K281A mutations result in 29-fold decrease in glycine potency (Fig. 5*C*). A related mutation, K276A, which is associated with startle disease, a rare neurological disorder, is known to produce a similar substantial decrease in glycine sensitivity (35) by impairing the opening of the channel rather than the binding of glycine (36).

DISCUSSION

The present study shows that the correct topology of the M3-M4 loop of the GlyR α1 subunit depends on a cluster of positively charged residues, ^{316}R*X*RRKRR, immediately downstream of the hydrophobic region M3. If one or more positive charges are neutralized within this motif, the GlyR α1 subunit adopts two topologies, the correct one with the hydrophobic region M3 spanning the membrane and the connecting loop being localized cytoplasmically, and an aberrant one with M3 being non-spanning and the M3-M4 loop being translocated into the ER lumen. This indicates that the cluster of basic residues contains topogenic information. Both the correctly and the incorrectly folded α1-His subunits assembled to homopentamers, but solely homopentamers consisting of correctly folded α1 subunits were exported to the plasma membrane, suggesting that the aberrant M3-M4 loop is recognized by the cellular quality control system. Also, when in our experiments the metabolic labeling period was followed by a 20-h chase, the intensity of the aberrant 54-kDa polypeptide decreased relative to that of the correctly folded α1 subunit. Together these data indicate that incorrectly folded receptor proteins are not only unable to reach the plasma membrane but are also subject to increased proteolytic degradation. The plasma membrane-bound mutant GlyRs, on the other hand, exhibited an electrophysiological phenotype identical to that of the parent α1 GlyR, indicating that the basic charges C-terminal to M3 are not directly involved in receptor functioning.

Functional Importance of the Basic Cluster for Correct GlyR Subunit Topogenesis—According to the classic model of membrane integration of polytopic proteins, the hydrophobic M3 region should follow the lead of the preceding transmembrane segment, M2. Because M2 has a N_{cyt}-C_{exo} orientation, M3 should adopt passively the opposite N_{exo}-C_{cyt} orientation, thus acting as a stop-transfer sequence that halts further translocation of the polypeptide chain across the membrane. Here, failure of the M3 segment of 30–80% of the newly synthesized α1 chains to span the membrane was demonstrated by the aberrant *N*-glycosylation of the M3-M4 loop after neutraliza-

tion of one or more basic residues 8–14 amino acids downstream to the C-terminal end of the M3 region. This indicates that proper membrane integration of the apolar M3 region depends critically on the presence of the highly charged basic motif. A similar role of positively charged residues in halting translocation of a hydrophobic segment has been described previously (37).

There is increasing evidence for polytopic proteins that topogenic information is not restricted to the most N-terminal hydrophobic domain but spread throughout the protein (for a recent review see Ref. 27). One of the determinants is apparently the transmembrane distribution of positive charges, which prevent not only the translocation of N- and C-terminal segments (38) but also of connecting loops of polytopic membrane proteins (39). In addition, internal loops of polytopic membrane proteins have on average a higher content of positively charged residues as compared with external ones (23). The failure of the hydrophobic M3 region to integrate into the membrane after neutralization of only a single positively charged residue was nevertheless unexpected, because seven positively charged residues are left within the 15 residues flanking the C-terminal end of the hydrophobic M3 region. When considering all charges within the flanking 15-residue windows on each side of the M3 segment, there remains a marked net positive charge difference Δ(C-N) of +4 (with net charges of +2 and +6, respectively) for the single charge neutralization mutants. According to the charge difference rule, this should be more than sufficient to dictate an N_{exo}-C_{cyt} orientation of a signal anchor sequence. However, despite this excess of positive charges only a minor fraction of the M3 segment adopted the correct N_{exo}-C_{cyt} orientation, and most of the M3-M4 loop was translocated incorrectly. This is also surprising in view of an excess of 11 positive charges within the entire M3-M4 loop, which harbors a total of 20 positively and nine negatively charged residues. In conclusion, neither the charge difference rule nor the positive inside rule provide any indication for a biased topology of the apolar M3 domain subsequent to neutralization of one or several positive charges of the cluster. This suggests that the M3 segment by itself is unable to reliably halt translocation.

Positive Charges on the Short M2-M3 Ectodomain Seem to Impair the Stop-transfer Function of the Apolar M3 Segment—Hydropathy analysis based on the Kyte-Doolittle algorithm with a window of five amino acids provided no indication that the M3 domain may not be sufficiently hydrophobic to partition by itself into the lipid bilayer. From our observation that unbiased folding can be restored by neutralization of positive charges on the M2-M3 ectodomain, we infer that the positive charges on the M2-M3 ectodomain prevent the M3 domain from positioning itself correctly. The three positive amino acids of the 14-amino acid-long M2-M3 loop may impose constraints to the M3 segment to adopt a N_{cyt}-C_{exo} orientation, which is obviously incompatible with the N_{cyt}-C_{exo} orientation of the preceding M2 domain. Therefore, the hydrophobic M3 domain may remain in an unstable state unless the downstream topogenic cluster of basic residues imposes the correct N_{exo}-C_{cyt} orientation. The extreme sensitivity of M3 transmembrane orientation to neutralization of single basic residues within the ^{316}R*X*RRKRR sequence suggests that the particular high density of positive charges is essential for keeping the M3-M4 loop on the Cis-side of the membrane. Hence, the basic cluster seems to serve as an accessory cytoplasmic stop-transfer signal which, by blocking translocation of the M3-M4 loop, forces the apolar M3 segment to insert properly into the membrane. Once inserted, hydrophobic interactions with the lipid bilayer may suffice to stabilize the M3 domain in the correct N_{exo}-C_{cyt} orientation.

Positive charges appear to be more easily translocated through the ER than through bacterial membranes, most likely because of the absence of a membrane potential in the ER (23). Our findings imply that the more frequent translocation of positive charges in eukaryotic systems requires additional topogenic signals, such as the basic cluster described here. Interestingly, clusters of basic charges have been shown recently (40) by computer analysis to occur more frequently in cytoplasmic loops of proteins near the cytoplasmic membrane surface than predicted from the abundance of Arg and Lys residues. It is likely that topogenic basic clusters act through electrostatic interactions with negative charges of lipids or proteins (or both). Proteins of the translocation machinery appear not to harbor relevant charged residues (27), but anionic phospholipids, at least in prokaryotes, are determinants of membrane protein topology because of the electrostatic interaction of their head groups with arginine and lysine residues (12, 41, 42). Interestingly, successful solubilization of the GlyR but not nicotinic acetylcholine receptors has been found to depend stringently on the presence of exogenous phospholipids (43). This is consistent with a role of lipids in the conformational stabilization of GlyR subunits. Whether the topogenic basic cluster identified here contributes to phospholipid stabilization of GlyR structure by ensuring its proper topology remains to be determined.

Acknowledgments—We thank Ursula Braam and Birte Steidl for technical assistance.

REFERENCES

1. Kuhse, J., Betz, H., and Kirsch, J. (1995) *Curr. Opin. Neurobiol.* **5,** 318–323
2. Harvey, R. J., and Betz, H. (2000) in *Handbook of Experimental Pharmacology* (Endo, M., Kurachi, Y., and Mishina, M., eds) Vol. 147, pp. 479–497, Springer-Verlag, Berlin
3. Langosch, D., Thomas, L., and Betz, H. (1988) *Proc. Natl. Acad. Sci. U. S. A.* **85,** 7394–7398
4. Kuhse, J., Laube, B., Magalei, D., and Betz, H. (1993) *Neuron* **11,** 1049–1056
5. Schmieden, V., Grenningloh, G., Schofield, P. R., and Betz, H. (1989) *EMBO J.* **8,** 695–700
6. Akagi, H., Hirai, K., and Hishinuma, F. (1991) *FEBS Lett.* **281,** 160–166
7. Kuhse, J., Schmieden, V., and Betz, H. (1990) *J. Biol. Chem.* **265,** 22317–22320
8. Griffon, N., Büttner, C., Nicke, A., Kuhse, J., Schmalzing, G., and Betz, H. (1999) *EMBO J.* **18,** 4711–4721
9. Blobel, G. (1980) *Proc. Natl. Acad. Sci. U. S. A.* **77,** 1496–1500
10. Rapoport, T. A., Jungnickel, B., and Kutay, U. (1996) *Annu. Rev. Biochem.* **65,** 271–303
11. Von Heijne, G., and Gavel, Y. (1988) *Eur. J. Biochem.* **174,** 671–678
12. van Klompenburg, W., Nilsson, I., Von Heijne, G., and de Kruijff, B. (1997) *EMBO J.* **16,** 4261–4266
13. Andersson, H., and Von Heijne, G. (1994) *EMBO J.* **13,** 2267–2272
14. Andersson, H., Bakker, E., and Von Heijne, G. (1992) *J. Biol. Chem.* **267,** 1491–1495
15. Nilsson, I., and Von Heijne, G. (1990) *Cell* **62,** 1135–1141
16. Hartmann, E., Rapoport, T. A., and Lodish, H. F. (1989) *Proc. Natl. Acad. Sci. U. S. A.* **86,** 5786–5790
17. Sato, T., Sakaguchi, M., Mihara, K., and Omura, T. (1990) *EMBO J.* **9,** 2391–2397
18. Wahlberg, J. M., and Spiess, M. (1997) *J. Cell Biol.* **137,** 555–562
19. Goder, V., Bieri, C., and Spiess, M. (1999) *J. Cell Biol.* **147,** 257–266
20. Wessels, H. P., and Spiess, M. (1988) *Cell* **55,** 61–70
21. Lipp, J., Flint, N., Haeuptle, M. T., and Dobberstein, B. (1989) *J. Cell Biol.* **109,** 2013–2022
22. Harley, C. A., and Tipper, D. J. (1996) *J. Biol. Chem.* **271,** 24625–24633
23. Gafvelin, G., Sakaguchi, M., Andersson, H., and Von Heijne, G. (1997) *J. Biol. Chem.* **272,** 6119–6127
24. Wilkinson, B. M., Critchley, A. J., and Stirling, C. J. (1996) *J. Biol. Chem.* **271,** 25590–25597
25. Beltzer, J. P., Fiedler, K., Fuhrer, C., Geffen, I., Handschin, C., Wessels, H. P., and Spiess, M. (1991) *J. Biol. Chem.* **266,** 973–978
26. Andrews, D. W., Young, J. C., Mirels, L. F., and Czarnota, G. J. (1992) *J. Biol. Chem.* **267,** 7761–7769
27. Goder, V., and Spiess, M. (2001) *FEBS Lett.* **504,** 87–93
28. Schmalzing, G., Gloor, S., Omay, H., Kröner, S., Appelhans, H., and Schwarz, W. (1991) *Biochem. J.* **279,** 329–336
29. Nicke, A., Bäumert, H. G., Rettinger, J., Eichele, A., Lambrecht, G., Mutschler, E., and Schmalzing, G. (1998) *EMBO J.* **17,** 3016–3028
30. Schägger, H., and von Jagow, G. (1987) *Anal. Biochem.* **166,** 368–379
31. Schägger, H., Cramer, W. A., and von Jagow, G. (1994) *Anal. Biochem.* **217,** 220–230
32. Nicke, A., Rettinger, J., Mutschler, E., and Schmalzing, G. (1999) *J. Recept.*

Signal. Transduct. Res. **19,** 493–507
33. Büttner, C., Sadtler, S., Leyendecker, A., Laube, B., Griffon, N., Betz, H., and Schmalzing, G. (2001) *J. Biol. Chem.* **276,** 42978–42985
34. Gafvelin, G., and Von Heijne, G. (1994) *Cell* **77,** 401–412
35. Langosch, D., Laube, B., Rundstrom, N., Schmieden, V., Bormann, J., and Betz, H. (1994) *EMBO J.* **13,** 4223–4228
36. Lewis, T. M., Sivilotti, L. G., Colquhoun, D., Gardiner, R. M., Schoepfer, R., and Rees, M. (1998) *J. Physiol* **507,** 25–40
37. Kuroiwa, T., Sakaguchi, M., Mihara, K., and Omura, T. (1991) *J. Biol. Chem.* **266,** 9251–9255
38. Zhang, J. T., Lee, C. H., Duthie, M., and Ling, V. (1995) *J. Biol. Chem.* **270,** 1742–1746
39. Sato, M., and Mueckler, M. (1999) *J. Biol. Chem.* **274,** 24721–24725
40. Juretic, D., Zoranic, L., and Zucic, D. (2002) *J. Chem. Inf. Comput. Sci.* **42,** 620–632
41. Gallusser, A., and Kuhn, A. (1990) *EMBO J.* **9,** 2723–2729
42. Bogdanov, M., Heacock, P. N., and Dowhan, W. (2002) *EMBO J.* **21,** 2107–2116
43. Pfeiffer, F., and Betz, H. (1981) *Brain Res.* **226,** 273–279

FEBS Letters 575 (2004) 52–58 FEBS 28779

Assembly of nicotinic α7 subunits in *Xenopus* oocytes is partially blocked at the tetramer level

Annette Nicke[1,2], Heike Thurau[1], Sven Sadtler, Jürgen Rettinger[3], Günther Schmalzing*

Department of Molecular Pharmacology, Medical School of the Technical University of Aachen, Wendlingweg 2, D-52074 Aachen, Germany

Received 5 June 2004; revised 11 August 2004; accepted 12 August 2004

Available online 28 August 2004

Edited by Maurice Montal

Abstract The assembly of nicotinic α1β1γδ, α3β4, and α7 receptors and 5-hydroxytryptamine 3A ($5HT_3A$) receptors was comparatively evaluated in *Xenopus* oocytes by blue native PAGE analysis. While α1β1γδ subunits, α3β4 subunits, and $5HT_3A$ subunits combined efficiently to pentamers, α7 subunits existed in various assembly states including trimers, tetramers, pentamers, and aggregates. Only α7 subunits that completed the assembly process to homopentamers acquired complex-type carbohydrates and appeared at the cell surface. We conclude that *Xenopus* oocytes have a limited capacity to guide the assembly of α7 subunits, but not $5HT_3A$ subunits to homopentamers. Accordingly, ER retention of imperfectly assembled α7 subunits rather than inefficient routing of fully assembled α7 receptors to the cell surface limits surface expression levels of α7 nicotinic acetylcholine receptors.

Keywords: Blue native PAGE; α7 Nicotinic acetylcholine receptor subunit; 5-Hydroxytryptamine receptor subunit; Quaternary structure; Sucrose density centrifugation

1. Introduction

The cation-conductive nicotinic acetylcholine receptors (nAChRs) are members of the cys-loop superfamily of ligand-gated ion channels (LGICs) that includes the closely related 5-hydroxytryptamine type 3 ($5HT_3$) receptors as well as the anion-permeable inhibitory γ-aminobutyric acid receptors and glycine receptors (GlyRs). Neuromuscular junction nAChRs are pentamers composed of four homologous gene products with a stoichiometry of $(\alpha1)_2\beta1\gamma\delta$ (fetal) or $(\alpha1)_2\beta1\varepsilon\delta$ (adult). In the mammalian nervous system, an additional repertoire of at least 11 nAChR gene products exists comprising eight α (α2–α7, α9, α10) and three β subunits (β2–β4) [1–3].

All nAChRs are thought to share a pentameric structure, in which homologous subunits surround a central aqueous pore whose opening and closing is regulated by neurotransmitter binding. When reconstituted in expression systems, most α subunits (α2–α6) need to heteropolymerize with at least one of the β subunit isoforms to form functional nAChRs, yielding multiple heterogeneous receptor assemblies with distinct pharmacological and functional phenotypes [1–3]. α7 and α9 subunits differ from other mammalian nAChRs subunits in their capacity to form evidently homomeric acetylcholine-gated ion channels when expressed in *Xenopus* oocytes [4–6], and certain cells of neuronal origin such as SH-SY5Y cells [7], GH_4C_1 cells [8], and PC12 cells [9,10]. The existence of endogenous α7 homopentamers has been convincingly demonstrated in a PC12 cell line and rat brain [11,12]. Transient transfection of non-neuronal cell lines with α7 subunit cDNA, however, resulted in little or no production of functional nAChRs, although high levels of α7 mRNA and α7 protein were observed [10,13]. Also certain neuronal cell lines, including those PC12 cells which lack endogenous α7 nAChRs, did not produce functional nAChRs from transfected α7 cDNA [9]. Apparently, the formation of functional nAChRs from α7 subunits requires cellular factors aiding in receptor assembly, maturation and/or stabilization [9,13–16] that occur only in a subset of cells. Cell-specific receptor formation is not found with homooligomeric $5HT_3A$ or GlyR α1 receptors.

In this study, we used the blue native PAGE technique to compare the assembly behavior of α7 subunits and $5HT_3A$ subunits in *Xenopus* oocytes. Among the members of the nicotinic superfamily, the $5HT_3A$ subunit is most closely related with the α7 nAChR subunit [17], with which it shares 51% amino acid sequence homology (28% sequence identity). We find that a majority of α7 subunits forms homotetramers and aggregates in *Xenopus* oocytes that are retained in the ER, whereas $5HT_3A$ subunits assemble rapidly and completely to homopentamers. Also heteropentameric nicotinic receptors are formed productively from co-expressed muscle α1β1γδ or neuronal α3β4 subunits. Our results imply that oocytes do not have the capacity to guide the polymerization of α7 subunits with the same efficiency as of other LGIC subunits and that surface receptor expression level is limited by imperfect subunit assembly rather than by impaired routing of fully assembled α7 receptors to the cell surface.

* Corresponding author. Fax: +49-241-8082433.
E-mail address: gschmalzing@ukaachen.de (G. Schmalzing).

[1] These authors contributed equally to this work.
[2] Present address: Max Planck Institute for Brain Research, Deutschordenstrasse 46, D-60528 Frankfurt am Main, Germany.
[3] Present address: Max Planck Institute of Biophysics, Marie-Curie-Strasse 13-15, D-60439 Frankfurt am Main, Germany.

Abbreviations: LGIC, ligand-gated ion channel; GlyR, glycine receptor; $5HT_3$, 5-hydroxytryptamine; nAChR, nicotinic acetylcholine receptor

0014-5793/$22.00 © 2004 Published by Elsevier B.V. on behalf of the Federation of European Biochemical Societies.
doi:10.1016/j.febslet.2004.08.035

2. Materials and methods

2.1. cDNA constructs

Mutations were inserted using the QuikChange™ site-directed mutagenesis kit (Stratagene). Plasmids containing cDNAs encoding the rat nAChR subunits α3, α7, and β4 were kindly provided by Dr. J. Patrick [6,18,19]. The complete coding regions of these cDNAs were subcloned into vector pNKS2 [20]. A plasmid (5HT$_3$A-pSGEM) containing the cDNA for the mouse 5HT$_3$A subunit [21] was kindly provided by Dr. M. Garcia-Guzman (Max Planck Institute for Experimental Medicine, Göttingen, Germany). Double stranded oligonucleotides encoding a C terminal His tag were inserted without changing any other amino acid into restriction sites generated just before the stop codons to generate nAChR α3-His, nAChR α7-His, nAChR β4-His, and 5HT$_3$A-His. All constructs were confirmed by sequencing. Plasmids encoding the muscle type rat nAChR α1-His subunit with a C-terminal hexahistidyl tag (His) as well as the non-tagged β1, γ and δ subunits were available from previous studies [22,23].

2.2. Expression of LGIC subunits in Xenopus laevis oocytes

Completely defolliculated oocytes were obtained by collagenase treatment [24] and maintained in sterile frog Ringer's solution (ORi: 90 mM NaCl, 1 mM KCl, 1 mM $CaCl_2$, 1 mM $MgCl_2$, and 10 mM HEPES, pH 7.4) supplemented with 50 μg/ml of gentamycin. Two-electrode voltage-clamp recordings were performed as described previously [23,25]. nAChRs and 5HT$_3$A receptors were activated by 200 μM (−)nicotine (hydrogen tartrate salt) or 10 μM serotonin (both from Sigma–Aldrich, Taufkirchen, Germany), respectively, in nominally Ca^{2+}-free ORi solution (designated Mg-ORi) to avoid Ca^{2+} activation of endogenous Cl-channels. The holding potential was −60 mV in all experiments.

For radiolabeling, cRNA-injected oocytes and non-injected control oocytes were incubated overnight with L-[^{35}S]methionine (>40 TBq/mmol, Amersham Biosciences) at ~25 MBq/ml in ORi (~0.1 MBq/oocyte). For selective labeling of plasma membrane bound proteins, cRNA-injected oocytes were kept for 3 days at 19 °C and then labeled with freshly radioiodinated (Na^{125}I, Amersham Biosciences) sulfo-succinimidyl-3-(4-hydroxyphenyl)proprionate (^{125}I-sulfo-SHPP) [26].

2.3. Ni^{2+}–NTA affinity chromatography, blue native PAGE and SDS–PAGE

Proteins were purified under non-denaturing conditions from digitonin or dodecylmaltoside extracts of radiolabeled oocytes in the presence of iodoacetamide and resolved by blue native PAGE as described previously [24,27]. For SDS–PAGE, proteins were denatured for 10 min at 37 °C with SDS sample buffer containing 20 mM dithiothreitol (DTT), and then electrophoresed in parallel with [^{14}C]-labeled molecular mass markers (Rainbow, Amersham Biosciences) on SDS–polyacrylamide gels. To investigate the glycosylation status, samples were treated for 1–2 h with either endoglycosidase H (Endo H) or PNGase F (New England Biolabs) in the presence of reducing SDS sample buffer supplemented with 1% (w/v) NP-40 to counteract SDS inactivation of PNGase F. Experiments were repeated at least three times with consistent results except of radioiodinations, which were reproduced only once.

2.4. Velocity gradient centrifugation

Metabolically labeled oocytes expressing α7-His or 5HT$_3$A-His LGICs were extracted with 1% digitonin as above. Cleared detergent extract (0.2 ml) was loaded atop of 11 ml of a 10–30% (w/v) linear sucrose gradient containing 150 mM NaCl, 50 mM Tris/HCl, pH 7.4, and 0.05% digitonin, and centrifuged at 40 000 rpm (~200 000*g*) for 16 h in a SW 41 Ti rotor (Beckman). 0.5-ml Gradient fractions were collected from the bottom of the tube and subjected to Ni^{2+}–NTA agarose affinity chromatography as above. Bound proteins were released by incubation with 250 mM imidazole/HCl, pH 7.4, and 1% digitonin, treated with the appropriate PAGE sample buffer, and resolved on both blue native PAGE gels and SDS–PAGE gels.

3. Results

3.1. Unlike 5HT$_3$A subunits, α7 subunits assemble inefficiently to homopentamers

The functional expression of the muscle type (αl-His)β1γδ nAChR, neuronal (α3-His)β4 and α7-His nAChRs, and 5HT$_3$A-His receptors in *Xenopus* oocytes was confirmed by two-electrode voltage-clamp electrophysiology. The introduction of a C terminal hexahistidine tag into the α7 subunit did not affect the shape of the current trace (Fig. 1A), but resulted in a ~25% reduction of the average current amplitude (Fig. 1B). Absolute amplitudes of the homomeric α7-His nAChR-mediated current of <0.6 μA were small when compared to >25 μA mediated by homomeric 5HT$_3$A-His receptors under equivalent conditions.

To assess the oligomeric state of the 5HT$_3$A-His and α7-His subunits, we exploited the blue native PAGE technique, which has been demonstrated to have the capacity to display the pentameric nature of other members of the nicotinic receptor superfamily such as the inhibitory $(\alpha_1)_5$ glycine receptor [28,29] and the muscle type $(\alpha1)_2\beta1\gamma\delta$ nAChR [23,24] (see also Fig. 2A, lanes 7–8). Also, recombinant 5HT$_3$A-His subunits isolated under non-denaturing conditions from *Xenopus* oocytes migrated predominantly as a single defined oligomer (Fig. 2A, lane 4). To display the number of 5HT$_3$A-His subunits incorporated in this oligomer, we exposed it to 8 M urea or 0.1% SDS to weaken non-covalent subunit interactions, thus inducing a dissociation into lower order intermediates. Consistent with the remarkable stability of LGIC complexes, these treatments did not lead to a complete dissociation into monomers, but generated a ladder of five bands, which

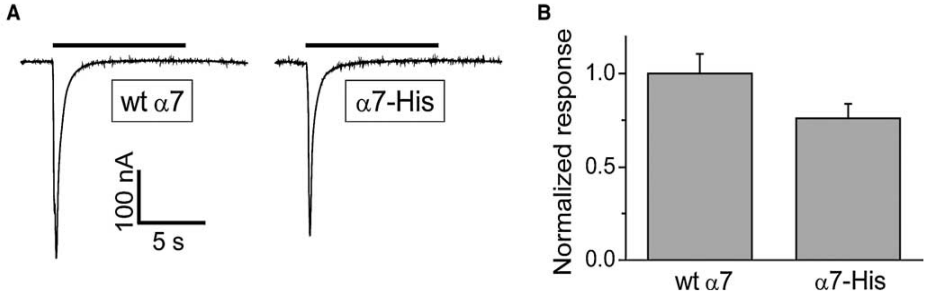

Fig. 1. Functional characterization of His-tagged α7 nAChR expressed in *Xenopus* oocytes. (A) Shown are typical current traces elicited at a holding potential of −60 mV by saturating test pulses of 200 μM nicotine (horizontal lines) in Mg-ORi two days after injection of the indicated cRNAs. (B) Bars are means ± S.E.M. of normalized current responses from two independent experiments, each with five oocytes per α7 type (unity corresponds to 340 ± 53 nA).

consisted of one, two, three, four and a maximum of five copies of the $5HT_3A$ subunit (Fig. 2A, lanes 5–6). Accordingly, the bulk amount of the non-treated $5HT_3A$ oligomer (lane 4) must be a pentamer, in agreement with previous studies [30,31]. The sole additional protein band resolved by blue native PAGE in the non-dissociated sample represents a minor

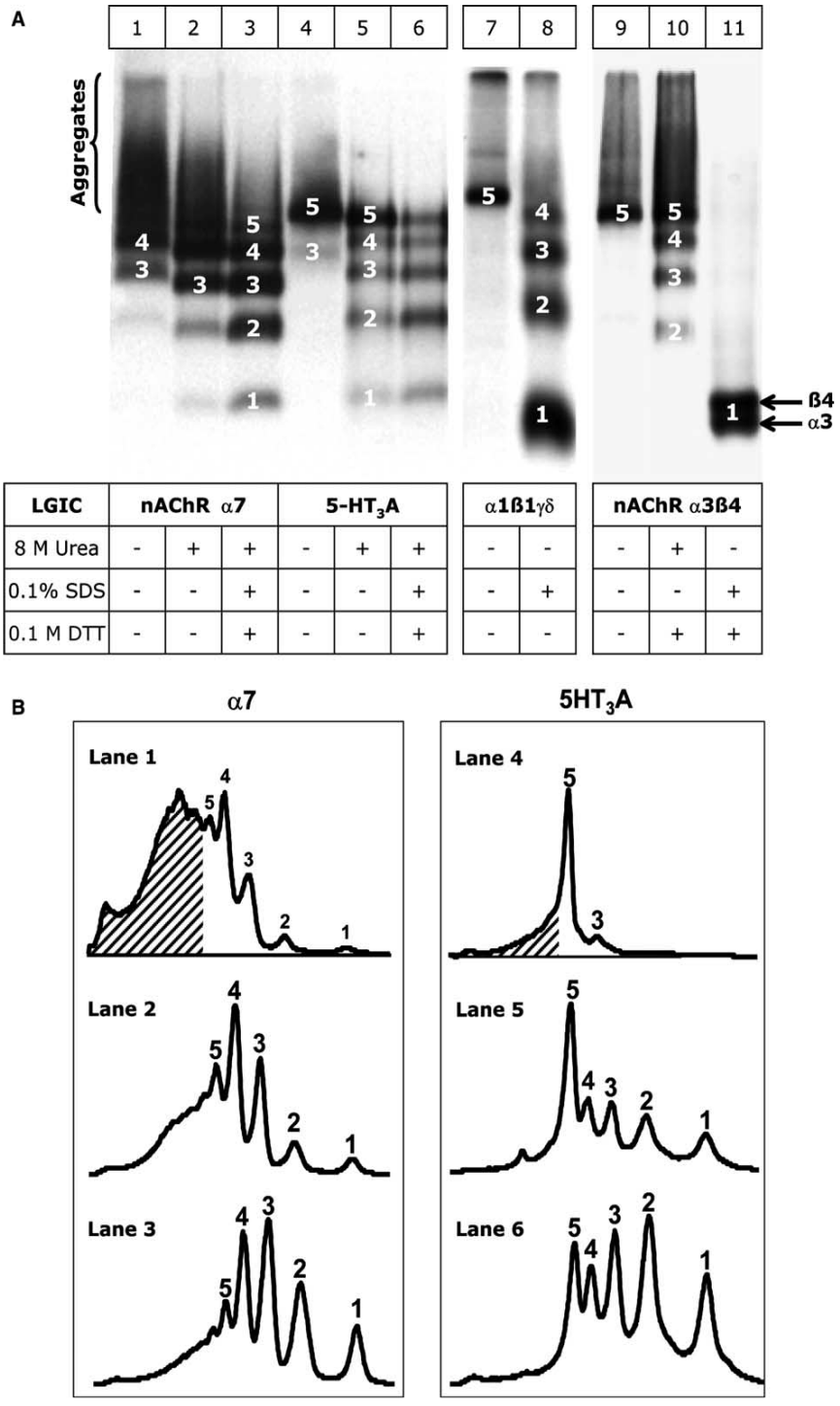

LGIC	nAChR α7			5-HT$_3$A			α1ß1γδ		nAChR α3ß4		
8 M Urea	-	+	+	-	+	+	-	-	-	+	-
0.1% SDS	-	-	+	-	-	+	-	+	-	-	+
0.1 M DTT	-	-	+	-	-	+	-	-	-	+	+

Fig. 2. Assembly state of homomeric nAChR α7-His and $5HT_3A$-His subunits and heteromeric nAChR subunit combinations shortly after their synthesis. (A) *Xenopus* oocytes were injected with cRNAs for His-tagged α subunits and non-tagged accessory subunits as indicated. After [^{35}S]methionine labeling, LGICs were natively purified from digitonin or dodecylmaltoside extracts of these cells. LGICs were immediately resolved by blue native PAGE either without further treatment or after a 1 h incubation at 37 °C in the presence of 8 M urea, 0.1 M DTT or 0.1% SDS as indicated. (B) A quantitative profile of the radioactivity incorporated in the various homooligomers was established by PhosphorImager analysis of individual lanes of the blue native PAGE gel shown in (A). The origin of the abscissa corresponds to the top of the blue native PAGE gel. Numbers indicate the oligomeric state of the corresponding protein bands. Hatched areas indicate aggregated protein. Lane numbers are the same as in (A). Experiments were repeated $\geqslant 3$ times with virtually identical results.

fraction of homotrimers (cf. Fig. 2B, right panel, lane 4). The absence of significant amount of intermediate assembly states indicates that the 5HT3A receptor attained a pentameric state during or shortly after synthesis while still in the ER.

In contrast, the recombinant α7-His protein isolated directly after a 4 h [^{35}S]methionine pulse existed in several oligomeric states and also in an aggregated form as indicated by the high molecular mass proteins that migrated at a broad range of masses above that of the pentameric receptor (Fig. 2A, lane 1). By comparison with the pattern of bands produced by dissociating treatment of the α7-His protein with urea or SDS (lanes 2–3), the discrete protein bands in lane 1 could be assigned to homotrimers and homotetramers of the α7-His subunit. Quantitative scanning of the protein bands with a PhosphorImager revealed the presence of monomers, dimers, and pentamers besides the dominant homotetramer (Fig. 2B, left panel, lane 1). From the quantitative profile, it is also apparent that another significant portion of α7-His subunits is contained in aggregates larger than the homopentamer. The relative amount of oligomers and aggregates did not change significantly during a subsequent 36 h chase interval (results not shown). Quantitative scanning established further that 5HT$_3$A-His subunits are largely incorporated in a homopentameric complex directly after a 4 h pulse (Fig. 2B). Primarily, properly assembled pentameric complexes were also formed from heteromeric nAChR combinations such as muscle type α1β1γδ subunits (Fig. 2A, lanes 7 and 8) and neuronal α3β4 subunits (lanes 9–11).

To assess the oligomeric state of α7-His subunits also by a method more commonly used in this respect, digitonin extracts of LGIC-expressing oocytes were subjected to sucrose density centrifugation. His-tagged LGICs were subsequently purified by native Ni^{2+}–NTA chromatography from each sucrose fraction. Blue native PAGE analysis (Fig. 3A) resolved the 5HT$_3$A receptor protein as a uniform homopentamer of identical mass in all the sucrose fractions where it was present. In contrast, the oligomeric state of the α7-His protein displayed by blue native PAGE increased with the sucrose density of the fraction from which the protein was purified. SDS–PAGE analysis of the same samples (Fig. 3A) followed by PhosphorImager quantification (Fig. 3B) showed a much broader distribution across the sucrose gradient for the α7-His protein than for the 5HT$_3$A-His protein. A similar broad sedimentation profile was previously observed for Triton X-100-solubilized recombinant α7 nAChRs isolated from HEK293 cells [10]. The similar results obtained by either method demonstrates that blue native PAGE represents a convenient alternative for sucrose density centrifugation.

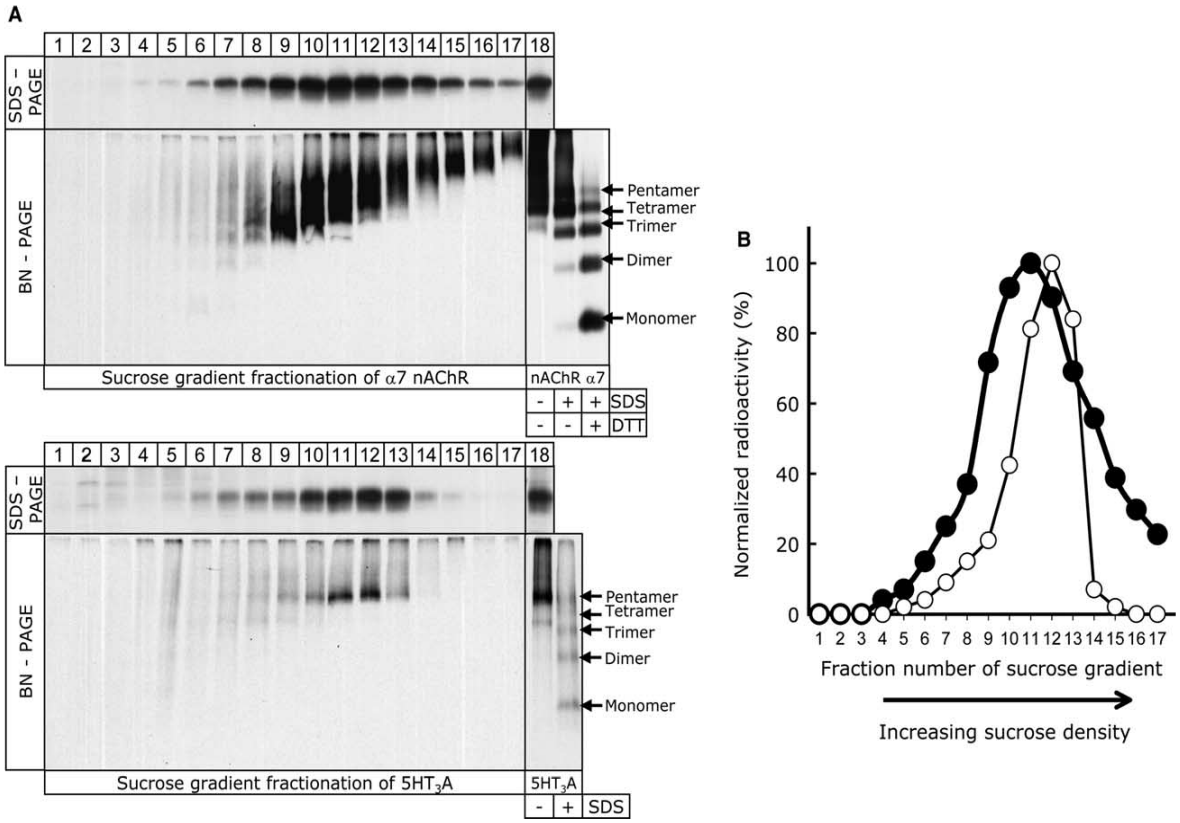

Fig. 3. Blue native PAGE and SDS–PAGE analysis of α7 nAChRs and 5HT$_3$A receptors purified from fractions derived from sucrose density centrifugation. (A) Autoradiographies of the indicated PAGE gels. LGICs purified directly from digitonin extracts of oocytes are also shown (lane 18). Samples analyzed by SDS–PAGE were denatured by reducing SDS–PAGE sample buffer before loading. (B) Radioactivity of the 5HT$_3$A-His polypeptide (○) and the α7-His polypeptide (●) as resolved by SDS–PAGE and shown in (A) was quantified by PhosphorImager analysis and normalized to the highest signal of the appropriate gel.

3.2. Solely complex-glycosylated α7 pentamers arrive at the cell surface

To allow for a direct comparison of the oligomeric state of the total pool of α7-His subunits with plasma membrane-bound α7-His subunits, α7-His protein was purified under non-denaturing conditions in parallel from surface-radioiodinated and metabolically labeled subgroups of cRNA-injected oocytes and resolved on the same blue native PAGE gel. While the metabolically labeled oocytes contained α7 subunits of different assembly states (Fig. 4A, lane 4), the plasma membrane contained exclusively homopentameric α7 nAChRs, albeit in comparably low amounts (lane 3). No intermediate bands corresponding to tetramers or lower order complexes were observed to exist at the cell surface. The muscle type $(\alpha 1)_2\beta 1\gamma\delta$ analyzed as a positive control appeared in significantly larger amounts at the cell surface (Fig. 4A, lane 2) than α7 nAChRs.

As an additional indicator for the subcellular localization of membrane proteins, we monitored the glycosylation status of the α7-His subunits. The [^{35}S]methionine-labeled α7 subunit migrated at around 63 kDa (Fig. 4B, lane 5) as compared to a protein core of 54 kDa calculated from the protein sequence. Deglycosylation with both Endo H or PNGase F resulted in a 8–9 kDa mass shift to about 55 kDa (Fig. 4B, lanes 6 and 7) consistent with the release of three high-mannose type *N*-glycans at N^{24}, N^{68}, and N^{111} of the mature α7-His polypeptide [32]. In contrast, the plasma membrane-bound α7 subunits migrated at 66 kDa and turned out to be entirely Endo H resistant (Fig. 4B, lane 5), indicating that all the α7-His subunits capable of reaching the plasma membrane acquired complex-type carbohydrates during transit of the Golgi apparatus. Accordingly, the apparent lack of Endo H-resistant complex-type α7-His subunits in metabolically labeled oocytes is consistent with the ER retention of the vast majority of α7-His subunits. As the fraction of complex-glycosylated α7-His subunits is low, their particular glycosylation status can be visualized only by selective labeling of the plasma membrane-bound pool of α7-His nAChRs.

4. Discussion

4.1. Incomplete assembly of α7 subunits in Xenopus oocytes

Many mammalian cell lines do not express functional nAChRs when transiently transfected with α7 subunits [10,33], even though α7 subunits are synthesized in substantial amounts. *Xenopus* oocytes are considered as an established exception of the rule that functional α7 nAChRs are produced by neuron-derived cells only. Accordingly, oocytes serve frequently in the analysis of electrophysiological and pharmacological properties of the homomeric α7 nAChR. We show here that α7 subunit assembly in *Xenopus* oocytes is also an only partially productive process that leads to fully assembled homopentamers, but also a large portion of homotetramers and aggregates. Both blue native PAGE analysis and sensitivity to Endo H of the oocyte expressed α7 subunits add to the view that only a limited fraction of the totally synthesized α7 subunits is able to polymerize to homopentamers capable of leaving the ER. En route to the plasma membrane, this small amount of homopentameric α7 nAChRs acquires complex-type carbohydrates in the Golgi apparatus. A majority of α7 polypeptides, however, remains trapped in the ER in the high-mannose form, apparently as a result of incomplete subunit assembly.

Incomplete homopolymerization in *Xenopus* oocytes is neither found with homooligomeric $5HT_3A$ subunits (present study) nor GlyR α1 subunits [28,29]. The small amount of $5HT_3A$ homotrimers observable directly after the [^{35}S]methionine pulse may represent a transient assembly intermediate equivalent to the αβγ trimer, which constitutes the earliest identifiable intermediate during assembly of muscle type nAChRs [23,34]. Consistent with this viewpoint, the $5HT_3A$ homotrimer disappeared completely during a subsequent chase period (unpublished results). In contrast, the relative amounts of α7 tetramers and aggregates, persisted during the chase, suggesting that a significant percentage of the α7 subunits is permanently misfolded and misassembled.

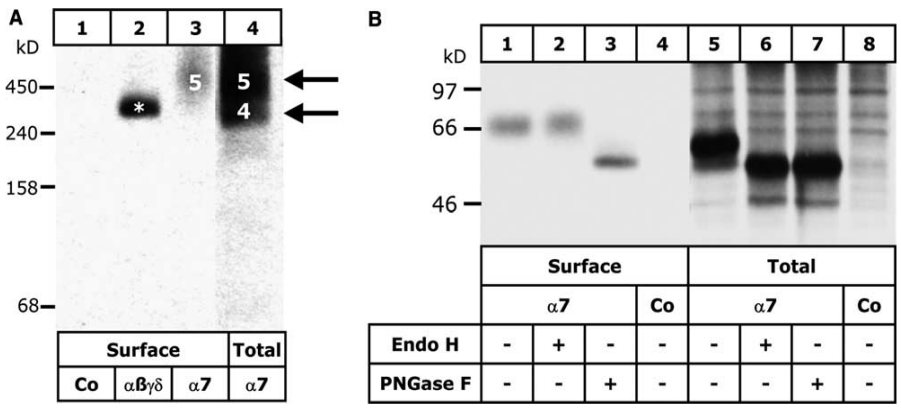

Fig. 4. Plasma membrane bound α7 nAChR is a complex-glycosylated homopentamer. (A) Three days after injection of the indicated cRNAs, oocytes were surface labeled with ^{125}I-sulfo-SHPP and extracted with digitonin. Proteins were purified under non-denaturing conditions and resolved by blue native PAGE (4–13% acrylamide). For direct comparison, α7-His protein isolated after an overnight [^{35}S]methionine pulse is also shown (lane 4). The asterisk indicates the pentameric surface-expressed muscle type nAChR, which was analyzed in parallel. (B) Glycosylation status of ^{125}I-labeled (surface) and [^{35}S]methionine-labeled (total) α7 subunits. The same samples as in (A) were denatured with reducing SDS sample buffer and then incubated for 2 h with Endo H or PNGase F as indicated. Note that the ^{125}I-labeled plasma membrane-bound α7 polypeptide is entirely Endo H resistant, whereas the [^{35}S]methionine-labeled α7 subunit is in an Endo H sensitive form. Co, non-injected control oocytes.

4.2. N-Glycan status of α7 nAChRs in Xenopus oocytes

Unexpectedly, the plasma membrane-bound α7 subunits turned out to harbor exclusively Endo H resistant, complex-type carbohydrates. In previous studies, α7 subunits were found to carry solely high-mannose type carbohydrates irrespective of whether they were isolated from native tissue, i.e., brain, or from host cells such as *Xenopus* oocytes or COS cells [32]. In our experiments, the detection of complex-type carbohydrates required the selective visualization of the plasma membrane-bound α7 nAChR by surface radioiodination. We were unable to detect complex-type α7 subunits among metabolically labeled α7 subunits, apparently because complex-glycosylated α7 subunits constitute only a minor fraction of the total α7 subunit pool. Hence, it is possible that a small amount of complex-glycosylated α7 subunits remained undetectable also in previous studies, in which the plasma membrane-bound nAChRs were not selectively labeled.

4.3. Incompletely assembled α7 nAChRs are retained by the quality control system in Xenopus oocytes

Surprisingly, the mechanisms that account for the paucity of functional α7 nAChRs at the cell surface of transiently transfected cells are cell type specific. In tsA201 cells of a human kidney epithelial cell line, α7 subunits arrive in substantial numbers as multimers at the cell surface, but neither function nor bind α-bungarotoxin [35]. COS cells, on the other hand, produce properly folded and assembled α7 nAChRs, yet these nAChRs remain located in an intracellular pool because they lack trafficking motifs needed for distribution to the plasma membrane [36]. In contrast, our results in *Xenopus* oocytes can be readily reconciled with selective retention of incompletely assembled α7 subunits by the ER quality control system [37]. A similar mechanism appears to be responsible for the low surface expression of functional α7 nAChRs in HEK293 and fibroblast QT6 cells. These cells also produce the α7 protein, but largely fail to assemble it properly, in contrast to neurons, which converted virtually all α7 subunits into nAChRs [13]. Both the need for structural subunits such as a homologous subunits, splice variants or folding isomers or specific helper proteins could explain the limited capacity of α7 subunits to polymerize. One such helper protein, RIC-3, has recently been identified to be involved in functional maturation of nAChRs in *Caenorhabditis elegans* [15].

4.4. Possible assembly pathway of α7 subunits in Xenopus oocytes

In *Xenopus* oocytes a major obstacle appears the addition of a fifth α7 subunit to the emerging receptor complex, leading to assembly block at the homotetramer level (Fig. 5 pathways A and C). Since α7 subunits must adopt two distinct conformations to assemble into functional nAChRs [35], homopentameric α7 receptors may be regarded as multimers composed of two folding isomers. In analogy to the "heterodimer" model of the assembly of the αβγδ subunits of the muscle type nAChRs [38,39], newly synthesized α7 subunits may first fold and combine to dimers of two isomers, which polymerize further to pentamers by enclosure of an unassembled α7 subunit (Fig. 5, B_1–B_3). *Xenopus* oocytes may belong to those cells in which α7 subunits fold mainly into only one conformation, and thus low levels of the second α7 folding isomer limit the formation of isomer dimers and eventually functional nAChRs. An "enclosed" tetramer may be formed preferentially and thus assembly interfaces needed for incorporation of the fifth subunit may become permanently inaccessible (Fig. 5, A_1–A_3). The incompletely assembled α7 oligomers may polymerize further giving rise to higher order oligomers that appear as undefined aggregates.

The alternative "sequential" assembly model takes into account that αβγ trimers represent the earliest assembly product of muscle type nAChRs [23,39], and could hence explain the existence of homotrimers in *Xenopus* oocytes. Trimer formation in the assembly pathway of the muscle type nAChR is

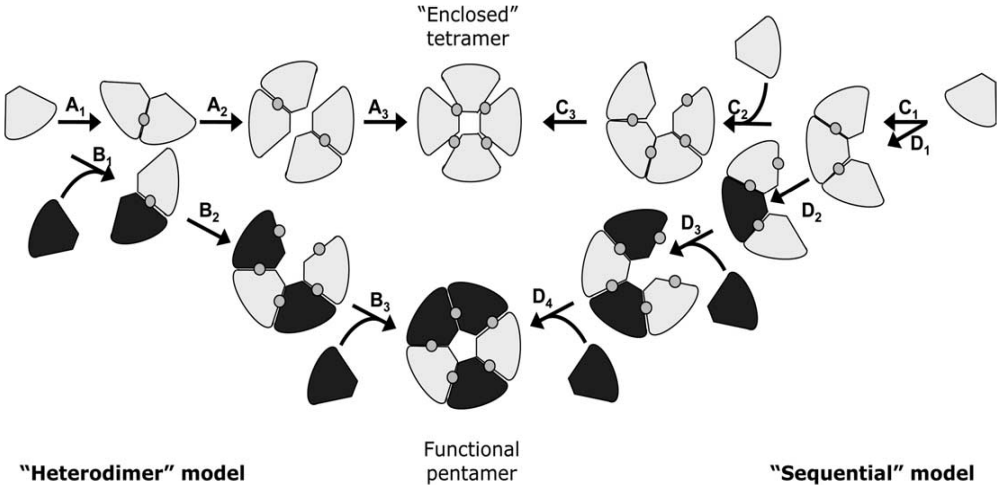

Fig. 5. Possible ER assembly pathway for α7 subunits in *Xenopus* oocytes. In analogy to the "heterodimer" model of the assembly of muscle type nAChR (for review, see [39]), functional α7 nAChRs may be formed by dimerization of two α7 dimers (B_1), each composed of two α7 folding isomers [35]. Limited availability of one of the folding isomers enables only a small portion of α7 subunits to assemble properly (B_1–B_3). The assembly of the remainder becomes blocked at the tetramer level (A_1–A_3). Alternatively, in analogy to the "sequential" model, a homotrimer may first be formed (C_1, D_1) as a prerequisite for subsequent folding steps (D_2) that generate recognition sites for the addition of the fourth and eventually the fifth α7 subunit (D_3–D_4). Like in the heterodimer model, lack of properly folded α7 subunits is proposed to block assembly at the level of the homotrimer and homotetramer (C_1–C_3). α7 folding isomers are shown in black and white; gray circles indicate subunit recognition sites.

considered as a prerequisite for subsequent slow posttranslational folding reactions of the α subunit (within the αβγ trimer) as part of a process that exposes appropriate amino acids for contact with the next incoming subunit (Fig. 5, D_1–D_4). Like in the adapted "isomer heterodimer" model above, the lack of appropriate folding isomers could explain the failure to complete the assembly process (Fig. 5, C_1–C_3). Interestingly, also the assembly of the muscle nAChR is blocked at the (αβγδ) tetramer level if a β subunit mutant is co-expressed that cannot form the cystine loop [40]. Although our data do not allow us to discriminate between the two assembly models, they provide additional support of the view that the α7 subunit itself contains insufficient information to warrant proper folding without support of cell specific helper proteins [13].

In summary, our results show that nicotinic α7 subunits are efficiently synthesized in *Xenopus* oocytes, but homopolymerize less faithfully than expected. Incomplete subunit assembly rather than a disturbed intracellular trafficking of fully assembled α7 receptors provides an explanation for why only a limited number of functional α7 nAChRs arrive at the oocyte surface. Efficient α7 nAChR formation apparently needs co-assembly with other nAChR subunit isoforms such as β2 [41] and β3 subunits [42] or support from cell type-specific chaperones that guide the assembly process.

Acknowledgements: We thank Dr. Jim Patrick for kindly providing us the neuronal nAChR plasmids. Also, we thank Dr. Cora Büttner for His-tagging of the nicotinic α7 and $5HT_3A$ cDNA constructs, and Silvia Detro-Dassen for subcloning and His-tagging of the nicotinic α3 and β4 cDNAs. This work was supported by grants of the Deutsche Forschungsgemeinschaft (Schm536/2-4, Schm536/4-1 and Ni 592/2-1).

References

[1] McGehee, D.S. and Role, L.W. (1995) Ann. Rev. Physiol. 57, 521–546.
[2] Sargent, P.B. (1993) Annu. Rev. Neurosci. 16, 403–443.
[3] Le Novere, N., Corringer, P.I. and Changeux, J.P. (2002) J. Neurobiol. 53, 447–456.
[4] Couturier, S., Bertrand, D., Matter, J.M., Hernandez, M.C., Bertrand, S., Millar, N., Valera, S., Barkas, T. and Ballivet, M. (1990) Neuron 5, 847–856.
[5] Anand, R., Peng, X. and Lindstrom, J. (1993) FEBS Lett. 327, 241–246.
[6] Séguela, P., Wadiche, J., Dineley-Miller, K., Dani, J.A. and Patrick, J.W. (1993) J. Neurosci. 13, 596–604.
[7] Puchacz, E., Buisson, B., Bertrand, D. and Lukas, R.J. (1994) FEBS Lett. 354, 155–159.
[8] Quik, M., Choremis, J., Komourian, J., Lukas, R.J. and Puchacz, E. (1996) J. Neurochem. 67, 145–154.
[9] Blumenthal, E.M., Conroy, W.G., Romano, S.J., Kassner, P.D. and Berg, D.K. (1997) J. Neurosci. 17, 6094–6104.
[10] Cooper, S.T. and Millar, N.S. (1997) J. Neurochem. 68, 2140–2151.
[11] Chen, D. and Patrick, J.W. (1997) J. Biol. Chem. 272, 24024–24029.
[12] Drisdel, R.C. and Green, W.N. (2000) J. Neurosci. 20, 133–139.
[13] Kassner, P.D. and Berg, D.K. (1997) J. Neurobiol. 33, 968–982.
[14] Helekar, S.A. and Patrick, J. (1997) Proc. Natl. Acad. Sci. USA 94, 5432–5437.
[15] Halevi, S., McKay, J., Palfreyman, M., Yassin, L., Eshel, M., Jorgensen, E. and Treinin, M. (2002) EMBO J. 21, 1012–1020.
[16] Helekar, S.A., Char, D., Neff, S. and Patrick, J. (1994) Neuron 12, 179–189.
[17] Ortells, M.O. and Lunt, G.G. (1995) Trends Neurosci. 18, 121–127.
[18] Boulter, J., Evans, K., Goldman, D., Martin, G., Treco, D., Heinemann, S. and Patrick, J. (1986) Nature 319, 368–374.
[19] Duvoisin, R.M., Deneris, E.S., Patrick, J. and Heinemann, S. (1989) Neuron 3, 487–496.
[20] Gloor, S., Pongs, O. and Schmalzing, G. (1995) Gene 160, 213–217.
[21] Maricq, A.V., Peterson, A.S., Brake, A.J., Myers, R.M. and Julius, D. (1991) Science 254, 432–437.
[22] Witzemann, V., Stein, E., Barg, B., Konno, T., Koenen, M., Kues, W., Criado, M., Hofmann, M. and Sakmann, B. (1990) Eur. J. Biochem. 194, 437–448.
[23] Nicke, A., Rettinger, J., Mutschler, E. and Schmalzing, G. (1999) J. Recept. Signal. Transduct. Res. 19, 493–507.
[24] Nicke, A., Bäumert, H.G., Rettinger, J., Eichele, A., Lambrecht, G., Mutschler, E. and Schmalzing, G. (1998) EMBO J. 17, 3016–3028.
[25] Rettinger, J. and Schmalzing, G. (2003) J. Gen. Physiol. 121, 451–461.
[26] Thompson, J.A., Lau, A.L. and Cunningham, D.D. (1987) Biochemistry 26, 743–750.
[27] Schägger, H., Cramer, W.A. and von Jagow, G. (1994) Anal. Biochem. 217, 220–230.
[28] Griffon, N., Büttner, C., Nicke, A., Kuhse, J., Schmalzing, G. and Betz, H. (1999) EMBO J. 18, 4711–4721.
[29] Büttner, C., Sadtler, S., Leyendecker, A., Laube, B., Griffon, N., Betz, H. and Schmalzing, G. (2001) J. Biol. Chem. 276, 42978–42985.
[30] Boess, F.G., Beroukhim, R. and Martin, I.L. (1995) J. Neurochem. 64, 1401–1405.
[31] Green, T., Stauffer, K.A. and Lummis, S.C. (1995) J. Biol. Chem. 270, 6056–6061.
[32] Chen, D., Dang, H. and Patrick, J.W. (1998) J. Neurochem. 70, 349–357.
[33] Rangwala, F., Drisdel, R.C., Rakhilin, S., Ko, E., Atluri, P., Harkins, A.B., Fox, A.P., Salman, S.S. and Green, W.N. (1997) J. Neurosci. 17, 8201–8212.
[34] Green, W.N. and Claudio, T. (1993) Cell 74, 57–69.
[35] Rakhilin, S., Drisdel, R.C., Sagher, D., McGehee, D.S., Vallejo, Y. and Green, W.N. (1999) J. Cell Biol. 146, 203–218.
[36] Dineley, K.T. and Patrick, J.W. (2000) J. Biol. Chem. 275, 13974–13985.
[37] Hurtley, S.M. and Helenius, A. (1989) Ann. Rev. Cell Biol. 5, 277–307.
[38] Kreienkamp, H.J., Maeda, R.K., Sine, S.M. and Taylor, P. (1995) Neuron 14, 635–644.
[39] Green, W.N. (1999) J. Gen. Physiol. 113, 163–170.
[40] Green, W.N. and Wanamaker, C.P. (1997) J. Biol. Chem. 272, 20945–20953.
[41] Khiroug, S.S., Harkness, P.C., Lamb, P.W., Sudweeks, S.N., Khiroug, L., Millar, N.S. and Yakel, J.L. (2002) J. Physiol. 540, 425–434.
[42] Jones, S., Sudweeks, S. and Yakel, J.L. (1999) Trends Neurosci. 22, 555–561.

doi:10.1016/j.jmb.2004.06.092 J. Mol. Biol. (2004) 342, 333–343

JMB

Available online at www.sciencedirect.com

SCIENCE DIRECT®

ELSEVIER

Trimeric Architecture of Homomeric $P2X_2$ and Heteromeric $P2X_{1+2}$ Receptor Subtypes

Armaz Aschrafi, Sven Sadtler, Cristina Niculescu, Jürgen Rettinger and Günther Schmalzing*

Department of Molecular Pharmacology, Technical University of Aachen Wendlingweg 2, D-52074 Aachen, Germany

*Corresponding author

Of the three major classes of ligand-gated ion channels, nicotinic receptors and ionotropic glutamate receptors are known to be organized as pentamers and tetramers, respectively. The architecture of the third class, P2X receptors, is under debate, although evidence for a trimeric assembly is accumulating. Here we provide biochemical evidence that in addition to the rapidly desensitising $P2X_1$ and $P2X_3$ receptors, the slowly desensitising subtypes $P2X_2$, $P2X_4$, and $P2X_5$ are trimers of identical subunits. Similar (heteromeric) P2X subunits also formed trimers, as shown for co-expressed $P2X_1$ and $P2X_2$ subunits, which assembled efficiently to a $P2X_{1+2}$ receptor that was exported to the plasma membrane. In contrast, $P2X_6$ subunits, which are incapable of forming functional homomeric channels in *Xenopus* oocytes, were retained in the ER as apparent tetramers and high molecular mass aggregates. Altogether, we conclude from these data that a trimeric architecture is the structural hallmark of functional homomeric and heteromeric P2X receptors.

Keywords: assembly; ligand-gated ion channels; protein–protein interactions; quaternary structure; *Xenopus* oocytes

Introduction

Ligand-gated ion channels (LGICs) serve to communicate chemical information rapidly across membranes. They achieve this by transducing the binding of extracellular ligands into a conformational change that results in the opening of an intrinsic transmembrane ion channel pore to allow for the flow of selected ions along their electrochemical gradient. On the basis of their amino acid sequences and membrane threading patterns, LGICs have been grouped into three major classes:[1,2] (i) the nicotinic acetylcholine receptor (nAChR) superfamily embracing the ionotropic receptors for acetylcholine, serotonin, glycine, and GABA (γ-aminobutyric acid); (ii) the cationic glutamate receptor (iGluR) family including AMPA (α-amino-3-hydroxyl-5-methyl-4-isoxazole propionic acid), NMDA (*N*-methyl-D-aspartate), and kainate receptors; and (iii) the ATP-gated P2X receptor family. The three LGIC classes do not share sequence homology. They possess, however, the same basic structural elements to fulfil their function such as large ligand-binding extracellular domains and smaller intracellular domains on either side of the membrane linked by transmembrane domains, some of which line the pore. Moreover, LGICs are organized by symmetric or pseudosymmetric arrangements of several subunits like their cousins, the voltage-gated channels.

To date, no 3D crystal structure of an intact member of one of the three major LGIC classes has been reported. The class I LGIC that is structurally best characterized is the nAChR at neuromuscular junctions. It consists of a pentameric barrel stave-like array of homologous subunits arranged in a circular order around a central ion channel. The overall shape and structural changes associated with nAChR activation have been visualized at 4.6 Å resolution by electron microscopy.[3] Atomic

Present addresses: A. Aschrafi, Department of Neurobiology, The Scripps Research Institute, 10550 North Torrey Pines Road, La Jolla, CA 92037, USA; J. Rettinger, Max Planck Institute of Biophysics, Marie-Curie-Strasse 13-15, D-60439 Frankfurt am Main, Germany.

Abbreviations used: ER, endoplasmic reticulum; LGIC, ligand-gated ion channels; nAChR, nicotinic acetylcholine receptor; ^{125}I-sulfo-SHPP, ^{125}I-sulfosuccinimidyl-3-(4-hydroxyphenyl)proprionate.

E-mail address of the corresponding author: gschmalzing@ukaachen.de

0022-2836/$ - see front matter

details of the ligand-binding domain have been revealed by the solved crystal structure of a soluble snail acetylcholine-binding protein that is homologous to the extracellular domain of the nAChR.[4]

iGluRs were first thought to share the pentameric architecture of the nAChRs. However, both biochemical and electrophysiological data favor the view that iGluRs form tetramers similar to K^+ channels (for references see Dingledine *et al.*[5]) Detailed structural information of the ligand-binding core is available from the crystal structure of a soluble fusion protein comprising two extracellular regions, which represent ~25% of the molecular mass of the complete subunit.[6] The ligand-binding cores tend to crystallize as dimers,[7] suggesting that the assembled tetramer represents a dimer-of-dimers.

P2X receptors open in response to extracellular ATP released from neuronal and non-neuronal cells[8] an intrinsic channel with almost equal permeability to Na^+/K^+ and a relatively high permeability to Ca^{2+}. All P2X subunits share a common membrane topology with cytosolic N and C termini, two membrane-spanning hydrophobic domains (M1 and M2), and a large intervening hydrophilic extracellular loop. On the basis of cysteine scanning mutagenesis, both M1[9] and M2[10,11] have been shown to contribute to the ion permeation pathway. Given that P2X subunits possess two transmembrane domains like inward rectifying K^+ channels, a tetrameric organization was anticipated. However, biochemical analyses of recombinant $P2X_1$ and $P2X_3$ receptors revealed an unexpected trimeric subunit organization[12] that is consistent with functional studies.[13,14]

Incorrect architectures have been initially assigned not only to iGluRs, but also to the bacterial mechanosensitive channel mscL, which was first determined by chemical cross-linking to be a hexamer, and later found by X-ray crystallography to be a pentamer.[15] It is not surprising therefore that concern about the validity of this unusual trimeric architecture of P2X receptors has been expressed,[16] and indeed, kinetic data have been reported that imply a tetrameric organization of $P2X_2$ receptors.[17] The aim of this study was to carefully re-evaluate biochemically the assembly properties and oligomeric state of slowly desensitizing homomeric P2X receptors by focusing in particular on $P2X_2$ homomers and $P2X_{1+2}$ heteromers. $P2X_6$ subunits were also studied because of their known inability to form functional homomeric receptors in *Xenopus* oocytes. In addition to blue native PAGE analysis, we used, as a novel independent approach, selective cell surface radioiodination followed by chemical cross-linking of plasma membrane-bound P2X receptors. We show that both non-desensitizing homomeric and heteromeric P2X receptors share a trimeric subunit organization with the previously described desensitising $P2X_1$ and $P2X_3$ receptors.[12]

Results

Intracellular rat and human $P2X_2$ subunits exhibit distinct assembly states

The $rP2X_2$ receptor, originally cloned from PC12 rat phaeochromocytoma cells,[18] is expressed in a variety of neurons in the peripheral and central nervous system, but also pancreas, cochlea, bone, and cardiac muscle.[16] The term $P2X_2$ distinguishes the non-desensitizing full length $P2X_2$ subunit from the desensitizing splice variant termed $P2X_{2B}$, which lacks a stretch of 69 amino acid residues C-terminal to M2.[19]

In contrast to $rP2X_1$ and $rP2X_3$ subunits,[12] the $rP2X_2$ protein did not migrate as a distinct band on the blue native PAGE gel, but mostly as an amorphous mass (Figure 1(a), lane 1). Treatment with urea (lanes 2 and 3) or low concentrations of SDS (Figure 1(b), lane 4) partially dissolved the aggregates, resulting in a ladder-like pattern of six or more bands, each spaced by the mass of a $rP2X_2$ monomer. Using this ladder as a mass marker, a trimeric state could be assigned to the faint band resolved in the non-denatured $rP2X_2$ sample (Figure 1(a), lane 1). The undefined assembly state of $rP2X_2$ subunits does not signify endoplasmic reticulum (ER) retention, as ~70% of metabolically labeled $rP2X_2$ subunits acquired Endo H resistance during an extended chase interval (results not shown).

To examine whether any other slowly desensitizing rat P2X subtype exhibits in its metabolically labelled, intracellular form an undefined assembly state, we expressed the $rP2X_2$ subtype in parallel with the receptor subtypes $rP2X_4$ and $rP2X_5$, and, in addition, the already previously studied rapidly desensitising subtypes $rP2X_1$ and $rP2X_3$ (Figure 1(b)). Because the X-ray film was partially overexposed to visualize also less prominent bands, higher order assemblies of the $rP2X_4$ receptor, most likely hexamers and nonamers, appear also as major bands. However, quantitative scanning clearly demonstrates that the trimers represent by far the predominant assembly state (scans not shown) and that an undefined assembly state is unique to $rP2X_2$ subunits.

Because of the unusual behavior of the $rP2X_2$ protein on blue native PAGE gels, we also examined its human orthologue. In striking difference to $rP2X_2$ subunits, metabolically labelled $hP2X_2$ subunits existed under virtually identical conditions in a defined assembly state (Figure 1(c), lane 1). The oligomer resisted largely to treatment with DTT (lane 2), whereas exposure to urea resulted in a dissociation into dimers (visible as a faint band) and monomers (lanes 3 and 4). Accordingly, a trimeric state can be assigned to the non-denatured $hP2X_2$ oligomer.

$rP2X_2$ receptors exist as individual homotrimers and clusters of homotrimers at the plasma membrane

Endo H resistance indicated that a major fraction

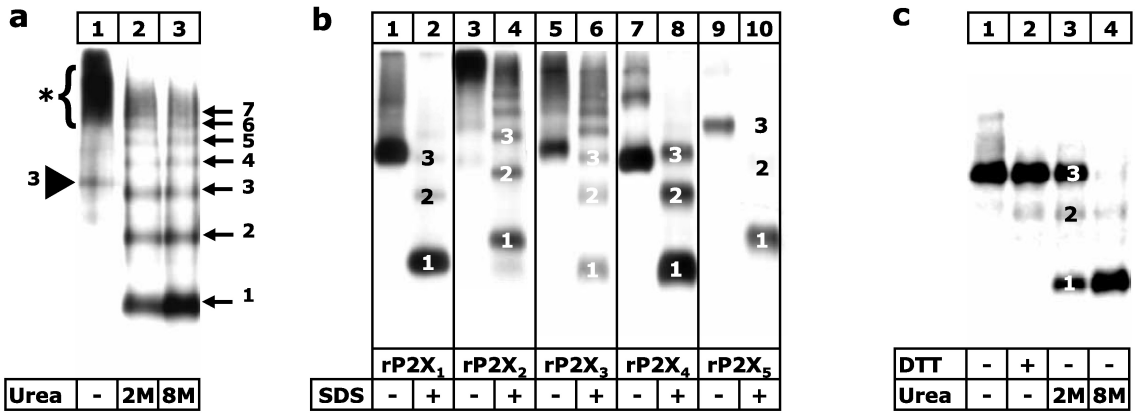

Figure 1. Undefined assembly state of intracellular rat but not human $P2X_2$ subunits. Shown is the migration on blue native PAGE gels of P2X receptors isolated after overnight [^{35}S]methionine labelling. Where indicated, samples were partially denatured by a one hour incubation at 37 °C in the presence of 2 or 8 M urea, 0.1 M DTT or 0.1% of SDS. (a) Metabolically labelled $rP2X_2$ subunits migrated as an amorphous mass of protein (asterisk) rather than in a defined assembly state except of a small amount of homotrimers (arrowhead). (b) An undefined assembly state is unique to the $rP2X_2$ subtype. (c) Under identical conditions, metabolically labelled $hP2X_2$ subunits migrated exclusively as DTT-resistant homotrimers.

of the metabolically labelled $rP2X_2$ protein was able to pass the ER quality control system. Accordingly, the undefined assembly state does not signify ER retention of aggregated $rP2X_2$ subunits. To analyze specifically the functional receptor form, which is biochemically accessible at the plasma membrane, we purified the His-$rP2X_2$ receptor from surface radioiodinated oocytes. For direct comparison, the $rP2X_1$ receptor was analyzed in parallel (Figure 2(a), lanes 2–5). The plasma membrane-bound His-$rP2X_2$ receptor migrated as several defined oligomers on blue native PAGE gels (lane 6). These oligomers resisted largely the denaturing effect of the reductant DTT (lane 8) in contrast to the His-$rP2X_1$ receptor, which dissociated readily when treated with DTT (lane 4; see also Nicke *et al.*[12]). Denaturing with urea produced $rP2X_2$ monomers, dimers, and trimers (lane 7), thus allowing us to identify the fastest migrating $rP2X_2$ oligomer as a homotrimer. Combined treatment with urea and DTT converted most of the $rP2X_2$ receptor oligomers into the monomeric form (lane 9). Resolution of the non-denatured $rP2X_2$ receptor on a lower percentage acrylamide gel (Figure 2(b), lane 1) resulted in a ladder-like pattern of three or four bands, each spaced by the mass of a $rP2X_2$ trimer. Accordingly, hexameric and nonameric states can be assigned to the higher mass oligomers. Thus, $rP2X_2$ receptors appear as homotrimers or multimers of homotrimers in the plasma membrane, whereas their intracellular assembly state appears to be less defined.

Cross-linking of plasma membrane-bound $rP2X_2$ receptors generates dimers and trimers

The experiments described above rely on the preservation of the quaternary structure of the purified rP2X receptors in digitonin. An unresolved and critical question therefore is whether functional P2X receptors include weakly bound subunits that are lost during receptor purification. To capture potentially existing loosely associated subunits, we performed the cross-linking reaction *in situ* with intact oocytes, i.e. prior to rP2X receptor purification (Figure 3(a)). Adduct formation is visible on reducing SDS-PAGE gels, which show a total of three bands at ~65, ~130, and ~190 kDa (Figure 3(b), lanes 3 and 4), corresponding in mass to the $rP2X_2$ monomer, dimer and trimer, with no bands larger than the 190 kDa band. Likewise, cross-linking of plasma membrane-bound $rP2X_1$ receptors yielded dimers and trimers, but no larger adducts (cf. Figure 4(e)). Altogether, these findings add further strong support to the view that functional $rP2X_2$ and $rP2X_1$ receptors are organized as homotrimers.

Polymerization of $rP2X_2$ and $rP2X_1$ subunits generates $rP2X_{1+2}$ heterotrimers

The $P2X_2$ subunit becomes incorporated not only into homomeric, but also in heteromeric assemblies with the $P2X_1$ subunit ($P2X_{1+2}$ receptor)[20] or the $P2X_3$ subunit ($P2X_{2+3}$ receptor).[21,22] To determine the subunit stoichiometry of heteromultimeric P2X receptors, oocytes co-expressing the hexahistidyl-tagged $rP2X_1$ subunit with the non-tagged $rP2X_2$ subunit were surface radioiodinated with [^{125}I]sulfo-SHPP. Purification of the rHis-$P2X_1$ receptor under non-denaturing conditions resulted in co-purification of non-tagged $rP2X_2$ subunits, as shown by SDS-PAGE analysis (Figure 4(a), lanes 3 and 4). Proteins isolated from oocytes expressing the His-$rP2X_1$ or the His-$rP2X_2$ subunit alone (lanes 1 and 2) or both His-tagged subunits together (lane 5) are shown to allow a direct comparison of the

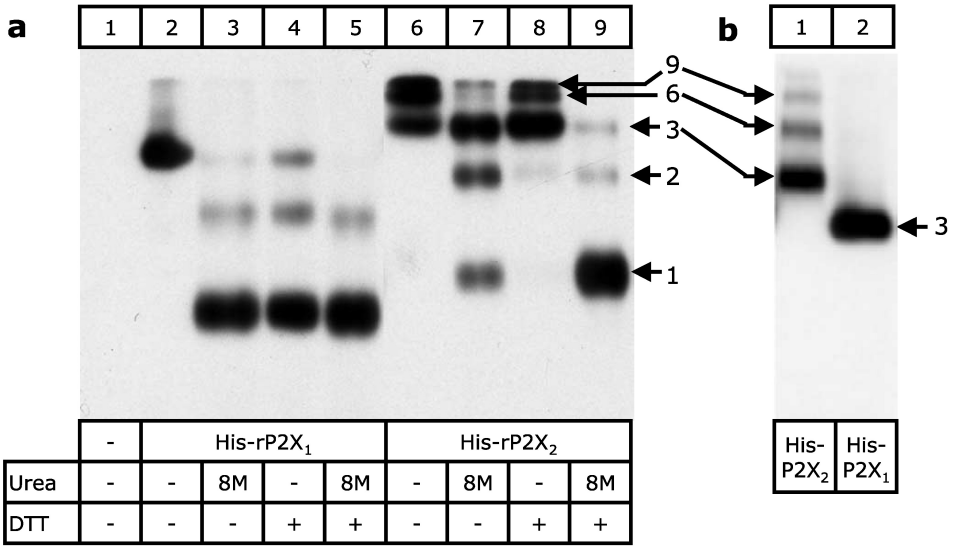

Figure 2. Plasma membrane-bound $rP2X_2$ receptors form as single and multiple homotrimers. Shown is the migration on blue native PAGE gels of the indicated P2X receptors isolated after cell surface radioiodination. (a) $rP2X_1$ and $rP2X_2$ receptors migrated in a single or several distinct assembly states, respectively. Weakening of non-covalent subunit interactions by urea or by reducing intrasubunit disulfide bonds resulted in the appearance of homodimers and monomers. DTT treatment resulted in a decrease of the higher order assemblies of the $rP2X_2$ receptor in favor of homotrimers, which, unlike $rP2X_1$ homotrimers, did not dissociate further when exposed to DTT alone. (b) A lower percentage blue native PAGE gel resolved the higher order assemblies of the $rP2X_2$ receptor as a ladder of bands, each spaced by the mass of a $rP2X_2$ trimer. Accordingly, hexameric and nonameric states can be assigned to the higher mass oligomers.

electrophoretic mobility of the different protein complexes.

The receptor isolated from oocytes co-expressing $rP2X_2$ and $rP2X_1$ subunits (Figure 4(b), lanes 3 and 4) migrated on blue native PAGE gels in between that of homotrimeric $rP2X_1$ receptors (lane 1) and homotrimeric $rP2X_2$ receptors (lane 2). Notably, oocytes co-expressing $rP2X_2$ and $rP2X_1$ subunits seemed not to contain homotrimeric $rP2X_1$ receptors, as the corresponding position of the gel did not contain protein. This suggests that heteromer formation represents the favored assembly pathway.

To display the number of subunits incorporated in the $rP2X_{1+2}$ receptor complex, we weakened non-covalent subunit interactions by exposing the isolated protein to urea or DTT. The homotrimeric $rP2X_2$ receptor required urea to dissociate partially

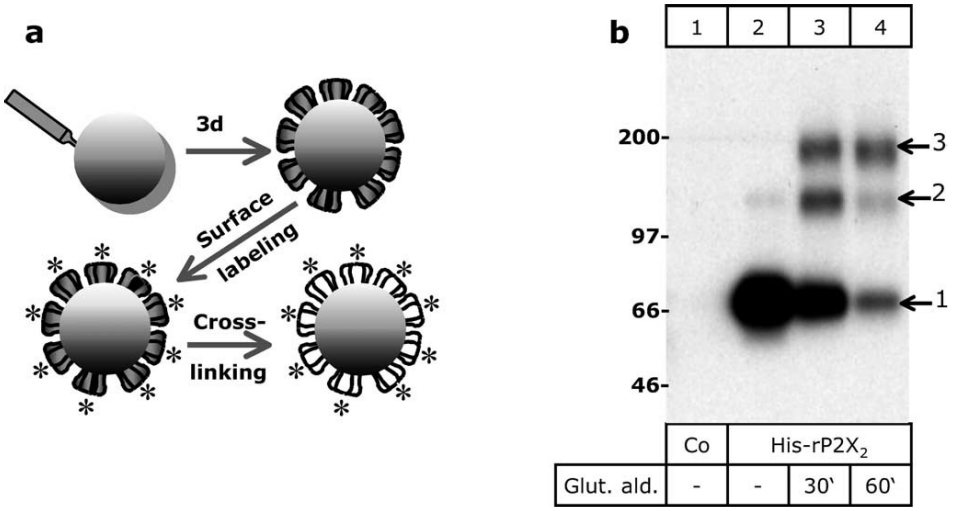

Figure 3. Cross-linking of $rP2X_2$ receptors *in situ* generated trimers as largest adducts. (a) Cartoon illustrating consecutive cell surface radioiodination and cross-linking of receptor subunits on intact P2X receptor-expressing oocytes. (b) $rP2X_2$ adducts generated by cross-linking with 100 µM glutardialdehyde for one hour on ice were resolved by reducing SDS-PAGE.

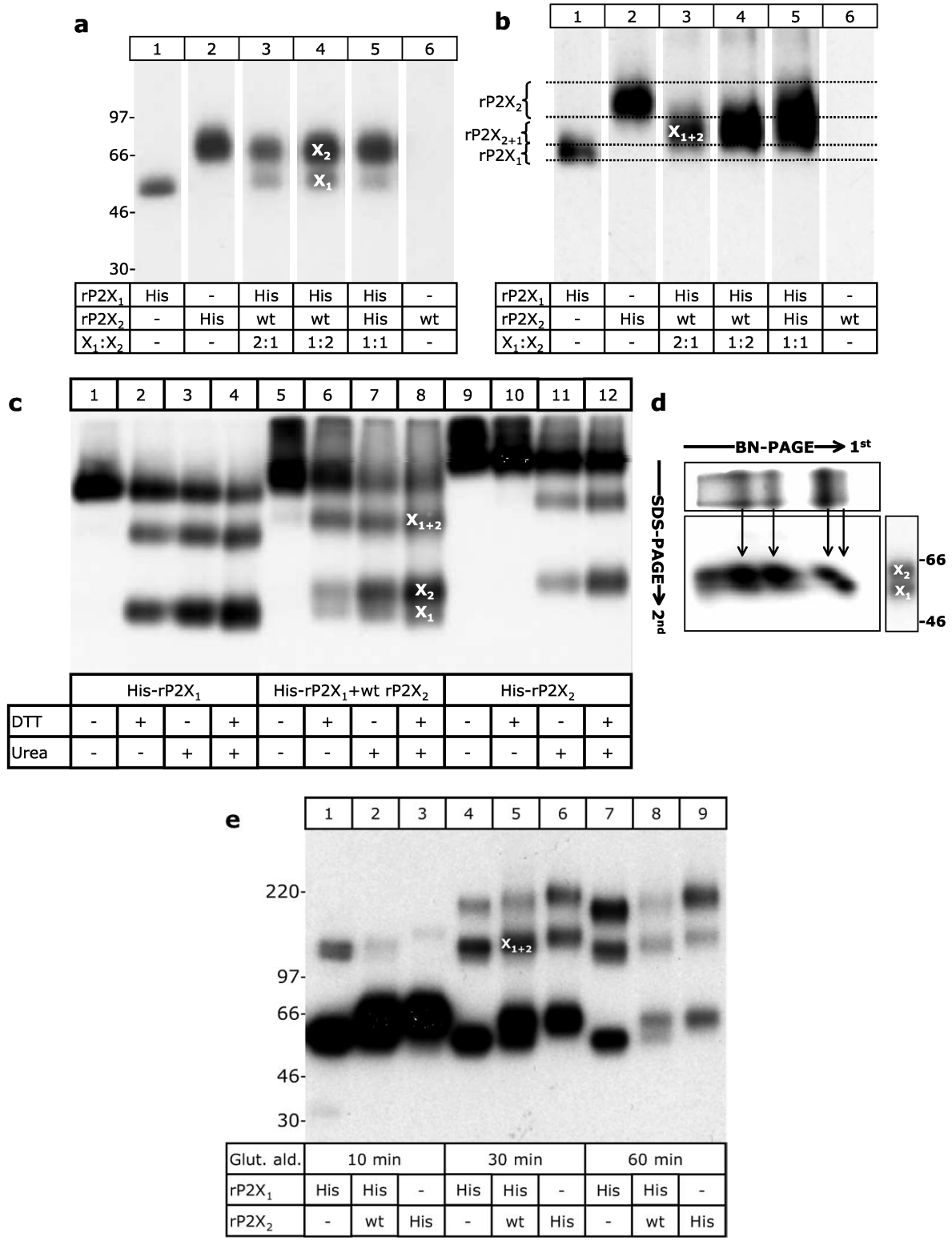

Figure 4. Plasma membrane-bound $rP2X_{1+2}$ receptors are heterotrimers. (a) SDS-PAGE analysis reveals co-purification of faster migrating His-$rP2X_1$ subunits with slower migrating non-tagged $rP2X_2$ subunits from surface-radioiodinated oocytes. A 73 amino acid residues longer polypeptide chain accounts for the larger mass of the $rP2X_2$ subunit. X1:X2, (wt/wt) ratio of co-injected cRNAs. (b) Co-expressed $rP2X_1$ and $rP2X_2$ subunits migrated as one single protein complex on the blue native PAGE gel with a mass slightly larger and smaller than the $rP2X_1$ and $rP2X_2$ homotrimers, respectively, as expected for a heteromeric protein complex composed of subunits of slightly different masses. Note the virtually exclusive formation of a $rP2X_{1+2}$ complex with no evidence for His-$rP2X_1$ homotrimers (lanes 3 and 4). (c) Weakening of subunit interactions by DTT and urea displays the homotrimeric state of $rP2X_1$ and $rP2X_2$

into dimers and monomers (Figure 4(c), lanes 9–12). In contrast, the homotrimeric $rP2X_1$ receptor (lanes 1–4) and also the heteromeric $rP2X_{1+2}$ receptor became unstable already by incubation with DTT at 37 °C (lane 5–8). Dissociation of the heteromeric $rP2X_{1+2}$ receptor produced a single defined intermediate, along with the two expected monomers, $rP2X_1$ and $rP2X_2$ (lanes 6–9). The $rP2X_{1+2}$ receptor intermediate migrated slightly slower and faster than the $rP2X_1$ and $P2X_2$ homodimers, respectively, which were run at adjacent positions of the same gel. This migration behavior identifies the $rP2X_{1+2}$ receptor intermediate as a complex of just one $rP2X_1$ and one $rP2X_2$ subunit. Reanalysis of the $rP2X_{1+2}$ receptor intermediate in the second dimension by SDS-PAGE corroborated this view by resolving two bands of ~57 kDa and ~62 kDa as expected for $rP2X_1$ and $rP2X_2$ monomers, respectively (Figure 4(d)).

To determine the quaternary structure of the hetero-assembled $rP2X_{1+2}$ receptor at the cell surface of intact *Xenopus* oocytes by an independent approach, we used surface radioiodination combined with glutardialdehyde-based *in situ* cross-linking as detailed above (cf. Figure 3(a)). SDS-PAGE analysis of the isolated cross-linked proteins revealed a total of four bands (Figure 4(e), lanes 5 and 8). The two bands migrating at ~57 kDa and ~65 kDa represent the His-$rP2X_1$ monomer and the co-isolated $rP2X_2$ monomers, respectively. The additional bands of ~117 kDa, and ~175 kDa represent adducts, which migrated in between the dimeric and trimeric adducts obtained by cross-linking of the homomeric His-$P2X_1$ and His-$P2X_2$ receptors, respectively (Figure 4(e), lanes 4 and 6). As in the blue native PAGE experiment, the cross-linking data are fully consistent with the view that $rP2X_{1+2}$ receptors are organized as trimers.

$hP2X_6$ subunits form tetramers and aggregates that are not exported to the plasma membrane of *Xenopus* oocytes

$P2X_6$ subunits are capable of heteropolymerizing with $P2X_4$ subunits,[23] yet are the sole P2X subunits that do not form as functional homomeric receptors in *Xenopus* oocytes.[16,24] Blue native PAGE analysis of the oocytes-expressed $hP2X_6$ protein revealed one major distinct protein band in addition to a slowly migrating amorphous protein mass indicative of aggregates (Figure 5(a), lane 3). Denaturing with urea resolved the aggregates and the distinct band to yield a ladder of bands, each spaced by the mass of a $hP2X_6$ monomer. Using this ladder as a mass marker, a tetrameric state could be assigned to the distinct band resolved in the non-denatured $hP2X_6$ sample (lane 4; see also Figure 5(b)). The co-analyzed $rP2X_3$ receptor and the α1 GlyR migrated as trimers (lanes 1 and 2) and pentamers (lanes 5 and 6), respectively. The $hP2X_6$ subunit was completely Endo H-sensitive after an extended chase interval (Figure 5(c)), and could not be detected to appear at the cell surface by surface radioiodination with sulfo-SHPP in experiments that showed high surface expression levels of other homomeric P2X receptors (results not shown). All these findings lend support to the hypothesis that the tetrameric $P2X_6$ complex is recognized and retained in the ER by the quality control machinery as an incorrectly assembled protein. Tetramers and aggregates were also observed for the rat ortholog, $rP2X_6$ (results not shown).

Discussion

The present study extends previous findings by showing that in addition to homomeric $P2X_1$ and $P2X_3$ receptors, natively purified $P2X_2$, $P2X_4$ and $P2X_5$ receptors and heteromeric $rP2X_{1+2}$ receptors are rather stable non-covalent assemblies of three subunits. This evaluation relies on a comparison of non-denatured and partially denatured P2X receptors on blue native PAGE gels, and, in addition, for the first time, on chemical cross-linking of plasma membrane-bound P2X receptors in the natural lipid environment of intact oocytes.

The assessment of the oligomeric organization of $rP2X_2$ receptors was unexpectedly complicated by an undefined intracellular assembly state that was not observed with any other P2X receptor. The amorphous migration of the $rP2X_2$ protein on blue native PAGE gels could signify that $rP2X_2$ subunits form aggregates and are therefore retained in the ER by quality control mechanisms. However, Endo H resistance of a large majority of $rP2X_2$ subunits clearly argues against ER retention. It is also unlikely that improperly assembled $rP2X_2$ subunits bypass the ER quality control system, as both blue native PAGE analysis and chemical cross-linking clearly indicated that all plasma membrane-bound $rP2X_2$ receptors exist in a defined assembly state of

receptors on the blue native PAGE gel. Note that the $rP2X_{1+2}$ complex dissociated into $rP2X_1$ and $rP2X_2$ monomers, and only one single intermediate, which migrated slower and faster than $rP2X_1$ and $rP2X_2$ homodimers, respectively. Consequentially, the lower order intermediate of the $rP2X_{1+2}$ receptor must be a (quite stable) heterodimer of one $rP2X_1$ and one $rP2X_2$ subunit. (d) 2D-PAGE analysis of partially dissociated $rP2X_{1+2}$ receptor complexes produced by a one hour incubation of the natively purified complexes with 8 M urea. After first dimension BN-PAGE, the lanes carrying the separated proteins were excised, polymerized into the stacking gel of a 8% SDS-PAGE gel, and then resolved in the second dimension by SDS-PAGE. (e) Cross-linking of plasma membrane-bound receptors on surface radioiodinated, intact oocytes expressing $rP2X_1$ and $rP2X_2$ subunits alone or together generated trimers as the larges adducts. Consistent with their composition of subunits of slightly different masses, the heteromeric adducts migrated in between the homodimeric and homotrimeric $rP2X_1$ and $rP2X_2$ adducts on the SDS-PAGE gel. Cross-linking was performed at 100 μM glutardialdehyde on ice for varying times as indicated.

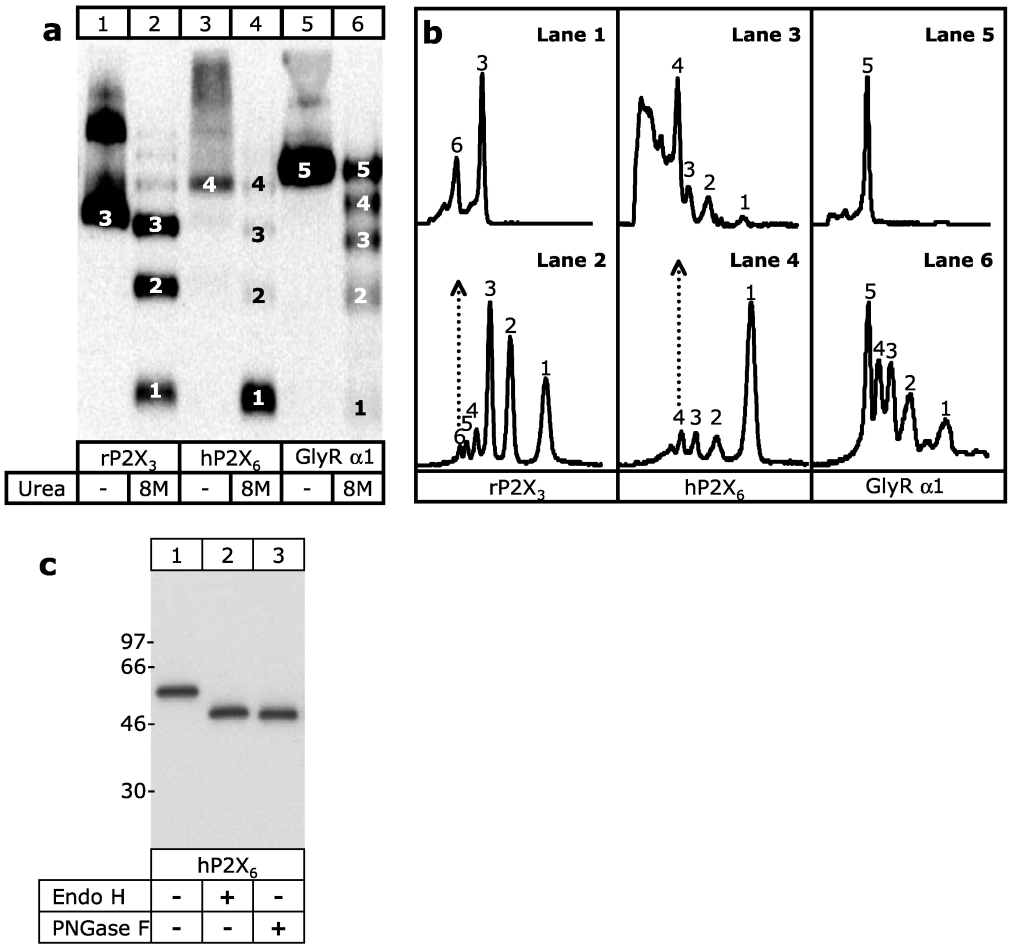

Figure 5. $hP2X_6$ subunits form aggregates and homotetramers in *Xenopus* oocytes. (a) Metabolically labelled GlyR hα1 subunits and $rP2X_3$ subunits, both known to form functional homomeric receptors, migrated as pentamers and trimers, respectively, on the blue native PAGE gel. In contrast, $hP2X_6$ subunits known for their inability to form a functional homomeric receptor in *Xenopus* oocytes, migrated as tetramers and aggregate. (b) Quantitative scans of lanes 3-6 of A are shown to display the relative amounts of the various protein bands. (c) *N*-glycan content of $hP2X_6$ subunits. The same samples as in (a) were deglycosylated as indicated and resolved by SDS-PAGE. The observed shift, from 56 to 48 kDa (49 kDa calculated protein core), is consistent with the presence of three *N*-glycans, suggesting that all three consensus sites (^{155}NGT, ^{185}NFT, ^{200}NFS) were used. No complex-glycosylated bands were observed.

homotrimers or multiples of homotrimers. These findings leave no doubt that homotrimers are the essential structural element of functional $P2X_2$ receptors.

Surprisingly, $hP2X_2$ subunits do not share with $rP2X_2$ subunits the amorphous migration on blue native PAGE gels, but migrate in their intracellular form as homotrimers. As sequence variability between human and rat $P2X_2$ subunits is almost confined to the C cytoplasmic domain, this observation points to a role of the long C-terminal tail for the unusual migration of $rP2X_2$ receptors. Indeed, preliminary results indicate that a functional splice variant, $rP2X_{2B}$, characterized by a 69 amino acid residue deletion within its cytoplasmic C-terminal tail as compared to the $rP2X_2$ subunit,[25] behaved entirely as a homotrimer on blue native PAGE gels (W. Duckwitz, S. Gendreau and G.S., unpublished results). The spliced domain, which shows only 65% similarity among human and rat, includes a proline-rich tubulin-binding domain.[26] We speculate that $rP2X_2$ homotrimers of the unspliced 472 amino acid residue form remain bound to cytoplasmic proteins, possibly cytoskeletal elements, during both non-denaturing purification and blue native PAGE, resulting in aberrant migration on the gels. A recently identified C-terminal trafficking motif, YXXXK, that has been suggested to tether P2X receptors to cytoskeletal proteins, is located a few amino acid residues upstream of the spliced exon.[27] As this motif is conserved among human and rat $P2X_2$ subunits, it is unlikely to play a role in the unusual migration of $rP2X_2$ receptors.

Higher order interactions of plasma membrane-bound homotrimeric $rP2X_2$ receptors: a possible structural basis of coupled gating

The $rP2X_2$ receptor differs also in its plasma membrane-bound form from other P2X receptors

by existing both as a homotrimer and multiples thereof, e.g. dimers, trimers, and tetramers of homotrimers. We have previously observed that $rP2X_1$ and $rP2X_3$ subunits had a certain propensity to form hexamers if *n*-octylglucoside was used as a detergent for receptor solubilization, which exerted a slight denaturing effect.[12] In contrast, the higher order complexes of plasma membrane-bound $rP2X_2$ homotrimers observed here were isolated in digitonin. The impossibility to fix these complexes in the oocytes plasma membrane by chemical cross-linking suggests that the spacer arm of glutardialdehyde of only ~5 Å may be too short to bridge the distance between two interacting homotrimers, although it efficiently cross-linked $rP2X_2$ subunits within a homotrimer. Thus, the interfaces mediating homotrimer formation and higher order interactions of homotrimers appear to be different. This view gains further support by the observation that the $rP2X_2$ receptor clusters dissociated into single $rP2X_2$ homotrimers when treated with DTT, whereas homotrimers resisted DTT treatment to dissociate into monomers.

The clusters of homotrimeric $rP2X_2$ receptors may be considered to form as artefacts similar to the $rP2X_1$ hexamers produced by *n*-octylglucoside in our previous study. An intriguing alternative possibility, however, comes from a kinetic study showing that multiple $rP2X_2$ receptors in a patch do not open and close independent of each other as expected for individual receptors, but are functionally coupled and partially synchronized.[28] Cooperative effects resulting from homomeric channel interactions have been demonstrated to occur with a variety of ion channels including nAChRs,[29,30] K^+ channels,[31] and Ca^{2+} release channels on the sarcoplasmic reticulum membrane.[32] Thus, the physical association between $rP2X_2$ homotrimers observed here could well represent the structural basis for the coupled gating behavior, leading to a synchronized opening of neighboring $rP2X_2$ receptors.

Tetrameric *versus* trimeric organization of P2X receptors

In vitro refolding of the bacterially expressed extracellular domain of the $P2X_2$ subunit yielded stable tetramers.[33] However, an important caveat to these experiments is that multimerization of full-length $P2X_2$ subunits is determined by the second transmembrane domain, and not by the extracellular loop.[34] In our experiments with full-length proteins, tetrameric assemblies were only observed upon expression of $P2X_6$ subunits, which are known for their incapability to form as functional homomeric receptors in *Xenopus* oocytes.[16] The persistence of oocyte-expressed $P2X_6$ subunits in the core-glycosylated ER form and their complete absence at the cell surface can be easily reconciled with the view that both $P2X_6$ aggregates and tetramers are recognized and permanently retained in the ER by the ER quality control system as incorrectly assembled proteins. Accordingly, failing to reach the native trimeric conformation rather than a genuine trafficking defect of properly assembled $P2X_6$ receptors appears to account for the inability to express functional homomeric $P2X_6$ receptors in *Xenopus* oocytes. This lends indirect support to the view that tetramers are not a functional oligomeric state of P2X receptors.

Unlike *Xenopus* oocytes, mammalian cell lines such as HEK293 cells do express non-functional $P2X_6$ protein at the cell surface in an unknown oligomeric state.[27,35] Although most attempts have failed to record functional responses from $P2X_6$ subunit-expressing mammalian cell lines, a novel αβ-methylene ATP-sensitive phenotype has recently been identified in a minute fraction of stably transfected HEK293 cell clones.[35] These findings may suggest that formation of functional P2X receptors from $P2X_6$ subunits requires specific helper proteins aiding in receptor assembly or maturation that occur in a small subset of mammalian cells, but evidently not in *Xenopus* oocytes.

A tetrameric organization was furthermore implicated by the inactivation rate of the $P2X_2$ receptor in excised patches, which increased with a Hill coefficient of 4, suggesting that the functional channel has at least four Ca^{2+} binding sites.[17] However, as mentioned by the authors, these data can also be reconciled with other stoichiometries if multiple Ca^{2+} binding sites are present per subunit. All other functional studies reported so far are in essence consistent with a trimeric channel. Experiments conducted before P2X receptors were cloned suggested that ATP-gated ion channels must bind ATP to each of three identical, non-interacting binding sites to open the channel.[36] In single channel studies with recombinant $rP2X_2$ receptors, ATP increased the open probability with a Hill coefficient of 2.3, implying that there are at least three positively cooperative ATP-binding sites in a functional $P2X_2$ receptor.[37] While this Hill coefficient does not exclude the existence of more than three such sites, the data fit best with a model in which the channel proceeds through three ATP-binding steps before opening.[37] Also when low agonist concentrations were used to minimize the contribution of cooperative interactions of subunits, initial slopes of 2.5 and 2.7 were derived for homo-oligomeric $rP2X_2$ and $rP2X_3$ receptors, consistent with three identical, independent binding sites.[13]

Experiments with concatenated P2X subunit cDNAs are also consistent with a trimeric channel. Contiguous copies of the $rP2X_2$ subunit carrying a functional reporter mutation could not be inhibited by a cysteine-reactive compound if the reporter mutation was introduced into the fourth copy. This suggests that the fourth subunit does not contribute to the $rP2X_2$ channel formation.[14] In a more biochemically oriented study with concatamers of up to six $rP2X_1$ subunits in series, significant problems were encountered in the interpretation of the electrophysiological data arising from the production of minute levels of lower order

by-products such as monomers and dimers.[38] These by-products combined to functional multimers equal in mass to the homotrimeric rP2X$_1$ receptor assembled from rP2X$_1$ monomers. Because multimers consisting of more than three rP2X$_1$ monomers were not observed to appear in the plasma membrane, these results also provide strong support for a trimeric architecture for rP2X$_1$ receptors.

Trimeric organization of heteromeric P2X$_{1+2}$ receptors

Biochemical evidence for a possible co-assembly of P2X$_1$ with P2X$_2$ receptors was first obtained by co-immunoprecipitation experiments of epitope-tagged P2X$_1$ and P2X$_2$ subunits expressed in HEK293 cells.[39] Phenotypically, heteromeric P2X$_{1+2}$ receptors and homomeric P2X$_1$ receptors are virtually identical, showing both rapidly desensitizing currents, and being only distinguishable on the basis of their distinct pH sensitivity.[20] Based on disulfide bond formation between engineered cysteine residues it has recently been suggested that a trimeric P2X$_{2+3}$ receptor would have the composition P2X$_2$(P2X$_3$)$_2$.[13] Our SDS-PAGE gels show significantly more radioactivity corresponding to co-isolated non-tagged P2X$_2$ subunits than to His-P2X$_1$ subunits. Provided that both subunits become labelled by [^{125}I]sulfo-SHPP with similar efficiency, this observation favors the view that the trimeric P2X$_{1+2}$ receptor incorporates one P2X$_1$ subunit and two P2X$_2$ subunits.

Surprisingly, our results clearly indicate that assembly of heteromeric P2X$_{1+2}$ receptors is favored over the respective homomeric P2X$_1$ receptors. Since P2X$_1$ and P2X$_2$ subunits co-exist in a variety of tissues,[20] the efficient formation of heteromeric P2X$_{1+2}$ receptors raises the intriguing possibility that ATP-gated currents attributed to homotrimeric P2X$_1$ receptors may at least in some native tissues be mediated by P2X$_{1+2}$ heterotrimers.

Materials and Methods

LGIC cDNA constructs

All LGIC cDNAs used here were subcloned into vector pNKS2, which contains a long poly(A) tract for efficient translation in *Xenopus* oocytes.[40] In addition, all the LGIC cDNA constructs were endowed with virtually the same 50 nucleotides long 5′ non-translated sequence between the SP6 polymerase-binding site and the initiating ATG corresponding to an optimized sequence that has been shown to support maximal protein synthesis in the rabbit reticulocyte system.[41] Cloned cDNAs, insertions and junction sequences were verified by dideoxynucleotide sequencing.

To indicate the species origin, LGIC subunit names are preceded by h or r for human or rat, respectively. cDNAs encoding the rP2X$_2$ subunit,[18] the hP2X$_2$ subunit,[19] the hP2X$_6$ subunit, and the rP2X$_4$ subunit[42] were isolated by RT-PCR from total RNA of NGF-treated PC12 cells, a human and a rat brain cDNA library (Life Technologies), respectively, using sequence-specific primers. rP2X$_5$ and rP2X$_6$ clones were kindly provided by Dr Florentina Soto.[43] Codons for six histidine residues (His) were introduced by QuikChange site directed-mutagenesis (Stratagene, La Jolla, CA) immediately behind the initiation ATG without changing any other amino acid to yield His-rP2X$_2$, His-hP2X$_2$, His-rP2X$_4$, His-rP2X$_5$ and His-rP2X$_6$. Constructs available from previous work include His-rP2X$_1$ and His-rP2X$_3$ encoding the rat P2X$_1$ and P2X$_3$ subunit with N-terminal His tags,[12] and GlyR hα1-His encoding the human GlyR α1-subunit with a C-terminal His tag.[44]

LGIC expression in *Xenopus* oocytes

Defolliculated *Xenopus* oocytes injected with capped cRNAs as described[45] were kept in parallel with non-injected control oocytes at 19 °C in sterile frog Ringer's solution (ORi: 90 mM NaCl, 1 mM KCl, 1 mM $CaCl_2$, 1 mM $MgCl_2$, 10 mM Hepes, pH 7.4) supplemented with 50 μg/ml of gentamycin. Oocytes injected with rP2X$_2$ or rP2X$_5$ cRNAs became occasionally unhealthy when kept in groups and were therefore cultured individually in microtiter plates, one oocyte per well. One to three days after cRNA injection, ATP responses were measured by two-electrode voltage-clamp recording at a holding potential of −60 mV as described.[46] Capping the N-terminal ends of the various rP2X subunits with a His tag for one-step affinity purification had virtually no effect on the electrophysiological phenotype of the corresponding receptor in *Xenopus* oocytes (results not shown).

Metabolic labelling and affinity purification of LGICs

For metabolic radiolabelling, cRNA-injected oocytes and non-injected controls were incubated overnight with L-[^{35}S]methionine (>40 TBq/mmol, Amersham Biosciences, Freiburg, Germany) at about 100 MBq/ml (0.4 MBq per oocyte) in ORi at 19 °C, and then chased as indicated. His-tagged receptors were purified by Ni^{2+} NTA agarose (Qiagen, Hilden, Germany) chromatography from digitonin (1.0%) extracts of oocytes as detailed previously.[12,47] LGICs were released from the Ni^{2+} NTA agarose with non-denaturing elution buffer consisting of 200 mM imidazole/HCl (pH 7.4) and 0.5% digitonin, and then kept at 0 °C until analyzed at the day of purification.

Cell surface radioiodination

Selective labelling of LGICs at the plasma membrane was achieved by incubating oocytes three days after cRNA injection with [^{125}I]sulfosuccinimidyl-3-(4-hydroxyphenyl)proprionate ([^{125}I]sulfo-SHPP), a membrane-impermeant derivative of the Bolton-Hunter reagent[48] exactly as described.[12,47] Proteins were purified from digitonin extracts of the oocytes by Ni^{2+} NTA agarose chromatography as detailed above.

In situ cross-linking of LGICs

For selective visualization of cross-linked plasma membrane-bound receptors, P2X receptor expressing oocytes were first surface radioiodinated with [^{125}I]sulfo-SHPP as described above. The oocytes were then washed several times with ice-cold cross-linking buffer (30 mM Na phosphate (pH 8.0), 1 mM $MgCl_2$, 0.1 mM $CaCl_2$), and glutardialdehyde was added to

initiate the cross-linking reaction on ice for the time indicated in the Figures. After the desired incubation time, residual glutardialdehyde was quenched with 10 mM lysine in cross-linking buffer. A digitonin extract was then prepared from the cells, from which rP2X receptors were isolated by Ni^{2+} NTA chromatography. Pilot experiments with $rP2X_1$ receptor-expressing oocytes revealed a 30–60 minutes incubation of intact oocytes at 100 μM glutardialdehyde on ice as optimal conditions.

Blue native PAGE and SDS-PAGE

Blue native PAGE[49,50] was carried out as described.[12] For partial dissociation of natively purified LGICs into lower order complexes down to monomers, samples were treated for one hour at 37 °C with 4 or 8 M urea or 0.1% (w/v) SDS as indicated. For SDS-PAGE, proteins were supplemented with SDS sample buffer containing 20 mM DTT and electrophoresed in parallel with ^{14}C-labelled molecular mass markers (Rainbow™, Amersham Biosciences) on SDS polyacrylamide gradient gels. In some experiments, samples were treated prior to SDS-PAGE for two hours at 37 °C with either Endoglycosidase H (Endo H) or Peptide:N-glycosidase F (PNGase F) (New England Biolabs, Frankfurt, Germany) in the presence of 1% octylglucoside to diminish inactivation of PNGase F. Both SDS and blue native polyacrylamide gels were fixed, dried, and exposed at −80 °C to BioMax MR or MS film (Eastman Kodak Co.) as appropriate. For quantification, the dried gels were exposed to a PhosphorImager screen and scanned using a Storm 820 PhosphorImager (Amersham Biosciences). Individual bands were quantified with the ImageQuant software.

Acknowledgements

We thank Dr Florentina Soto for providing the $rP2X_5$ and $rP2X_6$ clones. Also, we thank Drs Annette Nicke and Bruce A. Cunningham for critical reading and helpful comments on the manuscript. This work was supported by grants of the Deutsche Forschungsgemeinschaft to G.S. (Schm 536/2-3, 536/2-4, Schm 536/6-1, and GRK 137/2). We dedicate this paper to Professor Heinrich Betz on the occasion of his 60th birthday.

References

1. Le Novere, N. & Changeux, J. P. (2001). LGICdb: the ligand-gated ion channel database. *Nucl. Acids Res.* **29**, 294–295.
2. North, R. A. (1996). P2X receptors: a third major class of ligand-gated ion channels. *Ciba Found. Symp.* **198**, 91–105.
3. Unwin, N. (2003). Structure and action of the nicotinic acetylcholine receptor explored by electron microscopy. *FEBS Letters*, **555**, 91–95.
4. Brejc, K., van Dijk, W. J., Klaassen, R. V., Schuurmans, M., van Der, O. J., Smit, A. B. & Sixma, T. K. (2001). Crystal structure of an ACh-binding protein reveals the ligand-binding domain of nicotinic receptors. *Nature*, **411**, 269–276.
5. Dingledine, R., Borges, K., Bowie, D. & Traynelis, S. F. (1999). The glutamate receptor ion channels. *Pharmacol. Rev.* **51**, 7–61.
6. Gouaux, E. (2004). Structure and function of AMPA receptors. *J. Physiol.* **554**, 249–253.
7. Sun, Y., Olson, R., Horning, M., Armstrong, N., Mayer, M. & Gouaux, E. (2002). Mechanism of glutamate receptor desensitization. *Nature*, **417**, 245–253.
8. Bodin, P. & Burnstock, G. (2001). Purinergic signalling: ATP release. *Neurochem. Res.* **26**, 959–969.
9. Haines, W. R., Voigt, M. M., Migita, K., Torres, G. E. & Egan, T. M. (2001). On the contribution of the first transmembrane domain to whole-cell current through an ATP-gated ionotropic P2X receptor. *J. Neurosci.* **21**, 5885–5892.
10. Rassendren, F., Buell, G., Newbolt, A., North, R. A. & Surprenant, A. (1997). Identification of amino acid residues contributing to the pore of a P2X receptor. *EMBO J.* **16**, 3446–3454.
11. Egan, T. M., Haines, W. R. & Voigt, M. M. (1998). A domain contributing to the ion channel of ATP-gated $P2X_2$ receptors identified by the substituted cysteine accessibility method. *J. Neurosci.* **18**, 2350–2359.
12. Nicke, A., Bäumert, H. G., Rettinger, J., Eichele, A., Lambrecht, G., Mutschler, E. & Schmalzing, G. (1998). $P2X_1$ and $P2X_3$ receptors form stable trimers: a novel structural motif of ligand-gated ion channels. *EMBO J.* **17**, 3016–3028.
13. Jiang, L. H., Kim, M., Spelta, V., Bo, X., Surprenant, A. & North, R. A. (2003). Subunit arrangement in P2X receptors. *J. Neurosci.* **23**, 8903–8910.
14. Stoop, R., Thomas, S., Rassendren, F., Kawashima, E., Buell, G., Surprenant, A. & North, R. A. (1999). Contribution of individual subunits to the multimeric $P2X_2$ receptor: estimates based on methanethiosulfonate block at T336C. *Mol. Pharmacol.* **56**, 973–981.
15. Chang, G., Spencer, R. H., Lee, A. T., Barclay, M. T. & Rees, D. C. (1998). Structure of the MscL homolog from *Mycobacterium tuberculosis*: a gated mechanosensitive ion channel. *Science*, **282**, 2220–2226.
16. North, R. A. (2002). Molecular physiology of P2X receptors. *Physiol. Rev.* **82**, 1013–1067.
17. Ding, S. & Sachs, F. (2000). Inactivation of $P2X_2$ purinoceptors by divalent cations. *J. Physiol.* **522**, 199–214.
18. Brake, A. J., Wagenbach, M. J. & Julius, D. (1994). New structural motif for ligand-gated ion channels defined by an ionotropic ATP receptor. *Nature*, **371**, 519–523.
19. Lynch, K. J., Touma, E., Niforatos, W., Kage, K. L., Burgard, E. C., van Biesen, T. *et al.* (1999). Molecular and functional characterization of human $P2X_2$ receptors. *Mol. Pharmacol.* **56**, 1171–1181.
20. Brown, S. G., Townsend-Nicholson, A., Jacobson, K. A., Burnstock, G. & King, B. F. (2002). Heteromultimeric $P2X_{1/2}$ receptors show a novel sensitivity to extracellular pH. *J. Pharmacol. Expt. Ther.* **300**, 673–680.
21. Lewis, C., Neidhart, S., Holy, C., North, R. A., Buell, G. & Surprenant, A. (1995). Coexpression of $P2X_2$ and $P2X_3$ receptor subunits can account for ATP-gated currents in sensory neurons. *Nature*, **377**, 432–435.
22. Chen, C. C., Akopian, A. N., Sivilotti, L., Colquhoun, D., Burnstock, G. & Wood, J. N. (1995). A P2X purinoceptor expressed by a subset of sensory neurons. *Nature*, **377**, 428–431.
23. Le, K. T., Babinski, K. & Seguela, P. (1998). Central $P2X_4$ and $P2X_6$ channel subunits coassemble into a novel heteromeric ATP receptor. *J. Neurosci.* **18**, 7152–7159.

24. Collo, G., North, R. A., Kawashima, E., Merlo-Pich, E., Neidhart, S., Surprenant, A. & Buell, G. (1996). Cloning of $P2X_5$ and $P2X_6$ receptors and the distribution and properties of an extended family of ATP-gated ion channels. *J. Neurosci.* **16**, 2495–2507.
25. Brändle, U., Spielmanns, P., Osteroth, R., Sim, J., Surprenant, A. Buell, G. *et al.* (1997). Desensitization of the $P2X_2$ receptor controlled by alternative splicing. *FEBS Letters*, **404**, 294–298.
26. Gendreau, S., Schirmer, J. & Schmalzing, G. (2003). Identification of a tubulin binding motif on the $P2X_2$ receptor. *J. Chromatogr. B Analyt. Technol. Biomed. Life Sci.* **786**, 311–318.
27. Chaumont, S., Jiang, L. H., Penna, A., North, R. A. & Rassendren, F. (2004). Identification of a trafficking motif involved in the stabilization and polarization of P2X receptors. *J. Biol. Chem.* 2004;.
28. Ding, S. & Sachs, F. (2002). Evidence for non-independent gating of $P2X_2$ receptors expressed in *Xenopus* oocytes. *BMC. Neurosci.* **3**, 17.
29. Keleshian, A. M., Edeson, R. O., Liu, G. J. & Madsen, B. W. (2000). Evidence for cooperativity between nicotinic acetylcholine receptors in patch clamp records. *Biophys. J.* **78**, 1–12.
30. Schindler, H., Spillecke, F. & Neumann, E. (1984). Different channel properties of Torpedo acetylcholine receptor monomers and dimers reconstituted in planar membranes. *Proc. Natl Acad. Sci. USA*, **81**, 6222–6226.
31. Tytgat, J. & Hess, P. (1992). Evidence for cooperative interactions in potassium channel gating. *Nature*, **359**, 420–423.
32. Marx, S. O., Gaburjakova, J., Gaburjakova, M., Henrikson, C., Ondrias, K. & Marks, A. R. (2001). Coupled gating between cardiac calcium release channels (ryanodine receptors). *Circ. Res.* **88**, 1151–1158.
33. Kim, M., Yoo, O. J. & Choe, S. (1997). Molecular assembly of the extracellular domain of $P2X_2$, an ATP-gated ion channel. *Biochem. Biophys. Res. Commun.* **240**, 618–622.
34. Torres, G. E., Egan, T. M. & Voigt, M. M. (1999). Identification of a domain involved in ATP-gated ionotropic receptor subunit assembly. *J. Biol. Chem.* **274**, 22359–22365.
35. Jones, C. A., Vial, C., Sellers, L. A., Humphrey, P. P., Evans, R. J. & Chessell, I. P. (2004). Functional regulation of $P2X_6$ receptors by N-linked glycosylation: identification of a novel αβ-methylene ATP-sensitive phenotype. *Mol. Pharmacol.* **65**, 979–985.
36. Bean, B. P. (1992). Pharmacology and electrophysiology of ATP-activated ion channels. *Trends Pharmacol. Sci.* **13**, 87–90.
37. Ding, S. & Sachs, F. (1999). Single channel properties of $P2X_2$ purinoceptors. *J. Gen. Physiol.* **113**, 695–720.
38. Nicke, A., Rettinger, J. & Schmalzing, G. (2003). Monomeric and dimeric byproducts are the principal functional elements of higher order $P2X_1$ concatamers. *Mol. Pharmacol.* **63**, 243–252.
39. Torres, G. E., Egan, T. M. & Voigt, M. M. (1999). Hetero-oligomeric assembly of P2X receptor subunits. Specificities exist with regard to possible partners. *J. Biol. Chem.* **274**, 6653–6659.
40. Gloor, S., Pongs, O. & Schmalzing, G. (1995). A vector for the synthesis of cRNAs encoding Myc epitope-tagged proteins in *Xenopus laevis* oocytes. *Gene*, **160**, 213–217.
41. Kozak, M. (1994). Features in the 5′ non-coding sequences of rabbit α and β-globin mRNAs that affect translational efficiency. *J. Mol. Biol.* **235**, 95–110.
42. Soto, F., Garcia-Guzman, M., Gomez-Hernandez, J. M., Hollmann, M., Karschin, C. & Stühmer, W. (1996). $P2X_4$: an ATP-activated ionotropic receptor cloned from rat brain. *Proc. Natl Acad. Sci. USA*, **93**, 3684–3688.
43. Garcia-Guzman, M., Soto, F., Laube, B. & Stühmer, W. (1996). Molecular cloning and functional expression of a novel rat heart P2X purinoceptor. *FEBS Letters*, **388**, 123–127.
44. Büttner, C., Sadtler, S., Leyendecker, A., Laube, B., Griffon, N., Betz, H. & Schmalzing, G. (2001). Ubiquitination precedes internalization and proteolytic cleavage of plasma membrane-bound glycine receptors. *J. Biol. Chem.* **276**, 42978–42985.
45. Schmalzing, G., Gloor, S., Omay, H., Kröner, S., Appelhans, H. & Schwarz, W. (1991). Up-regulation of sodium pump activity in *Xenopus laevis* oocytes by expression of heterologous β1 subunits of the sodium pump. *Biochem. J.* **279**, 329–336.
46. Rettinger, J. & Schmalzing, G. (2003). Activation and desensitization of the recombinant $P2X_1$ receptor at nanomolar ATP concentrations. *J. Gen. Physiol.* **121**, 451–461.
47. Rettinger, J., Aschrafi, A. & Schmalzing, G. (2000). Roles of individual N-glycans for ATP potency and expression of the rat $P2X_1$ receptor. *J. Biol. Chem.* **275**, 33542–33547.
48. Thompson, J. A., Lau, A. L. & Cunningham, D. D. (1987). Selective radiolabeling of cell surface proteins to a high specific activity. *Biochemistry*, **26**, 743–750.
49. Schägger, H. & von Jagow, G. (1991). Blue native electrophoresis for isolation of membrane protein complexes in enzymatically active form. *Anal. Biochem.* **199**, 223–231.
50. Schägger, H., Cramer, W. A. & von Jagow, G. (1994). Analysis of molecular masses and oligomeric states of protein complexes by blue native electrophoresis and isolation of membrane protein complexes by two-dimensional native electrophoresis. *Anal. Biochem.* **217**, 220–230.

Edited by D. Rees

(Received 6 April 2004; received in revised form 25 June 2004; accepted 27 June 2004)

TABLE OF PUBLICATIONS, ORAL AND POSTER PRESENTATIONS

Sadtler, S., Büttner, C., Laube, B., Leyendecker, A., Griffon, N., Betz, H., Schmalzing G. (2001)
Ubiquitinierung des inhibitorischen Glycinrezeptors an der Plasmamembran von *Xenopus laevis*-Oocyten.
Oral presentation at the 42th Spring Meeting of the German Soc. for Exp. and Clin. Pharmacol. and Toxicol. 2001 in Mainz, Germany.

Büttner, C., Sadtler, S., Leyendecker, A., Laube, B., Griffon, N., Betz, H., Schmalzing, G. (2001).
Ubiquitination Precedes Internalization and Proteolytic Cleavage of Plasma Membrane-bound Glycine Receptors.
J. Biol. Chem. **276**, 42978-42985.

Sadtler, S., Leyendecker, A., Laube, B., Betz, H., Schmalzing, G. (2002)
Ubiquitination and Y^{339} are involved in internalization of the homomeric α1 glycine receptor.
Poster presentation at the 43th Spring Meeting of the German Soc. for Exp. and Clin. Pharmacol. and Toxicol. 2002 in Mainz, Germany.

Sadtler, S., Laube, B., Lashub, A., Nicke, A., Betz, H., Schmalzing, G. (2003).
A Basic Cluster Determines Topology of the Cytoplasmic M3-M4 Loop of the Glycine Receptor α1 Subunit.
J. Biol. Chem. **278**, 16782-16790.

Boldt, W., Klapperstück, M., Büttner, C., Sadtler, S., Schmalzing, G., Markwardt, F. (2003).
$Glu^{496}Ala$ polymorphism of human $P2X_7$ receptor does not affect its electrophysiological phenotype.
Am. J. Physiol. Cell Physiol. **284**, 749-756.

Aschrafi, A., Sadtler, S., Niculescu, C., Rettinger, J., Schmalzing, G. (2004).
Trimeric Architecture of Homomeric $P2X_2$ and Heteromeric $P2X_{1+2}$ Receptor Subtypes.
J. Mol. Biol. **342**, 333-343.

Nicke, A., Thurau, H., Sadtler, S., Rettinger, J., Schmalzing, G. (2004).
Assembly of nicotinic α7 subunits in *Xenopus* oocytes is partially blocked at the tetramer level.
FEBS Lett. **575**, 52-58

Lebenslauf

Persönliche Daten

Name	Sven Sadtler
Geburtsdatum, -ort	20.09.1972, Bad Homburg
Anschrift	Graf-Stauffenberg-Ring 139,
	61350 Bad Homburg

Schulischer Werdegang

1978 – 1983	Grundschule in Bad Homburg
1983 – 1992	altsprachliches Gymnasium in Bad Homburg,
	Abschluß: Abitur

Akademischer Werdegang

1992 – 1998	Diplomstudiengang Biochemie, Johann Wolfgang-Goethe-Universität, Frankfurt am Main bei Prof. Dr. H. Fasold Prüfungsfächer: Biochemie, Biophysikalische Chemie, Pharmakologie und Toxikologie Abschluß 1/98: Diplom-Biochemiker, Note der Diplomarbeit „sehr gut“, Gesamtnote: „sehr gut“ Thema der Diplomarbeit: *„Immunsuppressive Peptide endogener und exogener Retroviren – Wirkungsmechanismen und Bindungsproteine“*
9/1999 – heute	Promotion im Fachbereich chemische und pharmazeutische Wissenschaften am Pharmakologisches Institut für Naturwissenschaftler der Johann Wolfgang-Goethe-Universität, Frankfurt am Main bei Prof. Dr. G. Schmalzing, später bei Prof. G. Lambrecht. Fachrichtung: Molekulare Pharmakologie Liganden-gesteuerter Ionenkanäle Thema der Doktorarbeit: „*Synthesis, assembly, and intracellular trafficking of members of the cys-loop and P2X families of ligand-gated ion channels“* Abschluß geplant für 2. Halbjahr 2005

Beruflicher Werdegang

2/1993 – 4/1993	Praktikantentätigkeit am Paul-Ehrlich-Institut, Langen, im Fachbereich Immunologie. Erlernung und Anwendung diverser molekularbiologischer und immunologischer Testverfahren zur Feststellung endogener und exogener Retroviren
2/1997 – 9/1999	Aushilfstätigkeiten in der Parkapotheke, Bad Homburg mit den Aufgabenschwerpunkten Labortätigkeiten (Rezeptur, Defektur und Dokumentation), Lagerbestandspflege und Koordination der Botentätigkeiten
9/1999 – 3/2002	Wissenschaftlicher Angestellter im Fachbereich Chemische und pharmazeutische Wissenschaften am Pharmakologisches Institut für Naturwissenschaftler der Johann Wolfgang-Goethe-Universität, Frankfurt am Main bei Prof. Dr. G. Schmalzing. Forschungsprojekte: - Herstellung von zellulären Testsystemen für die Suche nach neuen Arzneistoffen (sog. High-Throughput-Screening, HTS) im Rahmen einer engen wissenschaftlichen Kooperation mit einem bekannten, pharmazeutischen Unternehmen. - Aufklärung grundlegender Vorgänge bei der Synthese und Regulation ligandgesteuerter Ionenkanäle, die potentielle Angriffspunkte von Arzneimitteln darstellen.
4/2002 – 12/2002	Wissenschaftlicher Angestellter am Institut für Pharmakologie und Toxikologie des Universitätsklinikum Aachen bei Prof. Dr. G. Schmalzing. Wechsel von Frankfurt nach Aachen wg. Umzug des Labors; Fortsetzung der Forschungsprojekte
1/2003 – heute	Aushilfstätigkeiten in der Parkapotheke, Bad Homburg mit den Aufgabenschwerpunkten Labortätigkeiten (Rezeptur und Dokumentation), Lagerbestandspflege und Koordination der Botentätigkeiten

Weiterbildung

9/2002 – 8/2004 Master of Business Administration (MBA),
Fachhochschule Mainz, Module:

- Buchführung,
- Kommunikation/Verhandlungsmanagement,
- Grundlagen des wissenschaftlichen Arbeitens,
- Volkswirtschaftliche Rahmenbedingungen unternehmerischer Entscheidungen,
- quantitative Methoden und Verfahren,
- Grundlagen der Betriebswirtschaftslehre,
- Human Resources,
- Financial Accounting,
- Marketing,
- Supply Chain Management,
- Managerial Finance,
- Management Accounting,
- Information Management,
- Grundlagen der Unternehmensführung mit Planspiel,
- Strategisches Management,
- Strategie Implementierung und Controlling,
- Entwicklung von Führungskompetenz,
- aktuelle Managementkonzepte,
- internationales Managementseminar einschließlich Exkursion

Abschlußnote: 1,7

2/2005 – 4/2005 Praktikum im Bereich „Communications“ bei einem internationalen, forschenden Pharmaunternehmen

Weitere Fähigkeiten

Sehr gute EDV-Kenntnisse (MS Office Programme)

Englisch, sehr gut in Wort und Schrift, verhandlungssicher

Französisch, ausbaufähige Grundkenntnisse

Italienisch, Grundkenntnisse

Wissenschaftliche Publikationen

1998 Denner, J., Sadtler, S., Chen, A., Kurth, R.:
The immunosuppressive Peptide of HIV-1:
Influence on the cytokine production of human lymphocytes.
12th World AIDS Conference, Geneva

1998 Denner, J., Sadtler, S., Chen, A., Lüttkopf, D., Kurth, R.:
Immunosuppression by Retroviruses: Role of transmembrane envelope protein and implications for AIDS and xenotransplantations.
2nd Congress of Molecular Medicine, Berlin

1998 Denner, J., Sadtler, S., Kurth, R.:
Influence of the immunosuppressive Peptide of HIV-1 on the cytokine production of human lymphocytes.
3rd European Conference on Experimental AIDS Research, Munich

2001 Büttner, C., Sadtler, S., Leyendecker, A., Laube, B., Griffon, N., Betz, H., Schmalzing G.:
Ubiquitination precedes internalization and proteolytic cleavage of plasma membrane-bound glycine receptors.
J. Biol. Chem. **276**, 42978-42985.

2003 Sadtler, S., Laube, B., Lashub, A., Nicke, A., Betz, H., Schmalzing, G.:
A basic cluster determines topology of the cytoplasmic M3-M4 loop of the glycine receptor alpha1 subunit.
J. Biol. Chem. **278**, 16782-16790.

2003 Boldt, W., Klapperstück, M., Büttner, C., Sadtler, S., Schmalzing, G., Markwardt, F.:
$Glu^{496}Ala$ polymorphism of human $P2X_7$ receptor does not affect its electrophysiological phenotype.
Am. J. Physiol. Cell Physiol. **284**, 749-756. Epub 2002 Nov 13.

2004 Aschrafi, A., Sadtler, S., Niculescu, C., Rettinger, J., Schmalzing, G.:
Trimeric architecture of homomeric $P2X_2$ and heteromeric $P2X_{1+2}$ receptor subtypes.
J. Mol. Biol. **342**, 333-43.

2004 Nicke, A., Thurau, H., Sadtler, S., Rettinger, J., Schmalzing, G.:
Assembly of nicotinic alpha7 subunits in Xenopus oocytes is partially blocked at the tetramer level.
FEBS Lett. **575**, 52-58.

Bad Homburg, den 27. Juni 2005

Sven Sadtler